Synthesis of silver nanoparticles and their role against human and *Plasmodium falciparum* leucine aminopeptidase

Thesis submitted in fulfilment of the requirements for the degree of

MASTERS OF SCIENCE IN BIOCHEMISTRY

In the

Department of Biochemistry, Microbiology and Biotechnology

Faculty of Science

Rhodes University

Grahamstown

South Africa

By

Dumisani Mnkandhla

G12M6048

March 2014

Supervisor: Prof C.G. Whiteley
Co-Supervisors: Dr B. Wilhelmi
Dr J. van Marwijk

Abstract

Antimalarial drug discovery remains a challenging endeavour as malaria parasites continue to develop resistance to drugs, including those which are currently the last line of defence against the disease. *Plasmodium falciparum* is the most virulent of the malaria parasites and it delivers its deadliest impact during the erythrocytic stages of the parasite's life cycle; a stage characterised by elevated catabolism of haemoglobin and anabolism of parasite proteins. The present study investigates the use of nanotechnology in the form of metallic silver nanoparticles (AgNPs) against *P. falciparum* leucine aminopeptidase (*Pf*LAP), a validated biomedical target involved in haemoglobin metabolism. AgNPs were also tested against the human homolog cytosolic *Homo sapiens* leucine aminopeptidase (*Hs*LAP) to ascertain their selective abilities. *Pf*LAP and *Hs*LAP were successfully expressed in *Escherichia coli* BL21(DE3) cells. *Pf*LAP showed optimal thermal stability at 25 °C and optimal pH stability at pH 8.0 with a K_m of 42.7 mM towards leucine-*p*-nitroanilide (L*p*NA) and a V_{max} of 59.9 μmol.ml^{-1}.min^{-1}. *Hs*LAP was optimally stable at 37 °C and at pH 7.0 with a K_m of 16.7 mM and a V_{max} of 17.2 μmol.ml^{-1}.min^{-1}. Both enzymes exhibited optimal activity in the presence of 2 mM Mn^{2+}. On interaction with polyvinylpyrrolidone (PVP) stabilised AgNPs, both enzymes were inhibited to differing extents with *Pf*LAP losing three fold of its catalytic efficiency relative to *Hs*LAP. These results show the ability of AgNPs to selectively inhibit *Pf*LAP whilst having much lesser effects on its human homolog. With the use of available targeting techniques, the present study shows the potential use of nanotechnology based approaches as "silver bullets" that can target *Pf*LAP without adversely affecting the host. However further research needs to be conducted to better understand the mechanisms of AgNP action, drug targeting and the health and safety issues associated with nanotechnology use.

Acknowledgements

Firstly I would like to thank the Lord for giving me the guidance, strength and ability which helped me see this project to completion. Secondly I want to express my deepest appreciation and gratitude to my supervisor, Professor Chris G. Whiteley whose unwavering encouragement and financial support gave me belief especially when things seemed hopeless. To my co-supervisor, Dr Jacqui van Marwijk, this project would have been impossible without you. Your guidance, patience and support were simply amazing to say the least and I can never thank you enough. To Dr Brendan Wilhelmi, my co-supervisor, your unwavering encouragement and support made life much easier and it was surely an honour to work under your guidance.

My sincere gratitude also goes out to family and friends, Mr R. Mnkandhla, Michael Cobb, J.J Mtupa, Victor Moyo, David Simba, Harold Moyo, Nichollas Nyoni, my brother Raphael Mnkandhla, Heidi Mnkandhla, my brother Ndumiso Mkandla and last but not least Nondumiso Fengu, my best friend. The role you all played in helping me accomplish this goal is priceless.
I would also like to extend gratitude to my lab mates for their help and advice, Jason Sterrenberg for assistance with westerns, everyone in the department of Biochemistry, Microbiology and Biotechnology for your kindness and assistance. I would also like to thank the National Research Foundation for the funding they availed for the completion of this project and Rhodes University for granting me the opportunity to use their resources and facilities.

I dedicate this thesis to the memory of my mother Ellen.

Table of Contents

List of abbreviations

Å	Angstrom
A_{280}	Absorbance at 280 nm
AgNPs	Silver nanoparticles
BCA	Bicinchoninic acid
BLAST	Basic Local Alignment Search Tool
BSA	Bovine serum albumin
cDNA	complementary DNA
cm	Centimeter
ddH_2O	Double distilled water
DDT	Dichloro-diphenyl-trichloromethane
DMSO	Dimethysulfoxide
DNA	Deoxyribonucleic acid
EDTA	Ethylenediaminetetraacetic acid
FPLC	Fast protein liquid chromatography
GDP	Gross domestic product
GNI	Gross national income
GNP	Gold nanoparticles
g	Gram
$g.l^{-1}$	Gram per liter
HIV	Human immunodeficiency virus
*Hs*LAP	*Homo sapiens* leucine aminopeptidase
IDA	Iminodiacetic acid
IDT	Integrated DNA technologies
IMAC	Immobilized metal affinity chromatography
kb	Kilo base pair
k_{cat}	Turnover number
k_{cat} / K_m	Catalytic efficiency

kDa	Kilo Dalton
K_m	Michaelis constant
LAP	Leucine aminopeptidase
LB	Luria-Bertani
L*p*NA	Leucine-*p*-nitroanilide
MCS	Multiple cloning site
µg	Microgram
$\mu g.ml^{-1}$	Microgram per milliliter
µl	Microliter
µm	Micrometer
µM	Micromolar
$\mu M.ml^{-1}$	Micromolar per milliliter
mA	Milliamps
M	Molar
mg	Milligram
$mg.ml^{-1}$	Milligram per milliliter
MHz	Megahertz
ml	Milliliter
$ml.min^{-1}$	Milliliter per minute
mm	Millimeter
mM	Millimolar
mRNA	messenger RNA
NCBI	National Center for Biotechnology Information
ng	Nanogram
$ng.\mu l^{-1}$	Nanogram per microliter
nm	Nanometer
NTA	Nitroloacetic acid
*Pf*M1, *Pf*AAP	*Plasmodium falciparum* alanine aminopeptidase
*Pf*M17, *Pf*LAP	*Plasmodium falciparum* leucine aminopeptidase
PCR	Polymerase chain reaction
PVP	Polyvinylpyrrolidone

RFLP	Restriction fragment length polymorphism
RNA	Ribonucleic acid
ROS	Reactive oxygen species
rpm	Revolutions per minute
SDS-PAGE	Sodium dodecyl sulphate polyacrylamide gel electrophoresis
SEC	Size exclusion chromatography
TED	Tris(carboxymethyl)ethylenediamine
TEM	Transmission electron microscope
T_m	Melting temperature
U	Units
UV	Ultraviolet
UV/Vis	Ultraviolet /visible
V	Volts
V_{max}	Maximum velocity
v/v	Volume per volume
W	Watt
WHO	World Health Organisation
w/v	Weight per volume
×	Times
×g	Times gravity

List of Figures

List of Tables

Chapter 1: Literature review

1.1. Introduction

Various infectious diseases have been known to mankind for generations and though some have been partially or totally eliminated from the planet, most still exist to this day. The Oxford dictionary of epidemiology (1988) describes an infectious disease as "an illness caused by a specific infectious agent or its toxic product that results from transmission of that agent or its products from an infected person, animal or reservoir to a susceptible host, either directly or indirectly through an intermediate plant or animal host, vector or inanimate environment". Some pathogens have evolved and developed drug resistance and outbreaks of new strains continue to threaten the health of the world population. The explosive characteristics and the unpredictability of epidemics are a cause of fear, insecurity and panic even today, as could be seen during the SARS epidemic in 2003 (Dwosh *et al*., 2003).

The above factors have kept the medical research world on its toes in efforts to curb the spread and the effects of infectious diseases worldwide. Advances in microbiology during the 19th century, particularly the works of Koch and Pasteur, confirmed the role of live microscopic agents as an immediate, fundamental cause of a wide range of illnesses (Rosen, 1958). These findings provoked profound changes in the understanding of the causes of infectious diseases and the consequent strategies for their prevention. The epidemiology of most diseases, whether infectious or non-infectious, is influenced by factors such as economic, climatic, evolutionary, social and cultural. These factors have restricted certain diseases or infections such as malaria to certain parts of the world where their impact is most severe and their control most challenging (Gething *et al.*, 2011).

1.2. Human malaria

Malaria is a widespread disease caused by parasites called *Plasmodia* and it falls under the category of infectious diseases (McGowan *et al*., 2010). By the year 1999, the world health organisation (WHO) reported that malaria was the fifth highest cause of death worldwide. In Africa the figures are staggering, mostly as a result of poverty (Teklehaimanot and Mejia, 2008).

The distribution of malaria as it stands today is, in part, a result of control measures taken during the 20th century which confined malaria to certain parts of the world (Hay *et al*., 2004). Areas such as Europe and North America once had widespread malaria which declined remarkably as the economies of these areas became well established. Stable economies made it possible to restrict the spread of malaria as resources for public health improvement became available. As a consequence malaria was eradicated in the United States between 1947 and 1951 (Zucker, 1996).

The eradication of malaria in countries such as the USA provided a blueprint which was to be followed in achieving similar results worldwide. WHO pioneered the global malaria eradication programme in 1955 (WHO, 1957). The programme depended on chloroquine and dichloro-diphenyl-trichloroethane (DDT) which helped with treatment and vector control, respectively (Greenwood *et al*., 2008). However there was very little success with the programme as international commitment to its fulfilment gradually ceased being a priority. It is highly likely that since the affluent regions of the world had succeeded in their fight against malaria, they felt the need to address other important issues in their own countries thereby leaving the poor countries at the mercy of malaria. To aggravate the situation, there was an emergence of chloroquine-resistant *Plasmodium* parasites and DDT-resistant *Anopheles* mosquitoes which made eradication of malaria almost impossible. This meant more resources had to be channelled into finding new solutions but with loss of political will and commitment this was not to be.

The goal of the global elimination of malaria was officially deserted in 1972, the same year DDT was banned. Malaria remains an important disease in the tropical regions of the world to this day, despite a revival of global interest to eradicate it (WHO, 2012). There has been vast research in order to understand the biology of the malaria parasites over the years. This has helped in elucidating various biological mechanisms and subsequently the chemotherapeutic targets of the malaria parasites. To date there have been a number of drugs that have been discovered and used in the fight against malaria as a result of continuous research efforts (Olliaro and Yuthavong, 1999; Rosenthal, 2003; Gelb *et al*., 2007).

1.2.1. The epidemiology of malaria

The epidemiology and clinical manifestation of malaria varies widely in different parts of the world. This variability is a consequence of a number of factors which include; (i) the species of malaria parasite prevalent in a given area, (ii) the efficacy of available chemotherapeutics against a particular malaria parasite, (iii) the occurrence and distribution of *Anopheles* mosquitoes in a given area, (iv) climate and other environmental conditions. Malaria is mainly prevalent in tropical and subtropical regions of sub-Saharan Africa, Central and South America, the Caribbean island of Hispaniola, the Middle East, the Indian subcontinent, South-East Asia and Oceania (figure 1.1) (Bell *et al*., 2006).

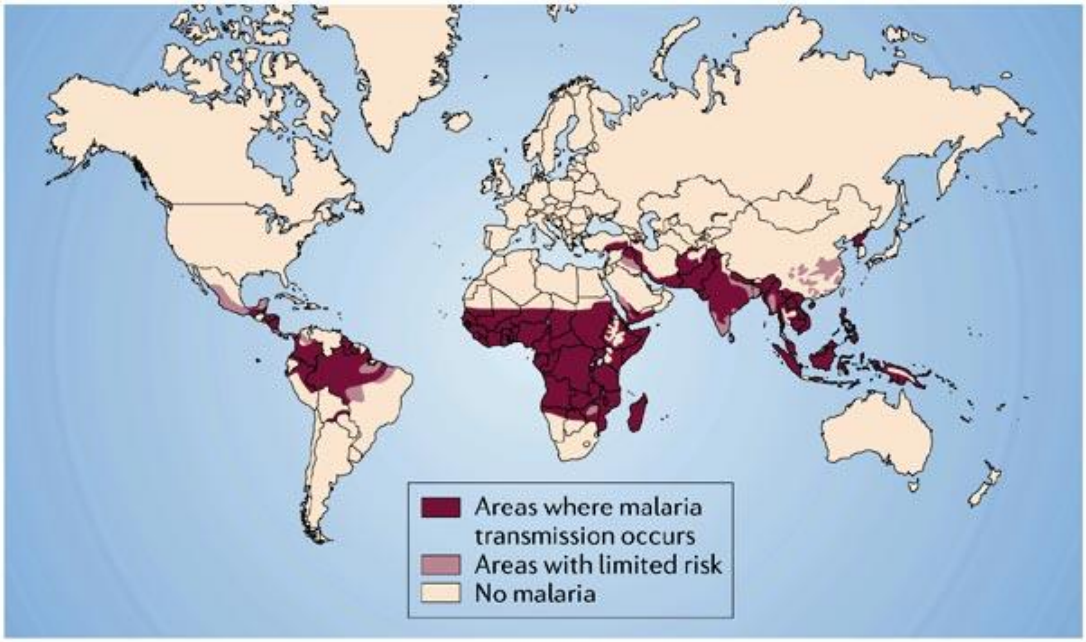

Figure 1.1 World map showing the global distribution of malaria (taken from Bell *et al*., 2006).

According to WHO (2012), there were an estimated 219 million cases of malaria and 660 000 deaths in 2010. Malaria remains prevalent in 104 countries of the tropical and semi-tropical world, with 35 countries in central Africa bearing the highest burden of cases and deaths (WHO, 2012). An estimated 74 % of the African population live in areas of high malaria transmission rates. The most susceptible population group in Africa are children. Kager (2002) estimated that 5 % of the children in Africa are highly likely to not reach 5 years of age and this accounts for a quarter of child mortality rates in Africa.

Hay and co-workers (2004) estimated that 48 % of the global population remains exposed to the risk of malaria despite attempts to eradicate it earlier in the 20th century. The spread of malaria has been exacerbated by the movement or migration of various populations as a result of wars, droughts, tourism or unfavourable socio-economic conditions (Nchinda, 1998). Due to these factors, malaria has re-emerged in areas where it once had been eradicated. Furthermore, the movement of people across borders and regions has made it possible to introduce drug resistant strains of malaria parasites to areas where the disease had been eliminated or was being adequately managed (Nchinda, 1998).

1.2.2. Malaria and poverty

The global distribution of malaria as stated in section 1.2.1 is known to be influenced by a variety of factors, most of which are natural; climatic conditions, ecology, vector distribution and parasite strain. A classic example is the African continent which is home to *Anopheles gambiae,* the most efficient malaria vector and *P. falciparum*, the most virulent of the malaria parasites. The distribution of malaria has also been observed to coincide with widespread poverty in the concerned areas (Teklehaimanot and Mejia, 2008). To reinforce this notion, the richest African countries, located in the northern and southern extremes, are also free of malaria. Other examples of poor and malarious countries include India, where the largest number of poor people per country live, and Haiti, the poorest country in the western hemisphere (Gallup and Sachs, 2001).

The global distribution of per-capita gross domestic product (GDP) shows an excellent correlation between malaria incidence and poverty, and malaria-endemic countries also have lower rates of economic growth. Malaria hinders economic growth and development in various ways which include loss of expertise through deaths, low productivity due to sick leave, poor saving by families, high fertility and high medical expenditures (Sachs and Malaney, 2002). A comparison of income in malarious and non-malarious countries indicates that average gross national income (GNI) per capita in malarious countries in 2007 was between USD900 or less and USD3 700, compared with USD11 500 in countries without intensive malaria (fig. 1.2), more than a tenfold difference in most cases (Barkan, 2011). The malaria and poverty situation is synonymous with the chicken and egg situation where it is not clear what causes the other.

Teklehaimanot and Mejia, (2008), suggest that causality runs in both ways, whereby the transmission and spread of malaria is boosted by poverty and in turn malaria impedes economic growth.

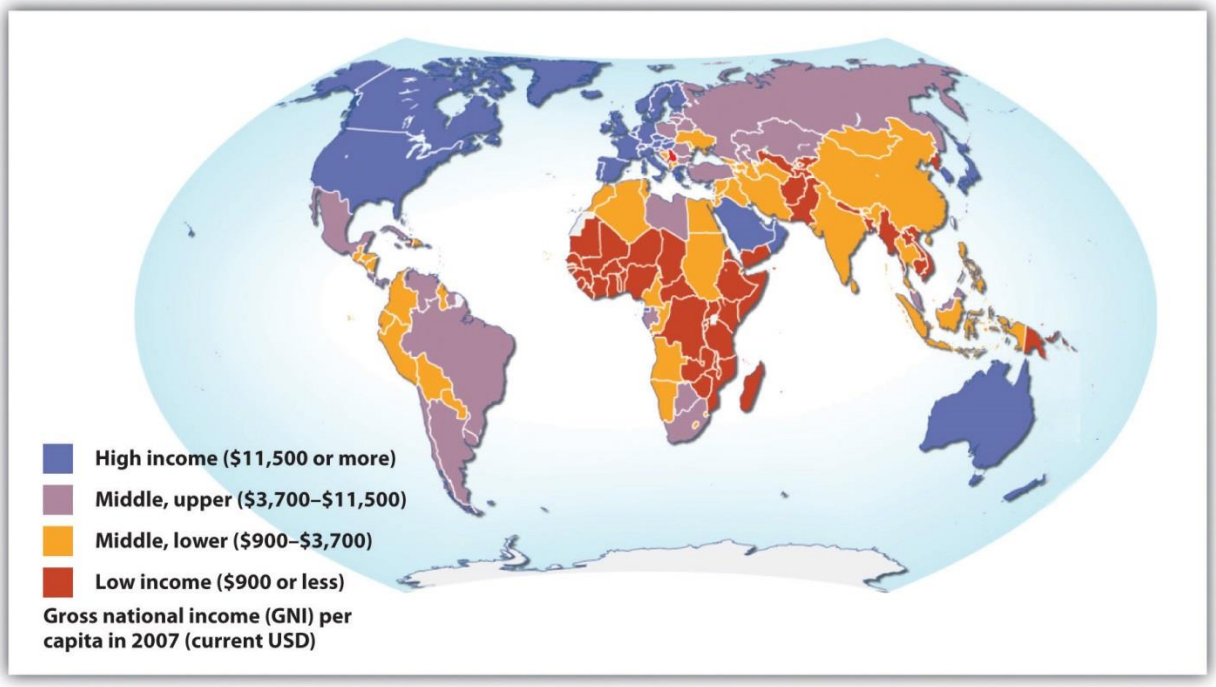

Figure 1.2 Global stratification map showing GNI per capita in 2007 (taken from Barkan, 2011).

As previously stated, malaria once existed in the affluent regions of the world and due to the availability of resources, it was eliminated. It may follow that given the same state of economic development as observed in the wealthy regions; the poor regions may succeed in the fight against malaria. Malaria incidence and deaths have dropped in the past decade owing to increased contributions to the global malaria fund (WHO, 2012). This shows that elimination of poverty and the subsequent availability of resources may be the answer to the fight against malaria.

1.2.3. The economic and social burden of malaria

Malaria has numerous economic and social burdens it presents to households and consequently at national level. Apart from the direct medical costs such as personal expenditures on prevention, diagnosis, treatment and care that families incur as a result of malaria, there are

behavioral changes which households implement in response to malaria which can result in various social costs (Sachs and Malaney, 2002). With high child and infant mortality rates, Yamada (1984) reported that malaria has been linked to high fertility rates. This is most likely an attempt by households to replace those children lost due to malaria.

Sachs and Mallaney (2002) have presented a hypothesis which they called the 'child-survivor' hypothesis whereby family planning in households is strongly influenced by the number of children that are likely to make it to adulthood. As a result parents may plan to have more children than necessary in order to increase their chances of getting their desired number to adulthood. This raises the demand of material resources and time needed to raise children. High child and infant mortality rates also mean that a great deal of resources is fruitlessly spent on raising those children that do not make it to adulthood. There are also social burdens associated with malaria as those that die leave behind grieving relatives who have to deal with emotional pain which may affect their performance at work or school. In cases where school children are infected with malaria, significant amounts of time are taken off school and this adversely affecting their education.

There are also costs that arise in response to malaria that are incurred at national level. Governments in malarious areas have expenditures on programs such as vector control, health facilities, education and research which are directed at combating the disease. Foreign investment and trade are affected as companies have reservations with investing in businesses in malaria infested areas due to health risks posed by these areas to employees. Tourism to these areas is most likely affected and great losses in income can be registered as a result. Economic growth in malaria endemic countries is very slow compared to non-malarious areas and economies that have overcome the malaria burden have shown remarkable growth afterwards (Gallup and Sachs, 2000).

1.2.4. *Plasmodium* parasites and malaria

The *Plasmodium* genus is a subset of the phylum Apicomplexa and it comprises of various species that are known to be parasites to different kinds of organisms (Dronamraju, 2006).

Human malaria is commonly known to result from infection with any of four *Plasmodium* species, namely *P. falciparum, P. vivax, P. ovale, and P. malariae. P. knowlesi,* though not a very common cause of malaria, has recently been making its presence and potency felt especially in the South East Asia region (White, 2007; Cox-Singh *et al*., 2010). The most common four parasites will be discussed further. *Plasmodium* resides in two different hosts during its life cycle; vertebrates being the intermediate hosts, and invertebrates being the final host. Invertebrates are also vectors of the parasites and they transmit the malaria parasites through their parasitism towards vertebrates. A great deal of the *Plasmodia* life cycle is spent inside the blood cells of vertebrates while the remaining time is spent in the invertebrates. With the exception of sand flies which spread *Plasmodium* parasites to reptiles, the typical invertebrate vectors feed on vertebrate blood such as mosquitoes (Kimsey, 1992).

1.2.4.1.P. falciparum

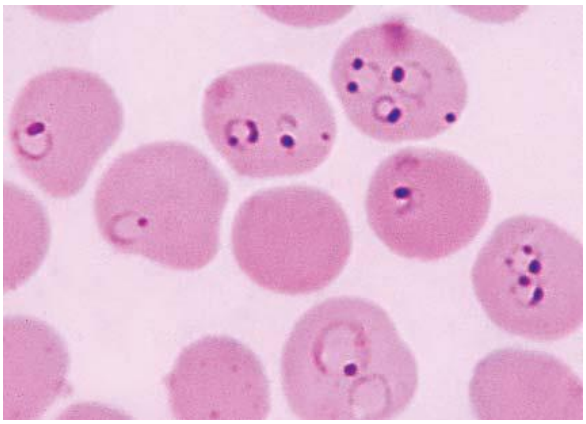

Figure 1.3 *P. falciparum* inside red blood cells. Multiple infections of a single red blood cell are common. Parasites can be seen as dark spots inside red blood cells. (taken from Pennisi, 2002).

P. falciparum (fig. 1.3) is the most virulent species of the malaria parasites (table 1.1) accounting for nearly 85 % of the total deaths. It accounts for an excess of three quarters of all malaria cases in Africa. The Sub-Sahara region has the highest prevalence. *P. falciparum* malaria does not relapse; this means the life cycle of the parasite does not include the formation of any dormant forms which may re-infect the red blood cells when the active parasites have been cleared by the host immune response or chemotherapeutic agents (Despommier *et al.*, 2000). *P. falciparum* is the only malaria parasite currently known to affect the brain and cause cerebral malaria. Cerebral

malaria is one of the attributes of *P. falciparum* that makes it the most fatal of the five known malaria pathogens. Amongst the malaria parasites, *P. falciparum* has exhibited the worst resistance to chemotherapeutic agents such as chloroquine, and now threatens to be resistant to the artemisinin therapeutics currently available (Bloland, 2001; Phyo *et al*., 2012).

Table 1.1 Different types of malaria, severity and duration (taken from Wiser, 2011).

	vivax	***ovale***	***malariae***	***falciparum***
Incubation Period (days)*	8-27	8-27	16->40	6-25
Severity of Initial Paroxysms	moderate to severe	mild	mild to moderate	severe
Average Parasitemia (per mm^3)	20,000	9,000	6,000	50,000-500,000
Maximum Parasitemia (per mm^3)	50,000	30,000	20,000	2,500,000
Typical Symptom Duration (untreated)	3-8 weeks	2-3 weeks	3-24 weeks	2-3 weeks
Maximum Infection Duration (untreated)	5-8 years**	12-20 months**	20-50 years	6-17 months
Anemia	++	+	++	++++
Other Complications			renal	cerebral***

* Incubation period defined as time from sporozoites infection until appearance of symptoms.
** Includes relapses due to 'hypnozoite' stage in the liver.
***Many other organs in addition to the brain are also affected in severe malaria.

1.2.4.2.P. vivax

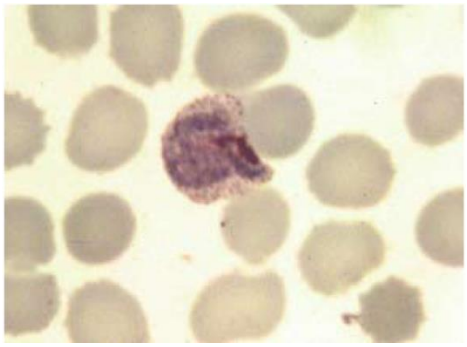

Figure 1.4 A trophozoite stage *P. vivax*. The parasite can be observed in the enlarged erythrocyte (taken from Despommier *et al*., 2000).

P. vivax (figure 1.4) may not be the most lethal malaria parasite but lends itself as the most geographically widespread malaria causing specie (Kim *et al*., 2010). Red blood cells infected with *P. vivax* are visibly larger than the uninfected cells (figure 1.4). Mendis *et al*. (2001) estimated *P. vivax* to account for 70–80 million clinical cases across much of Asia, Central and South America, the Middle East and parts of Africa. Unlike *falciparum* malaria which is very rife in the Sub-Saharan Africa, *P. vivax* malaria transmission is seldom reported in this region and in West Africa. This phenomenon is attributed to two factors; the prevalence of *P. falciparum* in Sub-Saharan Africa and the widespread presence of the Duffy negative trait in native West Africans (Miller *et al.,* 1976). The Duffy negative trait is a hereditary erythrocyte phenotype that does not possess the receptor to which *P. vivax* binds in order to gain access to the erythrocyte (Mendis *et al.,* 2001). *P. vivax* is known to relapse and the parasites can linger in the host for up to five years resulting in repeated malaria attacks on individuals that would have been previously cured (Despommier *et al.,* 2000).

1.2.4.3.P. malariae

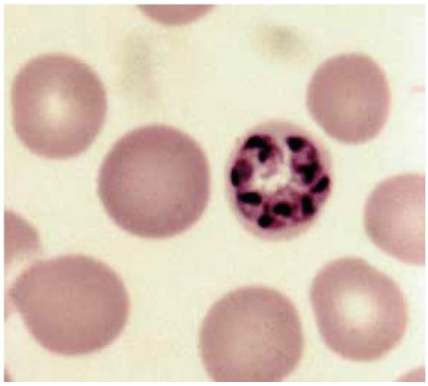

Figure 1.5 A schizont of *P. malariae* within a red blood cell. The size and shape of the infected cell remains the same (taken from Despommier *et al*., 2000).

P. malariae (figure 1.5) and *P. falciparum* are known to share the same geographical locations of prevalence (Mendis *et al.,* 2001). In Sub-Saharan Africa this has resulted in situations where *P. malariae* infections are mistaken for *P. falciparum* infections. *P. malariae* has the lowest average parasitemia of the four parasites (table 1.1) and its infections are not so easy to detect resulting in the need for polymerase chain reaction (PCR) techniques in numerous instances. Present knowledge of *P. malariae* suggests that it does not relapse and infected erythrocytes maintain the

same size and shape as the healthy ones (Collins and Jeffery, 2007). Parasite distribution is wide spread throughout Sub-Saharan Africa, South East Asia, Indonesia, and the Western Pacific (Collins and Jeffery, 2007).

1.2.4.4.P. ovale

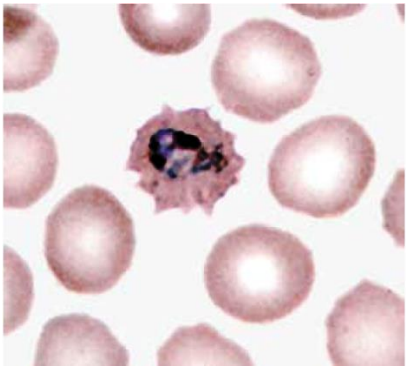

Figure 1.6 *P. ovale* trophozoite infected red blood cell. The deformed shape of the red blood cell is a result of infection (taken from Despommier *et al*., 2000).

P. ovale (figure 1.6) infections have very low parasitemia when compared to *P. falciparum* and *P. vivax* (table 1.1) and as a result their detection and diagnosis is difficult. These infections are known to cause illness but seldom result in death. It is for these reasons that *P. ovale* malaria is rarely researched and as documented as the other malarias. The parasite exists in dimorphic variants (*Plasmodium ovale curtisi* and *Plasmodium ovale wallikeri*) which are widely distributed in the tropics (Sutherland *et al*., 2010). *P. ovale* infections share a similarity with *P. vivax* infections in that they are also known to linger in the liver and cause a relapse of the disease (Despommier *et al*., 2000). Infected erythrocytes can be easily identified under the microscope as they lose their characteristic shape (figure 1.6).

1.2.5. The pathology of malaria

The life cycle of the malaria parasites occurs in both the human and the mosquito hosts as shown in figure 1.7. Malaria infections are initiated when an infected mosquito injects sporozoites into the human bloodstream during a blood meal. Sporozoites are transported to the liver through circulation and here they advance into pre- and exo-erythrocytic forms.

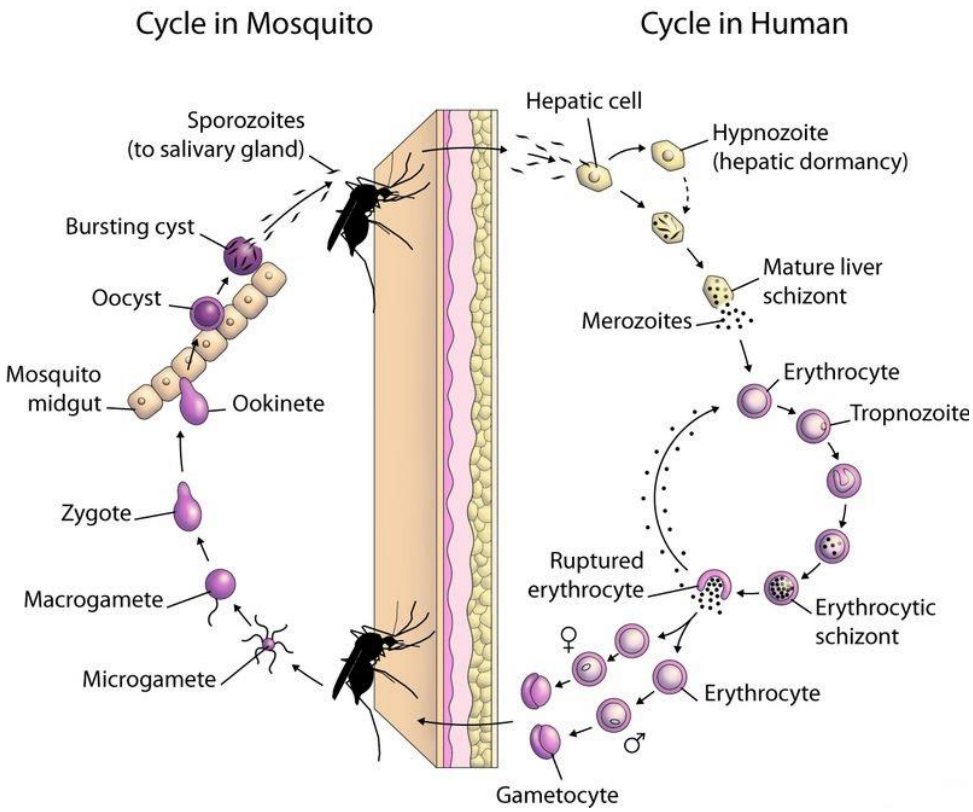

Figure 1.7 *Plasmodium spp*. life cycle. The life of the parasite in the mosquito and the human host are shown (taken from Malwest, 2012).

It is most probable that the sporozoites possess mechanisms to escape the immune system of the human; otherwise it is unlikely that they would survive the blood environment to reach the hepatocytes. Pre- and exo-erythrocytic forms of the parasite are not known to elicit an immune response prior to maturity. A process known as exo-erythrocytic schizogony, a form of asexual reproduction, occurs in the hepatocytes and produces exo-erythrocytic schizonts. Exo-erythrocytic schizonts are composite forms of the parasite with each containing nearly 30 000 merozoites which are released back into circulation (Thivierge *et al*., 2012). A fraction of the pre- and exo-erythrocytic forms of *P. vivax* and *P. ovale* go into dormancy instead of asexual reproduction. It is these dormant liver stage parasites that reside in the liver for periods of up to five years that are responsible for relapses of the disease.

Merozoites invade the erythrocytes and grow into larger "ring" forms, also known as trophozoites. The parasite utilizes the nutrients in the red blood cell in order to grow, and also facilitates the uptake of nutrients from the blood plasma. Haemoglobin is the principal molecule which is digested by the parasite within the erythrocyte to obtain nutrients and to maintain an osmotic balance within the erythrocytes (Florens *et al*., 2002). Nuclear division without cell division results in a parasite form known as a schizont and this marks the end of the feeding phase of the parasite. The schizont is able to yield merozoites through budding and this happens prior to the rupture of the erythrocyte to re-initiate the cycle. This blood stage is responsible for the pathology associated with malaria. The irregular fever paroxyms are a result of the rupture of the infected erythrocytes. The increased virulence of *P. falciparum* is due in part to the higher levels of parasitemia associated with *P. falciparum* infections (table 1.1) (Wiser, 2011).

The exo-erythrocytic forms of the parasite can differentiate into sexual forms known as macro- or micro-gametocytes. Gametocytes are mononucleic forms of the parasite and they grow to fill up the whole erythrocyte. When ingested by the *Anopheles* mosquito vector during a blood meal, the gametocyte is released from the erythrocyte and gametogenesis is triggered. In the mosquito, gametogenesis is induced by a temperature drop, a rise in CO_2 levels and changes in pH (WHO, 1987; Wiser, 2011). Microgametes, formed by a process known as exflagellation, are flagellated forms which will fertilize the macrogamete leading to a zygote. The zygote develops into a motile ookinete which penetrates the mosquito gut epithelial cells and develops into an oocyst. The oocyst undergoes multiple rounds of asexual replication resulting in the production of sporozoites. Rupture of the mature oocyst releases the sporozoites into the hemocoel of the mosquito. The sporozoites migrate to and invade the salivary glands, thus completing the life cycle (Wiser, 2011).

1.2.6. Early malaria control measures

The first documented malaria chemotherapeutic was a cinchona bark tree extract known as quinine. Quinine was in use as early as 1632 (Baird, 1996) until the production of more chemotherapeutics in the 20th century. Primaquine and quinacrine were produced after the First World War and chloroquine followed shortly thereafter in 1934 (Thompson and Werbel, 1972; Slater, 1993). By the middle of the 20th century chloroquine was the first choice remedy against

malaria (Coatney, 1963). Chloroquine discovery and use marked one of the most significant milestones in the history of the fight against infectious diseases. As mentioned in section 1.2, chloroquine alongside the pesticide DDT was responsible in for the eradication of malaria in various parts of the world. The efficacy and use of chloroquine lasted for 11 years before the development of resistance to the drug by some *Plasmodium* parasites especially *P. falciparum* (Wellems, 2002; Dondorp *et al*., 2010). To worsen the situation, the fight against *Anopheles gambiae* mosquitoes was lost as they became resistant to DDT. DDT was finally banned for ecological reasons.

1.2.7. Recent and current malaria control measures

With chloroquine and DDT having lost their efficacy in most parts of the world, new approaches to combat malaria had to be devised. One of the most effective approaches was the modification of existing drugs into analogues which proved potent even towards strains that were resistant to the parent drug. Examples included 4-aminoquinolines which are derivatives of chloroquine, and tafenoquine, a derivative of primaquine (Rosenthal, 2003). As research unveiled potential drug targets for malaria, new drugs were developed. These consisted of antifolates and artemisinins which have been used as combined therapies to effectively treat malaria (Olliaro and Yuthavong, 1999). Artemisinins are currently the last line of defense against malaria and some resistance towards them has been reported (Phyo *et al*., 2012).

With the malaria eradication programme having failed to achieve its goals, WHO embarked on a new project in 1998 called ‘Roll Back Malaria’. This was to coordinate a global fight against malaria and rally as much international support as possible (Hay, 2004). The aim was to reduce the risks and effects of malaria by 50 % by the year 2010. The control strategy of this program was aimed at preventing death, reducing illness and decreasing social and economic loss; not at eradication. Available tools were drugs, bed nets, especially insecticide- treated nets, insecticides and other measures aimed at the vector, and health education. However for a drastic reduction of the problem, let alone its resolution, new drugs and vaccines are needed.

1.2.8. Drug resistance

A major problem in the fight against malaria has been the emergence of drug resistant strains of the *plasmodium* parasites. According to WHO (2001), antimalarial drug resistance is the "ability of a parasite strain to survive and/or multiply despite the administration and absorption of a drug given in doses equal to or higher than those usually recommended but within tolerance of the subject". Resistance to antimalarial drugs has been described for two out of the four species that are known to affect humans, namely *P. falciparum* and *P. vivax. P. falciparum* drug resistance has been described against almost all antimalarial drugs currently in use. However resistance to any single drug is usually restricted to certain areas of the world and its distribution varies (Bloland, 2001; Phyo *et al*., 2012).

The general cause of resistance has been attributed to spontaneous mutations that confer reduced sensitivity to a given drug or class of drugs. Factors that have been associated with antimalarial drug resistance include human behavior, vector and parasite biology, pharmacokinetics and economics (Bloland, 2001). Programs which emphasize the use of one drug such as the malaria eradication programme exert a lot of pressure on the drug and increase the probability of the development of resistance.

1.2.9. Potential chemotherapeutic targets for malaria therapy

The life cycle of *Plasmodium* is complex and requires specialized protein expression for life in both invertebrate and vertebrate host environments (figure 1.7), for intracellular and extracellular survival, for invasion of multiple cell types and for evasion of host immune responses. In order to discover compounds that will be effective against malaria parasites it is essential to investigate the most critical metabolic pathways and to exploit the resulting knowledge for generating the appropriate compounds. Sequencing and annotation of the *P. falciparum* genome was completed in 2002 and offered the promise of identifying new and effective drug and vaccine targets (Gardner *et al*., 2002). A sufficiently good chemotherapeutic target for malaria would have to be a vital part of the parasite life cycle while differing from the corresponding process in the host. The parasite must also not have alternative routes of achieving the same goal as the target process.

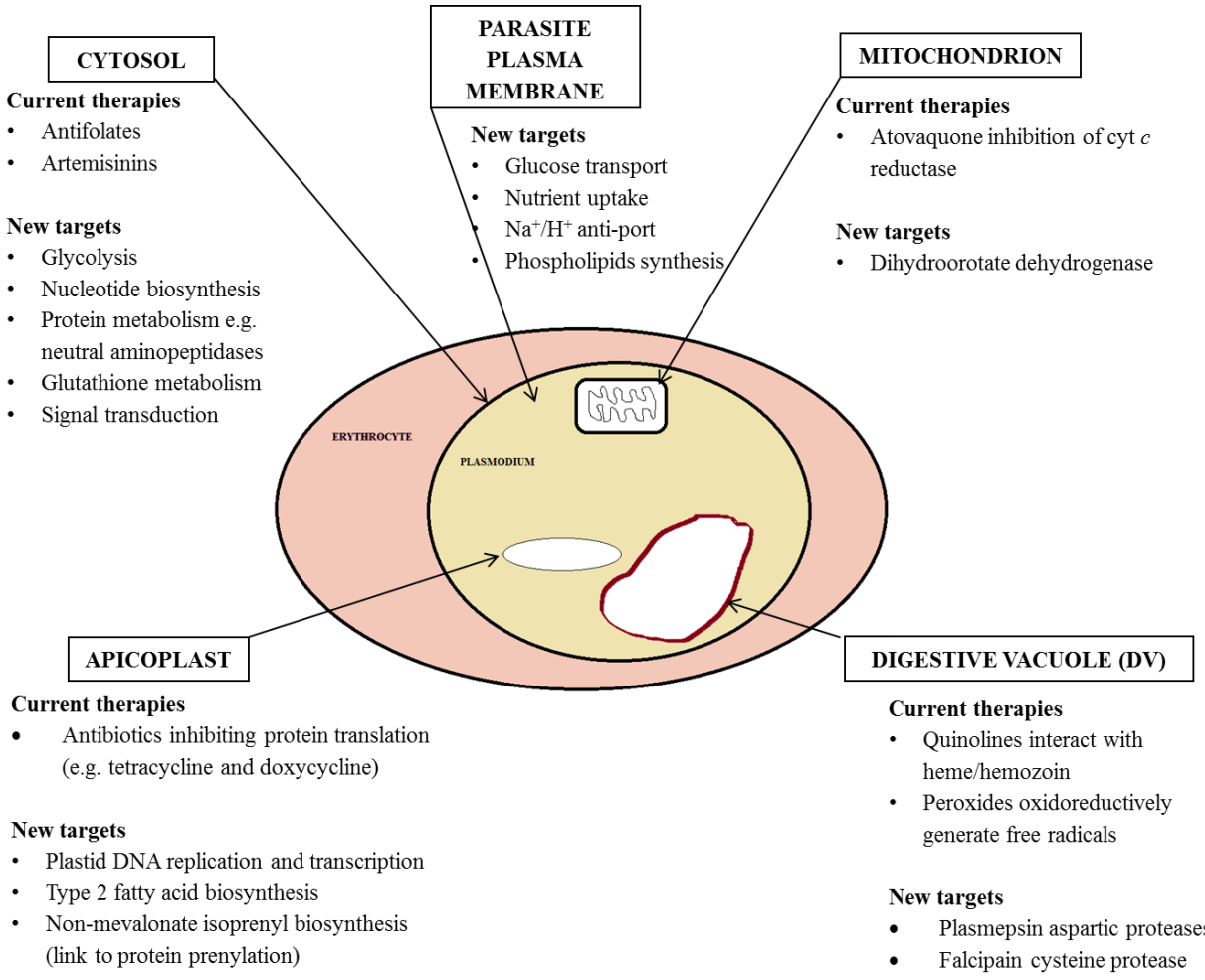

Figure 1.8 Schematic presentation of chemotherapeutic targets in plasmodia showing processes which can be targeted in different organelles/compartments of the parasite (adapted from Fidock *et al.*, 2004).

The target must be involved in a rate limiting biochemical process and finally have low chances of developing resistance (Olliaro and Yuthavong, 1999). There are several chemotherapeutic targets for malaria therapy that have been described and these are shown on figure 1.8 alongside the existing drug action targets. The current targets are found in the cytosol, mitochondrion, apicoplast, plasma membrane and the digestive vacuole of the parasite. As illustrated in figure 1.8, most of the research towards establishing putative targets for the treatment of malaria focuses on the erythrocytic stage of the parasite life cycle. This is because it is the stage associated with the typical clinical symptoms of malaria as stated in section 1.2.5. One such target is the neutral aminopeptidases which are found in the cytosol of the parasite (figure 1.8).

As stated in section 1.2.5, the digestion of haemoglobin is a pivotal process in supplying the parasite with vital amino acids which it uses for its own protein synthesis (Skinner-Adams *et al*., 2009). Neutral aminopeptidases are involved in the final stages of haemoglobin digestion thereby supplying free amino acids which the parasite uses for its own growth. Indeed the inhibition of neutral aminopeptidases during the trophozoite stage is lethal to the parasites (Gardiner *et al*., 2005). Bestatin is a dipeptide originally isolated from filtrates of *Streptomyces olivoretticuli* and inhibits aminopeptidases (Umezawa *et al*., 1976). In light of the importance of neutral aminopeptidases in the survival and proliferation of malaria parasites, the present study focuses on one of these enzymes, leucine aminopeptidase (LAP).

1.3. Aminopeptidases

1.3.1. Classification

Aminopeptidases are a class of enzymes that catalyse the successive cleavage of amino acids from the N-termini of proteins. They play a regulatory role between the break down and the building of proteins in biological systems (Gavigan, 2001). Aminopeptidases are found in a wide range of organisms and inside cells they are usually in subcellular organelles in the cytosol and as part of the cell membrane. Aminopeptidases are classified according to five different criteria, namely (i) the number of amino acids cleaved from the N-terminus of substrates (ii) optimum pH, (iii) the metal ion content, (iv) the location within the cell and (v) susceptibility to inhibition by bestatin (Taylor, 1993).

1.3.2. Mammalian aminopeptidases

In humans, aminopeptidases are usually zinc-metalloenzymes and they are generally found in body fluids (Rawlings and Barret, 1993) and are thought to be involved in the metabolism of proteins and various peptide hormones (Sanderink *et al*., 1988). Bovine lens LAP (Allen *et al*., 1983; Burley *et al*., 1991) and porcine kidney LAP (Spackman *et al*., 1955) are some of the most widely researched aminopeptidases in mammals. In humans, the placental (Matsumoto *et al*., 2000), kidney (Mantle, 1989) and liver LAPs (Kohno *et al*., 1985) and several skeletal muscle aminopeptidases have been purified and described. Human aminopeptidases often have large and overlapping specificities and this has led to confusion regarding their identification. Rawlings

and Barret (1993) described the evolutionary classification of peptidases and metallopeptidases. They are divided into 25 families with the M1 and M17 (M standing for metallopeptidase) LAPs being in the metallopeptidase category. In mammals, the M1 and M17 enzymes with LAP activity are involved in antigen presentation, processing of bioactive peptides (oxytocin, vasopressin, enkephalins), and vesicle trafficking to the plasma membrane (Matsui *et al*., 2006).

1.3.3. Malarial aminopeptidases

According to present knowledge the 26 Mb *P. falciparum* genome houses eight aminopeptidases (Stack *et al*., 2007). Some of these aminopeptidases comprise of a post-prolyl aminopeptidase that is located in the digestive vacuole, an aspartic aminopeptidase and a prolyl aminopeptidase located in the cytoplasm (Thivierge *et al*., 2012). Research over the years has, and is still revealing the importance of aminopeptidases in parasites from the protozoan kingdom as chemotherapeutic targets and vaccine candidates in infectious diseases (Jia *et al*., 2009). In addition, malaria parasites express two neutral aminopeptidases, a 122 kDa M1-family alanine aminopeptidase and a 67.8 kDa M17-family leucine aminopeptidase, sometimes termed *Pf*M1AAP and *Pf*M17LAP, respectively. Both have the ability to efficiently cleave N-terminal amino acids from peptide substrates. However as their names suggest, these enzymes have specificities that differ dramatically. *Pf*AAP exhibits far broader substrate specificity than *Pf*LAP and rapidly hydrolyses substrates containing alanine, leucine, arginine and lysine, but can also cleave substrates containing phenylalanine, tyrosine, serine and asparagine (McGowan *et al*., 2009). In contrast, *Pf*LAP possesses a severely restricted specificity for N terminally exposed leucine while alanine substrates are cleaved relatively poorly (Martin and Kirk, 2007).

These two neutral aminopeptidases are believed to be involved in the terminal stages of haemoglobin digestion (figure 1.9), thereby releasing free amino acids into the parasite cytosol (Poreba *et al*., 2012). During the erythrocytic stages of the growth of malaria parasites, as much as 65-75 % of erythrocyte haemoglobin is digested and used for parasite anabolism (Skinner-Adams *et al*., 2009). Malaria aminopeptidases are important in the generation and regulation of free amino acids that are used in protein anabolism, maintaining an osmotically stable environment and creating a gradient by which amino acids that are rare or not present in haemoglobin are drawn into the parasite from the host serum (Gardiner *et al*., 2006). Other

enzymes involved in the digestion of haemoglobin in the food vacuole have been investigated as targets for malaria therapy and have been found to have redundant functions.

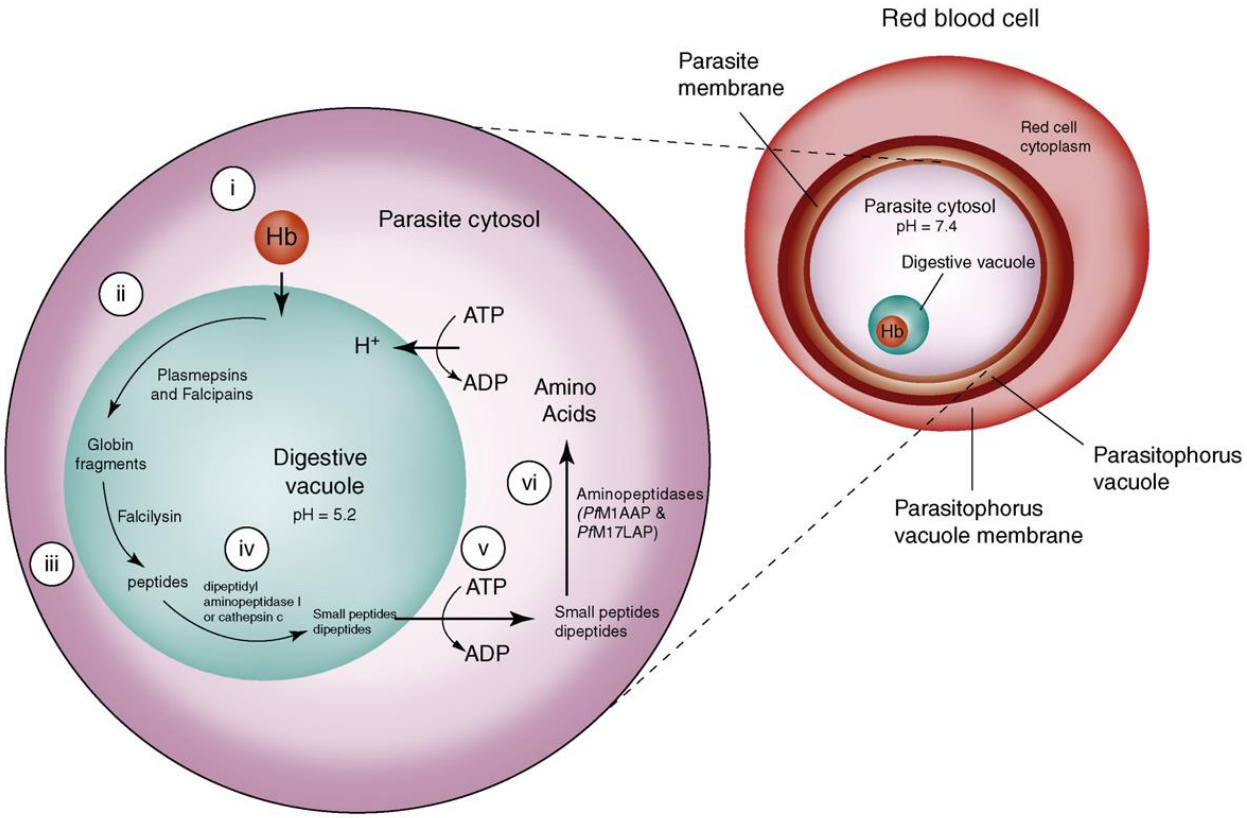

Figure 1.9 An overview of haemoglobin digestion in the malaria parasite *P. falciparum*. (i) transportation into the digestive vacuole, (ii) endopeptidase activity, (iii) metallo-protease activity, (iv) exopeptidases' activity, (v) transportation out of the digestive vacuole and finally (vi) neutral exopeptidases' activity (taken from Skinner-Adams *et al.*, 2009).

This means a good drug which targets haemoglobin digestion in the food vacuole would need to target more than one enzyme as other enzymes may carry out the functions of one whose function has been eliminated (Thivierge *et al*., 2012). The aminopeptidases *Pf*AAP and *Pf*LAP are critical to the growth and development of malaria parasites within the erythrocyte, as knockout of either aminopeptidase genes is lethal to the parasite (Dalal and Klemba, 2007). Prevention of *Pf*AAP and *Pf*LAP activity by aminopeptidase-specific inhibitors, such as bestatin, block development of malaria parasites *in vitro* and *in vivo*, showing a strong probability that these enzymes are attractive targets for the development of a new class of antimalarial drugs (Skinner-

Adams *et al.,* 2010). Of these two aminopeptidases *Pf*LAP exhibits narrower substrate specificity.

Matsui and co-workers (2006) stated that *Pf*LAP even exhibits narrower substrate specificity compared to its homologues in eukaryotes. Further research has shown that the digestion of red blood cell haemoglobin yields large amounts of leucine which is thought to be exchanged for extracellular isoleucine (Martin and Kirk, 2007). Isoleucine is abundant in *P. falciparum* proteins, present in 99.9% of its proteins, yet it is the only amino acid not found in human haemoglobin. This finding has prompted researchers to believe that the high specialization of *Pf*LAP is vital for the ultimate purpose of incorporation of isoleucine which is needed for parasite anabolism.

1.3.4. *Pf*AAP *vs Pf*LAP

Efforts to establish which of the two neutral aminopeptidases in the malaria parasite is the best antimalarial target for bestatin mediated killing of parasites have lead researchers to do further investigation on these enzymes. Gardiner and co-workers (2005) showed that parasites which over-expressed *Pf*LAP survived bestatin mediated killing compared to the normal parasites. McGowan (2009) and co-workers discovered the same phenomenon for *Pf*LAP. The malaria parasite expresses up to eighteen fold more *Pf*LAP compared to *Pf*AAP (LeRoch *et al*., 2003). Gardiner and co-workers (2005) found that parasites over-expressing *Pf*AAP did not have any increased resistance to bestatin mediated killing even though they concede that their results were not conclusive. Cunningham *et al.* (2008) found that inhibitory compounds appeared to have slightly higher inhibitory effects against the aminopeptidase activities of extracts under conditions favoring *Pf*LAP over *Pf*AAP although they also concede that due to differences in the K_m they could not directly compare the percentage inhibitions of the two enzymes.

Presently there is not enough conclusive evidence on which of the two neutral malarial aminopeptidase would be the better therapeutic target, however the available information has led current research to focus on *Pf*LAP as its role seems more critical (LeRoch *et al*., 2003; Cunningham *et al.,* 2008). However, the overlapping specifities of these two enzymes could be exploited to develop dual acting inhibitors such as bestatin. Bestatin use *in vivo* is restricted by

its high solubility and quick clearance via the kidneys which means it could be cleared from circulation before it kills the parasites (Skinner-Adams *et al*., 2007).

1.3.5. Leucine aminopeptidase

Leucine aminopeptidase (EC 3.4.11.1) was discovered by Linderstrom-Lang in 1929. LAPs are members of the M1 and the M17 peptidases and have distinctive structures, enzymatic mechanisms and biological roles in animals, plants and prokaryotes. While M17 LAPs are hexameric and have two cation binding sites per subunit, M1 LAPs are not hexameric but usually homomeric and have only one cation binding site (Matsui *et al*., 2006). As stated in section 1.3.3, LAPs of the M17 peptidase family are metal cation dependent exo-proteases that hydrolyze N-terminal residues from proteins and peptides. In bovine lens and the porcine kidney, LAP has been found to be a zinc-metalloenzyme, generally localized in the cytosol (Sanderink *et al*., 1988).

There is substantial literature characterizing the M17 LAPs from all three kingdoms at the biochemical level, and the three-dimensional structure has been determined for the bovine and *Escherichia coli* enzymes by X-ray crystallography (Coloms, 2004). Ledeme and co-workers (1983) characterized the human liver LAP as a hexamer *(Mr* 360 000) consisting of three dimers with two different subunits each *(Mr* 53 000 and 65 000) with optimum activity at pH 10. This enzyme is activated by Mg^{2+} and Mn^{2+}, and inhibited by Zn^{2+}, Co^{2+}, complexing agents, bestatin and amastatin. Apart from Ledeme *et al*. (1983) and Kohno *et al.* (1985), no documentation on the purification or expression of the human liver or cytosolic LAP has been published.

1.3.6. *Plasmodium falciparum* LAP

*Pf*LAP is a 320 kDa homo-hexamer that is optimally active at neutral or alkaline pH, is dependent on metal ions for activity and exhibits a substrate preference for N-terminally exposed hydrophobic amino acids, particularly leucine (Stack *et al*., 2006). As with M17 LAPs from other prokaryotes and higher organisms such as mammals, *Pf*LAP contains two metal binding sites in each subunit (Allen *et al*., 1983; Chi *et al*., 2007; Jia *et al*., 2009). The metal binding sites are designated site 1 and site 2, with site 1 being a loosely binding and readily exchangeable site, while site 2 is a tight binding site (Maric *et al.*, 2009).

It is believed that native *Pf*LAP contains zinc at site 2 while the occupant ion at site 1 is dependent on the type and the concentration of ions in the surrounding environment. Several divalent metal ions are known to bind to site 1 and these include Zn^{2+}, Mn^{2+}, Co^{2+}, Ni^{2+} and Mg^{2+}, while site 2 only accommodates Zn^{2+} and Co^{2+} (Allen *et al*., 1983). The *Pf*LAP active site with Zn^{2+} occupying the metal binding sites is illustrated by the stereo diagrams on fig. 1.10. The metal bound at site 1 influences the catalytic efficiency and the mode of binding by bestatin (Maric *et al*., 2009; Kang *et al*., 2010).

Metal ion chelators such as EDTA have been found to inactivate LAP and this confirms the importance of metal ions in the activity of this enzyme (McGowan *et al*., 2009). The overall sequence identity between the various malaria LAPs is high (65–69%), and within the C-terminal domain it is 80–85% (Cunningham *et al*., 2008). There are significant differences between LAPs from different kingdoms (plant, animal and microbes) as Gu and Walling (2002) demonstrated when they compared porcine LAP, *E. coli* PepA and tomato LAP-A. Gu and Walling (2002) suggested that differences in LAPs across different kingdoms, if sufficient, can be exploited in selectively targeting *Pf*LAP among other LAPs.

There are differences in the overall primary structure and in the residues that influence substrate binding in *Pf*LAP when compared to the mammalian homologues as shown by the sequence alignment (fig. 1.11) (Poreba *et al*., 2012). The significant differences in the S1 subsites of *Pf*LAP and the human LAP may be exploited to design more-potent and selective inhibitors (Cunningham *et al*., 2008). *Pf*LAP has been expressed in insect cells by Stack *et al*. (2007). The protein is encoded by a gene which consists of a single exon of 1 818 bp that is translated into a 605-amino-acid protein. *Pf*LAP was also expressed in *P. falciparum* by Gardiner *et al*. (2006) with a monomer size of 65 kDa. *Pf*LAP is produced by all stages of the intra-erythrocytic developmental cycle of malaria, but is most highly expressed by trophozoites, a stage at which hemoglobin degradation and parasite protein synthesis are elevated. The expression levels of *Pf*LAP as compared to *Pf*AAP are considerably high; approximately 18 fold, signifying the importance of *Pf*LAP (Gardiner *et al*., 2006).

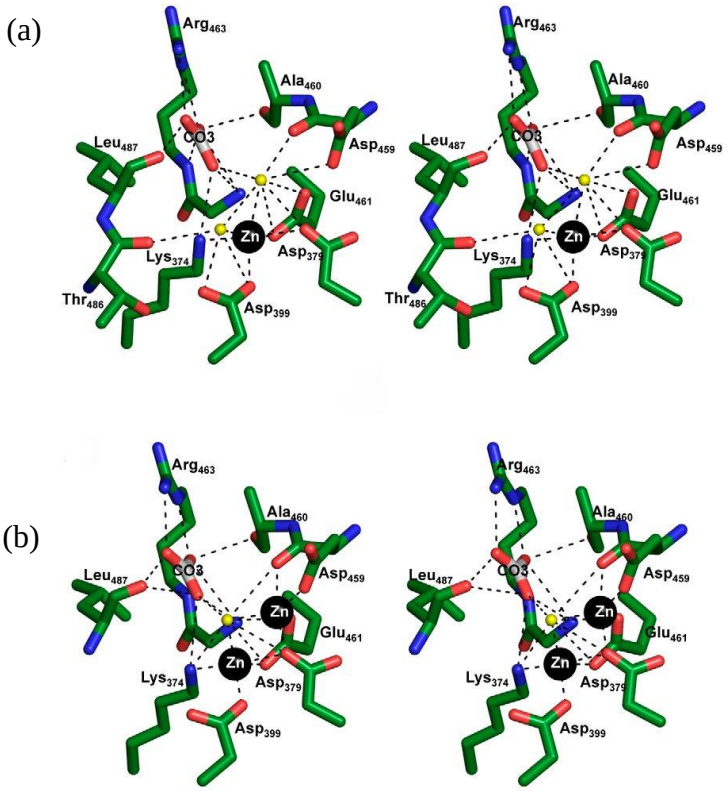

Figure 1.10 Stereo diagrams of the active sites of (a) 2.0 Å *Pf*LAP Zn^{2+} and (b) 2.4 Å *Pf*LAP $Zn^{2+}Zn^{2+}$. Carbon atoms of residues are colored by green. Water molecules are shown as yellow spheres. Hydrogen and metal bonds are indicated (dashed lines). Zn is shown as black spheres, and carbon atom of carbonate ion (CO_3) is colored grey (taken from McGowan *et al*., 2010).

Figure 1.11 Multiple sequence alignments of *Pf*LAP with mammalian orthologs, *Hs*: *Homo sapiens*, *Pf*: *Plasmodium falciparum*. Dashes represent gaps that optimize sequence adjustment. Small or hydrophobic amino acids are colored in magenta, acidic are red, basic are blue and amino acids with an amine or hydroxyl group are green. Conserved amino acids are highlighted in gray. Amino acids from active site residues are presented on a black background and those participating in metal binding are outlined (taken from Poreba *et al*., 2012).

Amino acid dipeptide analogs, such as bestatin and its derivatives, are potent inhibitors of the protease and also block the growth of *P. falciparum* malaria parasites in culture (Wilkes and Prescott, 1985; Skinner-Adams *et al*., 2007; Maric *et al*., 2009). *Pf*LAP has also been expressed in *E. coli* by Stack *et al*. (2007) and the present study aims to use this expression system.

1.3.6.1.*Pf*LAP crystal structure

The x-ray crystal structure of *Pf*LAP as reported by McGowan *et al*. (2010) resembles that of other LAPs reported (Burley *et al*., 1990; Matsui *et al*., 2006). This particular *Pf*LAP was obtained from expression in *E. coli* using a synthesized, truncated form of *Pf*LAP gene lacking the asparagine rich region as described by Stack *et al.* (2007). The structure exists as two hexamers in an asymmetric unit, with each hexamer consisting of six monomers assembled in a typical LAP fashion [figure 1.12(b)]. The active site on each monomer are oriented towards the interior of the hexameric assembly [figure 1.12(b)] and consists of negatively charged residues which are responsible for coordination of metal cations as shown on figure 1.10. Each monomer [figure 1.12(a)] consists of the catalytic C-terminal (residues 301-605) and the regulatory N-terminal (residues 85-276).

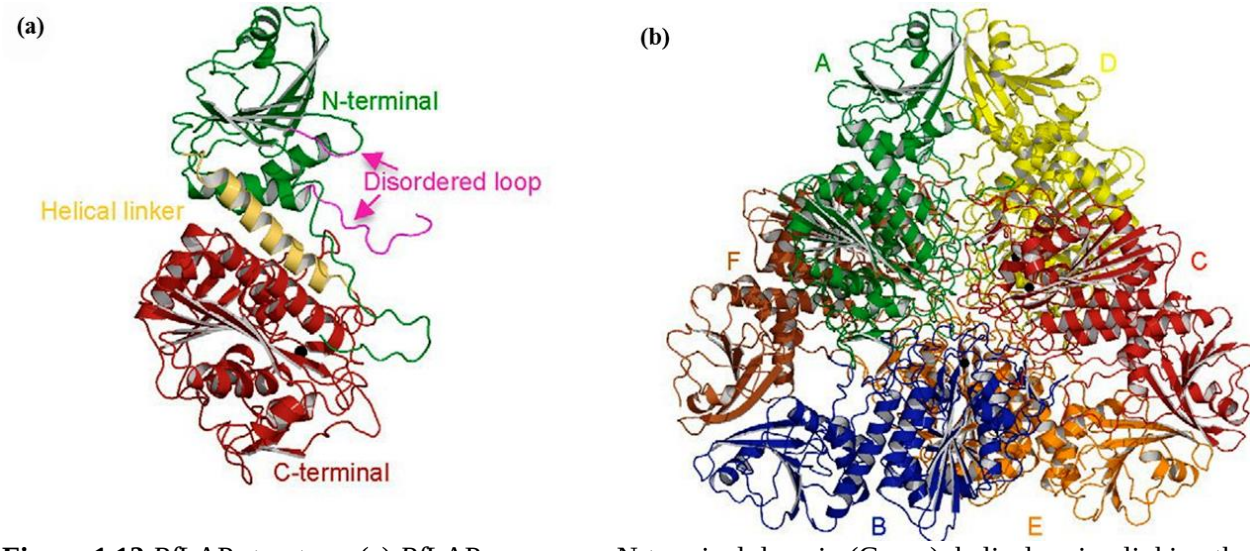

Figure 1.12 *Pf*LAP structure. (a) *Pf*LAP monomer: N-terminal domain (Green), helical region linking the two domains (Yellow), C-terminal catalytic domain (Red) and the partially disordered loop (Magenta). (b) *Pf*LAP hexamer coloured by monomer: A (Green); B (Blue); C (Red); D (Yellow), E (Orange) and F (Brown) (taken from McGowan *et al*., 2010).

The N-terminal is made up of a β-sheet and three α-helices, with the former assuming a central position. The C-terminal consists of nine α-helices which flank and an eight stranded β-sheet with a two stranded β-sheet capping one end of the catalytic domain. The dimensions of the active site are 18 Å by 18 Å and it is located near the central β-sheet of the C-terminal. The N-terminal and the C-terminal are linked by a 30 Å helix (residues 277-300). A 20 Å partially disordered loop lies at the mouth of the active site and it is believed that the flexibility of this loop regulates the entrance of substrates and the exit of products from the *Pf*LAP active site (McGowan *et al*., 2010).

1.4. Nanotechnology

Nanotechnology, the study of matter of sizes ranging between 1-100 nm is a fast growing field of research and has attracted considerable attention over the past several decades (Mohanraj and Chen, 2006; Zhang *et al*., 2008). Various fields such as physics, chemistry, engineering and biological sciences are associated with the use of nanotechnology. Spearheading the rise of nanotechnology is the use of nanodevices (table 1.2) which comprise of clusters (Zhao *et al*., 1998), nanoparticles (Pal *et al*., 2008), nanocrystals (Alivisatos, 1996), quantum dots (Larson *et al*., 2003), nanowires (Elechiguerra *et al*., 2005) and nanotubes (Iijima and Ichihashi, 1993).

The present study focuses on the use and application of various nanotechnologies in the field of medicine. The merge between nanotechnology and medicine is known as nanomedicine and involves the exploitation of materials at the nanoscale to develop novel therapeutic and diagnostic agents. The nanoscale is where most natural processes take place and the integration of nanotechnology and biology presents great potential in solving a number of today's biomedical problems and revolutionizing the medical field (Sahoo *et al*., 2006).

Table 1.2 Some of the nanodevices commonly used in nanotechnology and nanomedicine.

Nanodevices	TEM image	Source
Quantum dots are colloidal fluorescent semiconductor nanocrystals (2–10 nm). The central core of quantum dots consists of combinations of elements from groups II–VI of the periodic table.	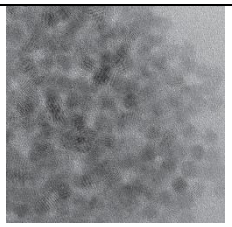	Talgorn *et al*., 2011
Nanotubes are self-assembling sheets of atoms arranged in tubes. Nanotubes come as either single- or multi-walled carbon nanotubes.		Iijima and Ichihashi, 1993
Nanowires are nanostructures of diameter 100 nm or less and usually have a length 1 000 times their diameter.	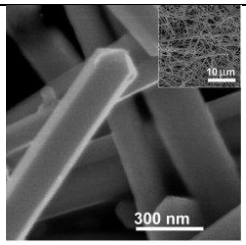	Elechiguerra *et al*., 2005
Nanoparticles nanosized metal structures consisting of 10^3 metal atoms. They have various shapes and sizes.	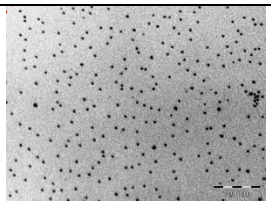	Pal *et al*., 2008
Liposomes are spherical bilayered vesicles with an aqueous interior surrounded by a phospholipid	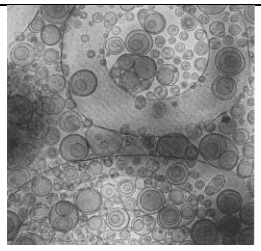	Al-Jamal and Kostarelos, 2011

1.4.1. Nanomedicine: potential and promise

The first recorded example on the use of nanomedicine dates back to 1965 when liposomes were first used in medicine (Deamer and Bangham, 1965). Today more nanodevices such as gold nanoparticles (GNPs) can be functionalized to make them even more versatile (Ghosh *et al*.,

2008). Functionalized nanodevices can be conjugated to therapeutic agents and used to carry and deliver the agents to their target site. The release of the drug is typically triggered by a change in the environment such as the low pH in tumor tissues or the presence of a substance that has a higher affinity for the nanodevice than the drug, e.g. glutathione inside cells (Han *et al*., 2005; Sahoo *et al*., 2006; Ghosh *et al*., 2008). Glutathione is known to exist in higher concentrations inside cells than outside and this can be exploited to deliver drugs that are attached to GNPs via thiol linkages as glutathione has a higher affinity for GNPs via the same linkages (figure 1.13) (Sies, 1999; Ghosh *et al*., 2008).

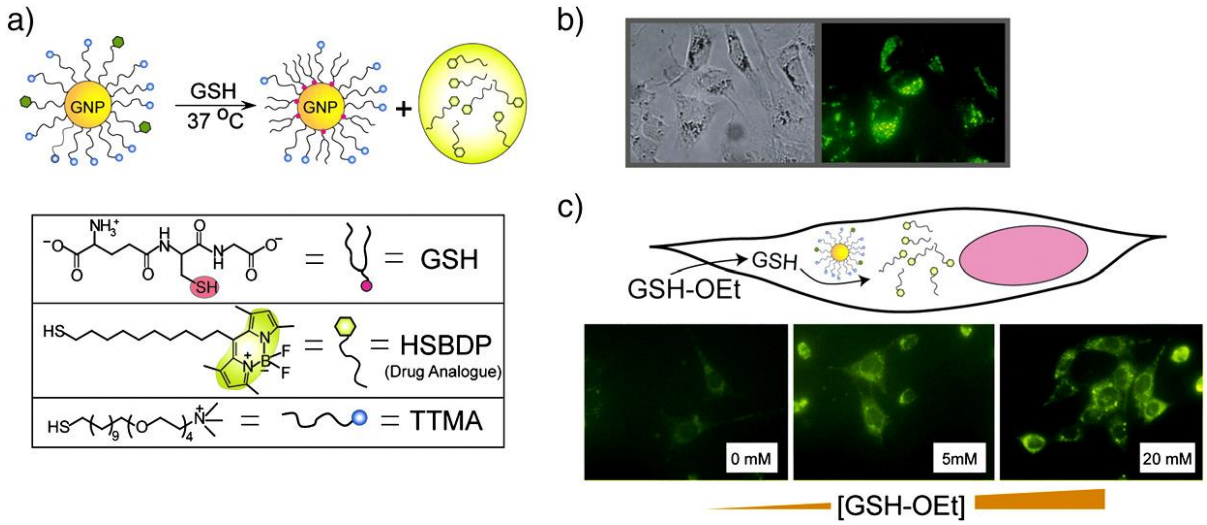

Figure 1.13 GNP modes of action. **a)** An illustration of the glutathione-mediated drug release by GNPs via a displacement reaction. **b)** Bright field and fluorescence micrographs of human Hep G2 cells after incubation with GNPs for 96 h. **c)** Fluorescence images showing dose-dependent release of drugs (taken from Ghosh *et al*., 2008).

The deviation of diseased tissues from normal metabolism results in pathophysiological conditions which may also be exploited for drug release at the target site (Prato *et al*., 2008). Ideally, while in transit, the nanodevice is meant to shield the therapeutic agent from degradation or any form of alterations by many of the body's metabolic processes. The small size and solubility of nanodevices are essential for the movement of drugs across barriers such as the blood brain barrier which drugs cannot otherwise pass through (Calvo *et al*., 2001; Sahoo *et al*., 2006). The small size and the inert nature of nanodevices also enables them to be transported undetected by the immune system thereby making them able to deliver drugs effectively without eliciting immune responses (Emerich and Thanos, 2007). Targeting can be accomplished by the

conjugation of ligands which are able to bind to specific receptors at the target site. Targeting ensures bioavailability of the drug to the target site and prevents toxicity in the rest of the body where the drug is not needed (Emerich and Thanos, 2007; Prato *et al*., 2007). Nanodevices are also capable of carrying biomolecules such as nucleic acids (Han *et al*., 2005; Han *et al*., 2006) and proteins (Bhumkar *et al*., 2007) and releasing them at target sites. This property, especially in GNPs makes them potential alternatives for gene therapy and delivery of proteins such as insulin to target sites. These are just but a few examples of the potential uses of nanotechnology in medicine. For a field that is relatively new, nanomedicine presents exciting opportunities for novel drug discovery and the improvement of existing drugs to enhance their effects.

1.4.2. Current nanotechnology based therapies

One of the most successful applications of nanotechnology in pharmacology is in cancer therapy with several marketed compounds and others being currently investigated in clinics (Couvreur and Vauthier, 2006). Examples of cancer therapy drugs currently in use include Caelyx® and Doxil® while those under investigation and trials in clinics include Transdrug®, Abraxane® and ABI-007. Zhang *et al.* (2008) reported that by 2008 there were 24 nanotechnology based chemotherapeutic agents in clinical use with the majority being liposome based. Liposomes are the most clinically established nanodevices and were among the first to be used for medical purposes (Mohanraj and Chen, 2006; Sanvicens and Marco, 2008). Liposomes are able to encapsulate various payloads of both hydrophilic and hydrophobic nature in their interior and shield them from the systemic barriers and modifications (Zhang *et al*., 2008; Al-Jamal and Kostarelos, 2011).

Advances taking place in nanomedicine are impressive but a lot of work still lies ahead. The field of infectious diseases is in great need of medical breakthroughs as cures and vaccines are needed to combat diseases such as HIV and malaria which threaten a very significant fraction of the world's population. The discovery of new treatments for infectious diseases has been complicated by various factors which include the constant modification of pathogen patterns because of the emergence of resistant strains of bacteria, parasites, fungus and viruses. New pathogens such as the SARS virus, bird flu and swine flu also continue to emerge (Guan *et al*., 2002; Dwosh *et al*., 2003; Zimmer and Burke, 2009). The application of nanotechnology in the

fight against infectious diseases is promising and some studies have already shown improved drug efficacy as a result of applying nanotechnology in drug delivery (Owais *et al*., 1995; Couvreur and Vauthier, 2006; Zhang *et al*., 2008).

Singh *et al.* (2008) stated that in the fight against bacterial infections, metallic nanoparticles have proved to be the best among other nanodevices. Morones *et al.* (2005) and Lara *et al.* (2009) documented the bactericidal effect of silver nanoparticles (AgNPs). The anti-HIV properties of AgNPs have also been documented, signifying their potential use against infectious diseases (Elechiguerra *et al*., 2005; Lara *et al*., 2010). Other diseases whose proliferation has been shown to be inhibited by AgNPs include hepatitis B and Dalton's lymphoma (Lu *et al*., 2008; Sriram *et al*., 2010). The efficacy of AgNPs against a wide range of microorganisms influenced the present study to incorporate them for the interaction with *Plasmodium* and human LAP.

1.4.3. AgNPs synthesis and the importance of morphology

There are various methods which have been proposed for the effective synthesis of AgNPs and they mostly include the reduction of a silver salt and stabilization using an appropriate agent (Sun and Xia, 2002; Pastoriza-Santos and Liz-Marzan, 2002; Dominiguez-Vera *et al*., 2007; Pal *et al*., 2008; Saxena *et al*., 2010). The nanoparticles are stabilized to prevent agglomeration and corrosion and to ensure particle monodispersion (Ghosh *et al*., 2008). The size and shape of nanoparticles, especially in medicine, has been found to be of great importance in their efficacy against microbes with sizes of 10 nm or less having been reported to have the best bactericidal activity (Morones *et al*., 2005).

Elechiguerra *et al.* (2005) and Lara *et al.* (2010) found that the anti-HIV-1 effects of AgNPs were strongly dependent on their size, with only sizes from 1-10 nm being able to bind to the virus. Recently Argawal *et al.* (2013) found that mammalian epithelial, endothelial and immune cells have a strong preference for nanodiscs compared to nanorods. In most cases, as reported by Elechiguerra *et al.* (2005), Lara *et al.* (2010) and Argawal *et al.* (2013), it has been observed that spherical or disc shaped nanoparticles interact better with biomolecules than nanorods and nanowires (Brust *et al*., 2005; Lu *et al.*, 2008). Thus the shapes of nanoparticles influence the reaction of nanoparticles with biomolecules. The size and shape of the nanoparticles can be

controlled by variations of stoichiometry of the precursors and parameters such as the pH of the reactions (Ishii *et al*., 2003; Chithrani *et al*., 2006; Ji *et al.*, 2007).

1.4.4. AgNPs mechanism of action

The use of silver as an antibacterial agent dates back several decades, with some articles even dating back centuries (Singh *et al*., 2008). Silver nitrate was used in the 20th century to treat wounds and burns (Moyer *et al*., 1965). The lethal effects of AgNPs towards other microbes other than bacteria and cancerous cells have been investigated and are well documented (Elechiguerra *et al*., 2005; Morones *et al*., 2005; Lu *et al*., 2008; Lara *et al*., 2009; Lara *et al*., 2010; Sriram *et al*., 2010). The antimicrobial effect of AgNPs has been shown to be a size dependent phenomenon but the finer details of their mechanism are still a subject of discussion. Possible mechanisms of action are presented in figure 1.14.

Morones *et al.* (2005) proposed that AgNPs interact with bacterial membranes and disrupt their integrity or they can penetrate the cell membrane and interact with sulphur and/or phosphorus containing compounds such as DNA. Choi *et al.* (2003) reported the interaction of AgNPs with thiol groups of organic compounds, while Elechiguerra *et al.* (2005) and Lara *et al.* (2010) proposed that silver nanoparticles exert their anti-HIV-1 effects by binding to the gp120 glycoprotein on the virus thereby preventing its binding and entry into CD4 cells.

The inactivation of microbes by the interaction of AgNPs with thiol groups of proteins such as enzymes and trans-membrane proteins was proposed by Klueh *et al.* (2000). Though the mechanism of AgNPs may not be entirely understood, their efficacy as an antimicrobial has been demonstrated. The present study seeks to interact AgNPs with LAP enzymes from human and *Plasmodium* sources in an attempt to evaluate their therapeutic nature towards malaria.

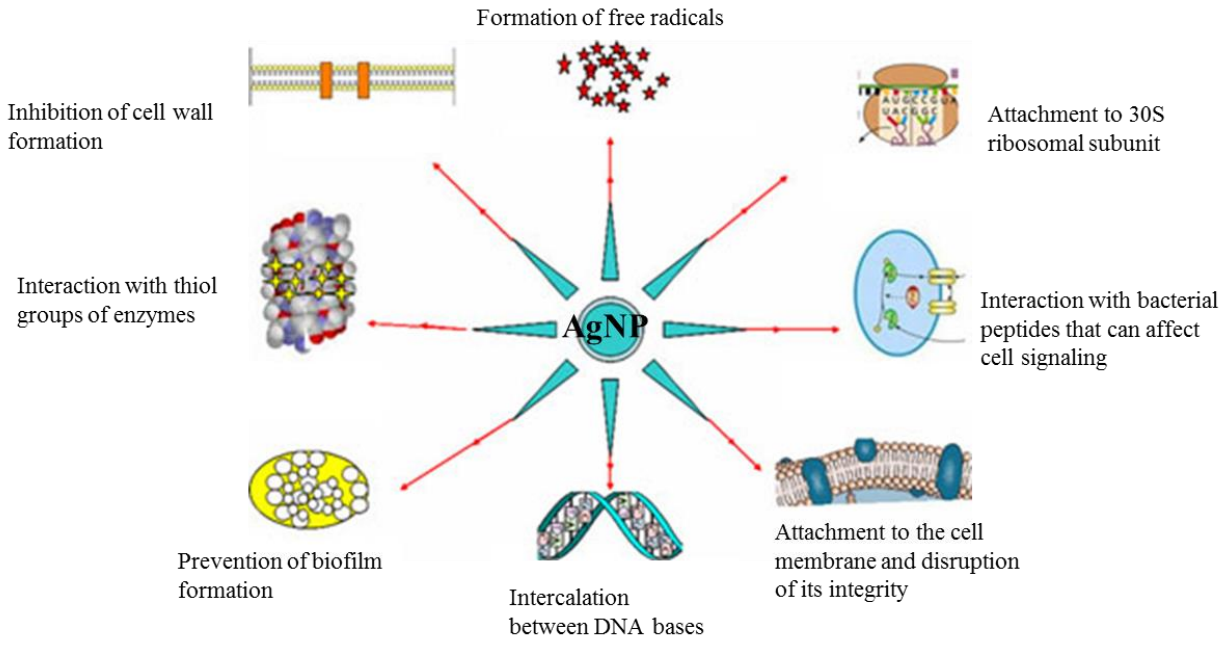

Figure 1.14 An illustration of various antimicrobial mechanisms of AgNPs (adapted from Rai *et al*., 2012).

1.4.5. Health and safety implications of nanoparticles

The rapid growth of nanotechnology and its promise to revolutionize medicine has not come without reservations on the potential negative impacts that may be inflicted by this technology. Various studies have been conducted to ascertain the health and safety implications on the use of nanoparticles. Pujalte *et al.* (2011) reported the *in vitro* nephrotoxicity of ZnO and CdS through the generation of reactive oxygen species (ROS) and consequent oxidative stress. Pujalte *et al.* (2011) found that TiO_2 did not exhibit these toxic effects and they also conceded that *in vitro* studies show exaggerated cell damage as compared to *in vivo* studies. AshaRan *et al.* (2009) conducted a study on the cytotoxicity and genotoxicity of starch coated AgNPs on normal lung fibroblasts. AshaRan *et al.* (2009) observed a marked difference in morphology and cytotoxicity of cells treated with nanoparticles from the normal cells, (figure 1.15) and attributed this to the disruption of the cytoskeleton and necrosis. AshaRan *et al.* (2009) concluded that the silver nanoparticles are cytotoxic, genotoxic with potential to be carcinogenic and antiproliferative.

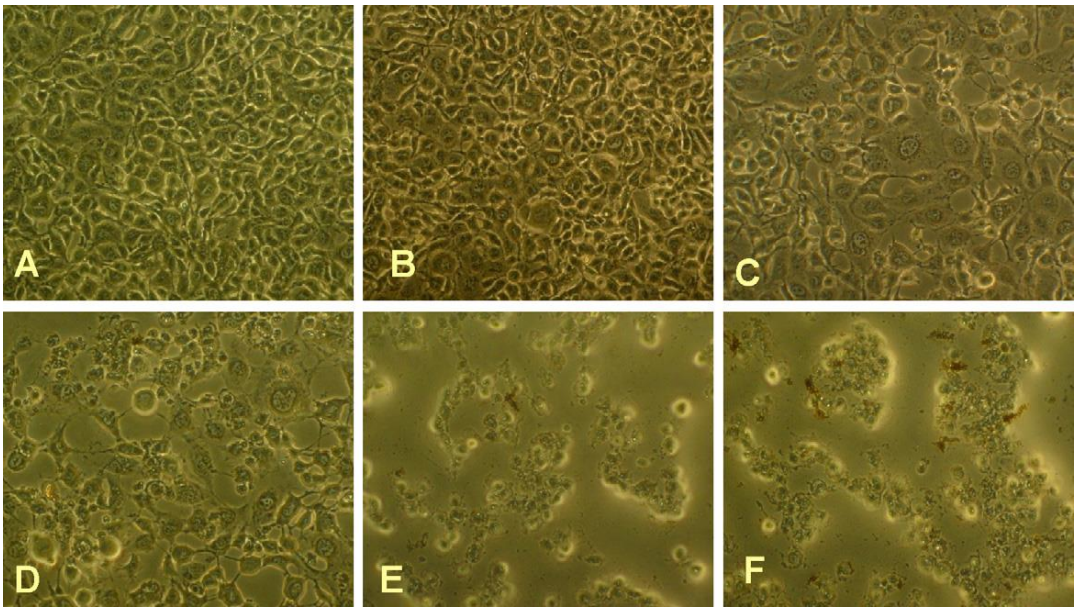

Figure 1.15 AgNP toxicity. Phase contrast micrographs of (A) unexposed cells; (B–F) 24 h after the cultures were exposed to 3.12, 6.25, 12.5, 25 and 50 $g.ml^{-1}$ AgNPs, respectively, (magnification 200×) (taken from Arora *et al.*, 2008).

A few other research groups have investigated the toxicity of AgNPs and found them toxic to rat cells (Lesniak *et al*., 2009), rat spermatogonial stem cells (Braydich-Stolle *et al*., 2005), rat liver cells (Hussain *et al*., 2005) and human fibrosarcoma cells (Arora *et al*., 2000). The finding that AgNPs also have deleterious effects on normal cells requires that their use in therapeutics be approached with caution. However it is worth noting that most research on the toxicity of nanoparticles has been conducted *in vitro* and gives exaggerated results which may not be reproducible *in vivo* (Pujalte *et al*., 2011). Furthermore nanoparticles may be functionalized and engineered to target specific cells, a property which would circumvent their potential effects on healthy cells in the body (Emerich and Thanos, 2007; Prato *et al*., 2007). Conor *et al.* (2005) found that GNPs did not have deleterious effects on human leukemia cells but that the precursors to the nanoparticles had negative effects. These findings show that nanotechnology still holds great promise in the medical field and more research needs to be conducted to understand their acute and chronic effects, not just in living organisms but also on the environment.

1.5. Conclusions

The critical role of LAP in the most menacing strain of malaria parasites, *P. falciparum* has been discussed and illustrated. LAP's importance in protein metabolism, particularly hemoglobin digestion makes it a potential biomedical target for the treatment of malaria. There are differences in amino acid composition and the S1 subsites between *Pf*LAP and *Hs*LAP; these differences may be exploitable in the design of a selective inhibitor for *Pf*LAP. Among potential inhibitors, AgNPs provide an attractive candidate as they have already been shown to interact and inhibit several biomolecules including enzymes (Elechiguerra *et al*., 2005; Morones *et al*., 2005; Lu *et al*., 2008; Lara *et al*., 2010). AgNPs are known to interact with thiol groups in biomolecules thereby disrupting their normal function. Structural differences in *Pf*LAP and *Hs*LAP may aid selective inhibition since the exposed thiol containing amino acids (cysteine and methionine) may differ in each enzyme. Therefore the interaction of silver nanoparticles with *Pf*LAP may prove to fatal to *P. falciparum*. Since inhibition of other microbes is already known, it is speculated that *Pf*LAP may also be a susceptible target.

1.6. Hypothesis

The differences in amino acid sequences of *Pf*LAP and *Hs*LAP are sufficient for silver nanoparticles to selectively inhibit *Pf*LAP without adverse effects on *Hs*LAP function.

1.7. Aims of study

1. Obtain the coding sequence for *Pf*LAP, design primers and PCR amplify the gene using *P. falciparum* cDNA as a template.
2. Obtain the coding sequence for *Hs*LAP and get the gene synthesized.
3. Amplify *Pf*LAP and *Hs*LAP genes and sub-clone them into the expression vector pET 28b(+).
4. Transform *E. coli* BL 21 (DE3) cells with pET 28b(+) inserted with LAP genes for the over-expression of *Pf*LAP and *Hs*LAP.
5. Purify both *Pf*LAP and *Hs*LAP using nickel affinity chromatography and assay for their activity using a suitable assay.

6. Characterize both recombinant *Pf*LAP and *Hs*LAP by assessing their metal ion dependence, pH and temperature stability, and their kinetic parameters.
7. Synthesize and characterize silver nanoparticles using UV/VIS spectroscopy, TEM and also assess their size distribution and stability.
8. Interact both *Pf*LAP and *Hs*LAP with silver nanoparticles and assess changes in their kinetic parameters.
9. Suggest mechanisms and reasons for differences in the effects of nanoparticles on *Pf*LAP and *Hs*LAP.

Chapter 2: Molecular cloning of leucine aminopeptidase

2.1. Introduction

2.1.1. Molecular cloning

Molecular cloning involves the insertion of a gene into a DNA molecule otherwise known as a cloning vector. Cloning vectors are carrier DNA molecules whose important features among others include (i) the ability to replicate autonomously (Struhl *et al*., 1979), (ii) a number of unique restriction endonuclease cleavage sites that are present only once in the vector, (iii) a selectable marker (Rao and Rogers, 1979) and (iv) can be easily retrieved from a host cell. Commonly used vectors include plasmids, bacteriophages and cosmids, while more recently bacterial artificial chromosomes (BACs), yeast artificial chromosomes (YACs) and mammalian artificial chromosomes (MACs) have been used for housing large DNA fragments (Collins and Hohn, 1978; Monaco and Larin, 1994; Hamilton, 1997). The isolation of DNA and the production of recombinant DNA make use of two classes of enzymes, namely restriction endonucleases and DNA ligases which function to cut and to link DNA fragments respectively (Wright, 1986).

Using a suitable host organism such as yeast or bacteria, large amounts of the inserted gene can be produced by proliferation of the vector. Typically, molecular cloning using plasmid vectors involves five steps, namely, (i) the construction of a recombinant DNA molecule (foreign DNA ligated into a plasmid) using restriction endonucleases and DNA ligases (Struhl, 1985), (ii) the transfer of the recombinant DNA molecule into the host strain. Bacterial transformations commonly use competent *E. coli* strains (Srivastava, 2013), while yeast transformation most commonly use competent *Saccharomyces* / *Pichia* strains (Cereghino and Cregg, 2000), (iii) selection of recombinant clones using a selectable marker (Rao and Rogers, 1979), (iv) multiplication of plasmid DNA molecules by division of host cells and finally, (v) the purification of recombinant plasmid DNA (Shiloach *et al*., 1996).

PCR, an *in vitro* technique, can also be used for the amplification of particular segments of DNA (Mullis *et al*., 1986). PCR can produce a billion-fold of a target sequence in several hours and

makes use of DNA polymerase, a DNA template, primers and free nucleotides. PCR involves 3 steps, namely; (i) denaturation, where the double stranded template is rendered single stranded by heat to expose the strands for amplification, (ii) annealing, where the reaction is cooled to allow primers to bind to the appropriate complementary strand, and finally (iii) primer extension, where DNA polymerase, in the presence of Mg^{2+} extends the primers in the 5′ to 3′ direction. The template is the DNA sample to be amplified and may be in the form of genomic DNA, complementary DNA (cDNA), a previous PCR product or a synthesised DNA fragment (Schochetman *et al*., 1988). Primers are usually designed and synthesised while DNA polymerase is commercially available. The most popular polymerase is *Taq* polymerase from the thermophilic bacteria *Thermus aquaticus* (Chien *et al*., 1976; Tindal and Kunkel, 1988; Holland *et al*., 1991; Pluthero, 1993). The DNA polymerase employed in the present study was Phusion hot start II DNA polymerase which has an error rate 50 fold lower than *Taq* polymerase and has proof reading abilities (Pezza *et al*., 2012).

Vectors can be engineered to possess control sequences which trigger RNA synthesis and consequently protein synthesis. This way, if a cloned gene is flanked by properly situated control sequences for RNA and protein synthesis, the host cells are able to produce large quantities of the messenger RNA and the protein coded for by that gene. Vectors which contain control sequences for mRNA and protein synthesis are called expression vectors. When previously isolated clones are transferred into a different vector for other applications, this is called "sub-cloning."(Struhl, 1987).

2.1.2. Bacterial transformation

Transformation is a naturally occurring phenomenon which results from the uptake of exogenous genetic material by competent bacterial cells (Tortosa and Dubnau, 1999). This process can be artificially induced and has been exploited in the field of recombinant DNA technology to facilitate the uptake of foreign DNA by cells which would otherwise not take up the DNA. In the present study *E. coli* BL21(DE3) was the expression system of choice and competency in these cells was induced chemically using divalent metal ions and DMSO, with the latter serving as a stabiliser of the frozen cells (Inoue *et al*., 1990). *E. coli* BL21(DE3) was chosen due to its

possession of an inducible T7 RNA polymerase system and its protease deficiency (Timmons *et al*., 2001).

The principle of this method is described by Srivastava (2013) and lies in the destabilisation of the chemical structure of the outer membrane of *E. coli* by divalent metal ions. The metal ions increase the ionic bonding and disrupt the internal membrane interactions which are vital for the maintenance of the membrane integrity. The metal ions also confer an overall positive charge on the membrane which carries an overall negative charge under physiological conditions thereby allowing DNA which is negatively charged to pass through the cell membrane (Bergmans *et al*., 1981).

The current study made use of Ca^{2+} and Mn^{2+} to render the *E. coli* cells competent before snap freezing them in liquid nitrogen and storage at -80 °C for future use. The competent cells were transformed by thawing on ice, followed by incubation with the pET 28b(+) plasmid on ice to facilitate plasmid DNA uptake (Dagert and Ehrlrich, 1979). A brief heat shock at 42°C was performed and it is believed that this step melts the membrane structure and completes the uptake of plasmid DNA (Srivastava, 2013). The transformed cells were allowed to grow briefly under highly favourable conditions to allow the DNA to stabilise before plating on agar plates. Kanamycin resistance, a trait which is conferred on *E. coli* by the pET 28b(+) plasmid was used as a selectable marker to screen for positive transformants. Transformation yielded *E. coli* BL21(DE3) cells which contained the pET 28b(+) plasmid housing either *Pf*LAP or *Hs*LAP.

2.2. Aims and objectives

The aims of this section were to obtain the genes for *Pf*LAP and *Hs*LAP and clone them into an expression vector. The *Pf*LAP gene was to be PCR amplified using *P. falciparum* cDNA as a template while the *Hs*LAP gene was to be artificially synthesised as a template for its amplification was not available. The initial step was to design primers for *Pf*LAP amplification and perform virtual cloning using software such as pDraw and BioEdit to confirm the insertion of the genes into the expression vector and the expression of the genes with the His-tag in frame. The *Pf*LAP gene would be inserted into a cloning vector, amplified and digested out using *Eco*RI and *Nde*I. These same enzymes would be used to digest open the circular expression vector pET

28b(+) prior to ligation of the gene into the expression vector. The bacterial cell lines to be used for the proliferation of the cloning vector and protein expression were *E. coli* JM109 and *E. coli* BL21(DE3) respectively. Competent cells would be prepared using the chemical method. Agarose gel electrophoresis and DNA sequencing were the methods chosen for confirming the identity of the relevant DNA fragments after the steps where this was necessary.

2.3. Methods and materials

2.3.1. Primer design and virtual cloning

The *Pf*LAP nucleotide sequence was obtained from the National Center for Biotechnology Information (NCBI) Genbank (accession code: XM_001348577.1) and used for primer design. The primer sequences (Table 2.1), containing either an *Nde*I or *Eco*RI restriction site, were analysed using the free online OligoAnalyzer tool on the Integrated DNA Technologies (IDT) website to obtain their properties. The specificity of the primers to the target gene sequence was determined using the bioinformatics tool, Basic Local Alignment Search Tool (BLAST) on the NCBI website. Using the pET 28b(+) (Novagen) vector sequence, the designed primers and the software pDraw32 version 1.1.116, virtual cloning of the gene was done.

The first step in virtual cloning was to enter the primer sequences into the oligonucleotide database on the software pDraw32. The coding sequence for *Pf*LAP was entered into pDraw32 as a new sequence and the relevant restriction enzymes (*Eco*RI and *Nde*I) were explicitly selected for the cloning of the sequence. The fragment produced from this step was saved in pDraw32 format as the *Pf*LAP PCR fragment. The vector sequence was obtained from the Novagen website and also entered into pDraw32 as a new fragment and then saved in pDraw32 format. Then the option "cloning of sequences" was selected on pDraw32 and the vector sequence was selected from its file location as the first sequence followed by the PCR fragment sequence. *Eco*RI and *Nde*I were selected as the enzymes for the cloning process. The vector sequence was marked as circular and inverted before the virtual cloning process was performed. After virtual cloning the presence of six histidine residues, otherwise known as a His-tag and the in-frame expression was checked using the open reading frames of the protein to be expressed which are available as a viewing option in pDraw32. The -His-tag is necessary for the downstream purification of the expressed protein using affinity chromatography.

Table 2.1 Oligonucleotide primers used for PCR amplification.

Primer	Sequence	T_m (°C)
Pf-LeuPEP_*NdeI*_F	5′ – **CAT ATG** TAT TTT TCT TCC TTA TGT AAA TTT TTG C – 3′	53.4
Pf-LeuPEP_*EcoRI*_R	5′ – **GAA TTC** TTA TAG AGC GTC ATT GAG TAC – 3′	53.4

2.3.2. Polymerase chain reaction

P. falciparum 3D7 cDNA (MRA-156, MR4, and ATCC® Manassas Virginia) was used as template for the amplification of the *Pf*LAP gene. PCR reactions were performed in a total reaction volume of 50 µl using a BIO-RAD T100™ Thermal Cycler. The reaction mixture contained 1 µl of 2 ng.µl^{-1} *P. falciparum* cDNA, 10 µl of the 5× HF buffer, 1.25 µl of 10 µM *Pf*-LeuPEP_*NdeI*_F primer, 1.25 µl of 10 µM *Pf*-LeuPEP_*Eco*RI_R primer, 1 µl of 10 mM dNTPs, 0.5 µl of 2 U.µl^{-1} Phusion hot start II DNA polymerase and 35 µl double distilled water (ddH_2O). Gradient PCR was performed at T_m temperatures ranging from 50-65 °C. The PCR reaction conditions consisted of an initial denaturation step (98 °C; 3 minutes), followed by 35 cycles each consisting of a denaturation (98 °C; 30 seconds), annealing (50-65 °C; 15 seconds) and elongation (60 °C; 165 seconds) step. This was followed by a final elongation step (60 °C; 10 minutes) to ensure complete elongation of the amplified product. The optimised PCR reaction followed the same steps save for the annealing temperature which was selected to be 65 °C.

2.3.3. Agarose gel electrophoresis

Agarose gel electrophoresis was used for the analysis of DNA products. Agarose gels (0.8 %) were prepared by dissolving agarose powder in 1×TAE buffer (0.04 M Tris-HCl, 1 mM EDTA, pH 8.0 and 0.021 mM glacial acetic acid) with 0.6 µg.ml^{-1} ethidium bromide. DNA was allowed to separate on the agarose gels for one hour at 90 V and was visualised using a UVITEC Uvipro Chemi high UV radiation source. DNA to be extracted from the agarose gels for downstream applications was visualised using a Vilber Lourmat low UV radiation source.

2.3.4. DNA extraction and quantification

DNA was extracted from agarose gels using the Bioflux Biospin Gel Extraction Kit according to the manufacturer's recommendation (Bioer Technology Co., Ltd). The DNA containing part of the gel was excised from the rest of the gel and dissolved in extraction buffer through heating. A spin column was used to retain and wash the DNA. The DNA was eluted using elution buffer. Nucleic acid concentrations were determined using a Nanodrop® ND-1000 spectrophotometer (NanoDrop Technologies, Inc). A GeneRuler™ DNA ladder Mix (100 – 10,000 bp) (Thermo Scientific) was run alongside the sample DNA to allow fragment size estimation based on electrophoretic mobility of the fragment relative to that of the DNA Ladder.

2.3.5. Ligations

The purified DNA products were ligated into the cloning and expression vector systems. CloneJet® (Fermentas®) was the cloning vector of choice while pET 28b(+) was the expression vector. The maps of both plasmids are shown in figure 2.1. The LAP gene was inserted into the multiple cloning site (MCS) close to the T7 promoter. In CloneJet® this site is within the lethal gene (eco 47IR) and therefore disrupts this gene. This was first done through virtual cloning as described in section 2.3.1 making use of the selected restriction enzymes *Eco*RI and *Nde*I before being done in practice. The *Pf*LAP PCR product obtained in section 2.3.2 was ligated into the CloneJet® vector system. Ligations were performed as per manufacturer's instructions. Ligations were performed in a total reaction volume of 20 µl and consisted of 2 µl T4 DNA ligase buffer (10×), 0.5 µl CloneJet® vector (50 ng. μl^{-1}), 7.5 µl of 9.1 ng.μl^{-1} DNA insert, 0.5 µl of 5 U.μl^{-1} T4 DNA ligase and 9.5 µl ddH_2O. A molar ratio of insert:vector DNA of 3:1 was used for all CloneJet® vector system calculations. The ligation reactions were incubated at room temperature for 5 minutes and transformed into chemically competent *E. coli* JM109 cells (as described in section 2.3.6). Gene sequences synthesised by GenScript (New Jersey, USA), as described in section 2.3.10, were sub-cloned into linearised pET 28b(+).

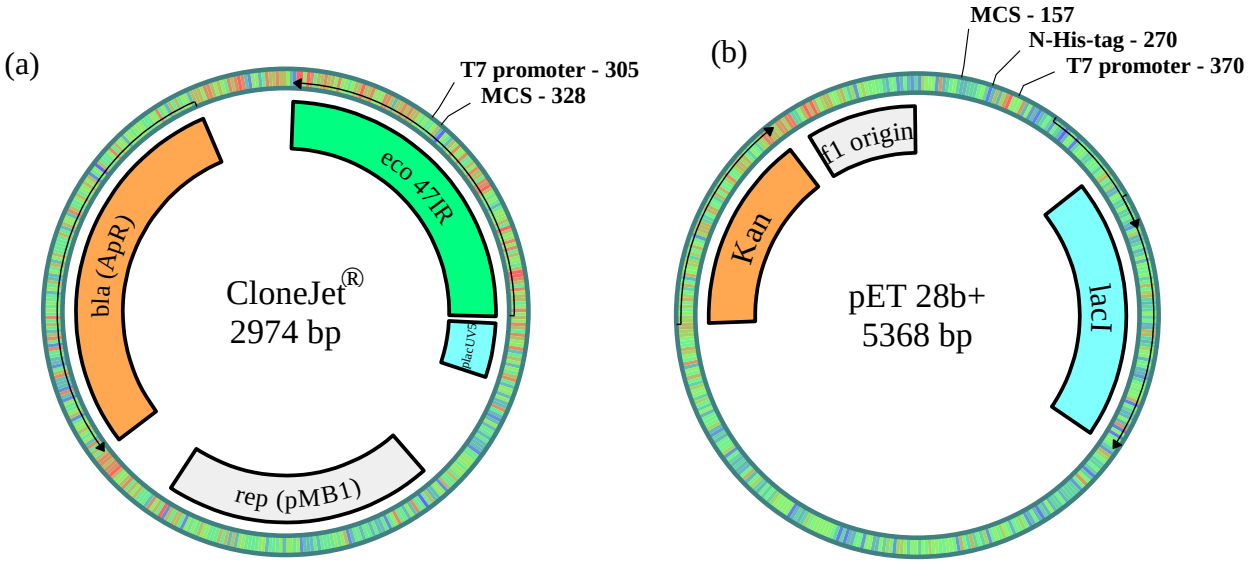

Figure 2.1 Plasmid maps of (a) CloneJet® and (b) pET 28b(+). On the CloneJet® image: bla (Ap^R) is the β-lactamase gene conferring resistance to ampicillin, eco 47IR is a lethal gene enabling selection, rep (pMB1) is a replicon from the pMBI plasmid responsible for the replication of CloneJet® and P_{lacUV5} is a modified P_{lac} promoter for expression of the *eco47IR* gene at a level sufficient to allow for positive selection. On the pET 28b+ image: Kan is the kanamycin gene conferring resistance to kanamycin, lacI is the promoter and f1 origin is the origin of replication (adapted from Novagen and Thermo Scientific).

Ligations into pET 28b(+) were carried out in a total reaction volume of 20 µl and consisted of 2 µl T4 DNA ligase buffer (10×), 7 µl pET 28b(+) vector (6.5 $ng.\mu l^{-1}$), 10 µl DNA insert (4.3 $ng.\mu l^{-1}$), 0.5 µl of 5 $U.\mu l^{-1}$ T4 DNA ligase with a 1:1 molar ratio of insert:vector DNA and 0.5 µl ddH_2O. The ligation reactions were incubated at 4 °C overnight. The plasmids were transformed into *E. coli* BL21(DE3) cells as described in section 2.3.7.

2.3.6. Chemically competent cell preparation

Competent *E. coli* JM109 and BL21(DE3) cells were prepared according to the method described by Inoue *et al*. (1990). Two test tubes containing 5 ml LB broth were inoculated with 5 µl stock JM109 or Bl21(DE3) cells and grown overnight at 37 °C on a shaker at 150 rpm. The cultures were used to inoculate two flasks containing 100 ml SOB media (20 $g.l^{-1}$ tryptone, 5 $g.l^{-1}$ yeast extract, 0.584 $g.l^{-1}$ NaCl, 0.186 $g.l^{-1}$ KCl, 2.034 $g.l^{-1}$ $MgCl_2$ and 2.464 $g.l^{-1}$ $MgSO_4$) and grown at 37 °C on a shaker at 150 rpm until an absorbance of ~0.55 at 600 nm was reached. The cells were put on ice for 10 minutes and then collected by centrifugation (2 500 ×g; 10 minutes; 4 °C). Cells were re-suspended in 80 ml ice cold TB buffer

(10 mM HEPES pH 6.7, 15 mM $CaCl_2$, 250 mM KCl and 55 mM $MnCl_2$) and incubated on ice for 10 minutes. Cells were collected by centrifugation (2 500 ×g; 10 minutes; 4 °C) and re-suspended in 20 ml TB buffer. DMSO to a final concentration of 7 % was added to 20 ml cell suspension. Cells (100 µl) were aliquoted in pre-cooled eppendorf tubes and snap frozen in liquid nitrogen followed by storage at -80 °C.

2.3.7. Transformation protocol

Competent *E. coli* cells were transformed with ligation mixture / plasmid. This was done by first retrieving an aliquot (section 2.3.6) from -80 °C and thawing it on ice. The ligation mixture / plasmid were added to the competent cells and the reaction mixture kept on ice for 30 minutes. This was followed by incubation at 42 °C for 42 seconds (heat-shock) and 2 minutes on ice. Two hundred and fifty microliters of pre-heated (37 °C) SOC media (SOB media supplemented with 20 $ml.l^{-1}$ of 1 M glucose after autoclaving) was added to the transformation mixture and incubated at 37 °C for 1 hour. Positive transformants were obtained by plating the transformation mixture onto antibiotic (ampicillin / kanamycin) containing LB agar plates and incubated overnight at 37 °C. Single colonies were inoculated into 5 ml LB broth containing the desired antibiotic (100 $\mu l.ml^{-1}$ ampicillin / 30 $\mu l.ml^{-1}$ kanamycin) to maintain selective pressure and grown overnight at 37 °C.

2.3.8. Plasmid extraction and restriction enzyme digestions

Plasmids were retrieved from the overnight cultures (section 2.3.7) using the BioFlux BioSpin Plasmid Extraction Kit as per manufacturer's recommendations (Bioer Technology Co., Ltd). The bacterial cells were spun down and pelleted in 1.5 ml Eppendorf tubes using an Eppendorf MiniSpin Plus microcentrifuge and then resuspended in re-suspension buffer. The cells were lysed by the addition of lysis buffer and neutralised before spinning down to separate the cell debris and the DNA containing supernatant. Using a spin column, the DNA in the supernatant was washed and eluted in 50 µl elution buffer. Restriction fragment length polymorphism (RFLP) was used as a screening method to verify insertion of the gene into the vector. The plasmid DNA was digested using *Eco*RI and *Nde*I in a 20 µl, double digestion reaction which consisted of 4 µl of 127 $\mu g.\mu l^{-1}$ *Pf*LAP (and 4 µl 131 $\mu g.\mu l^{-1}$ in the case of *Hs*LAP) plasmid

DNA, 2 µl of reaction buffer (buffer O), 0.4 µl *Eco*RI, 0.4 µl *Nde*I of 10 $U.\mu l^{-1}$ and 13.2 µl of ddH_2O. The reaction was incubated at 37 °C overnight. The mixture was separated on agarose gel and visualised as described in section 2.3.3.

2.3.9. Sequence verification

The plasmids with the desired gene (section 2.3.8) were sent to Inqaba Biotech™ for sequencing to confirm the nucleotide composition of the relevant gene. The DNA fragments were purified using Zymo Research Sequencing Clean-up Kit (Zymo Research) and subsequently analysed on a 3500xl Genetic Analyser (ABI, Life Technologies). The termination reactions were performed using BigDye version 3.1 (ABI, Life Technologies) according to the manufacturer's instructions. Electropherograms were analyzed and edited using Geospiza's FinchTV version 1.4.0. Reverse complementation was performed using BioEdit version 7.3.1.0. Sequence alignments were performed using DNAssist version 3.0.

2.3.10. Gene synthesis

The gene sequences for *Pf*LAP (3D7) and *Hs*LAP were obtained from the NCBI Genbank (accession codes: XM_001348577.1 and BC065564.1 respectively). The *Pf*LAP sequence was confirmed by performing a BLAST on the Plasmodb database. The *Pf*LAP gene sequence was truncated by the removal of the first 246 bases and base replacements were done as follows; (i) at position 454, A was replaced with C, (ii) at position 456, T was replaced with G, (iii) at position 1543, A was replaced with C, (iv) at position 1636, A was replaced with C and (v) at position 1638, T was replaced with G. The truncated and modified nucleotide sequences were translated into protein sequences using the software BioEdit version 7.3.1.0. The resulting amino acid sequences were checked for possible glycosylation sites using the post translational modification prediction tool from the ExPASy Bioinformatics Resource Portal website. The *Hs*LAP gene was not truncated but was only inspected for glycosylation sites

Artificial genes were optimised for expression in *E. coli* and synthesized by GenScript (GenScript USA Inc.). The genes were supplied in the pUC 57 vector which is shown in figure 2.2. Lyophilised plasmids were reconstituted in 20 µl Tris (10 mM; pH 8.0) before being

transformed into competent *E. coli* JM109 cells for plasmid propagation as described in section 2.3.7. The plasmids were extracted and subjected to RFLP analysis as described in section 2.3.8.

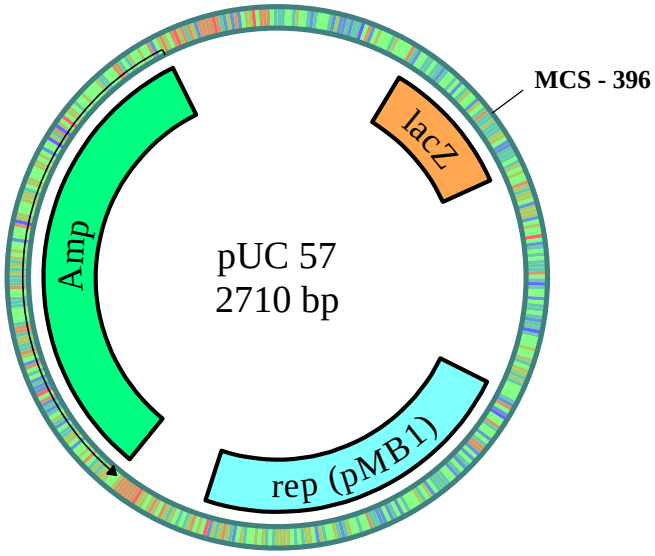

Figure 2.2 pUC 57 plasmid map. Amp is a gene conferring resistance to ampicillin, rep (pMB1) is a replicon from the pMBI plasmid responsible for the replication of the plasmid and lacZ is the promoter (adapted from GenScript).

The DNA bands corresponding to the correct size were cleaned from the gel as described in section 2.3.4 and sub-cloned into the pET 28b(+) expression vector as described in sections 2.3.5. Positive plasmids were sent for sequencing to confirm the nucleotide composition of the relevant genes (section 2.3.9) and the expression of the His-tag in the correct frame.

2.4. Results and discussions

2.4.1. Primer design and virtual cloning

In the present study the use of free online designing tools and free software were implemented in primer design and virtual cloning. Primer design is of paramount importance in running a successful PCR reaction. The design of primers that will efficiently produce the desired product is dependent on several factors namely; (i) T_m, (ii) primer length, (iii) primer G+C content, (iv) the 3′ end of the primer sequence, (v) and the lack of further possible hybridisation sites along the template (Wilson and Walker, 2007). Innis and Gelfand (1990) stated that ideally primers should have between 18 and 28 nucleotides and have a G+C content between 50 % and 60 %. *P.*

falciparum has the lowest reported G+C content (17-19 %) of a living organism, hence a compromise needed to be reached between keeping the primers within recommended lengths and getting the best G+C content (Pollack *et al*., 1981).

Due to the stronger hydrogen bonding between G and C compared to that between A and T, a good G+C content in a primer means annealing to the template during the reaction will be efficient. The *Pf*LAP forward primer was 27 nucleotides while the reverse primer was 34 nucleotides long. The G+C content for the forward primer was 23.5 % while that of the reverse primer was 37 % and this was the best possible G+C content and length combination for each of the primers. The use of pure cDNA as a template compared with the use of genomic DNA minimised the risk of non-specific primer/template binding and gave room for the design of short primers (Dieffenbach *et al*., 1993). Despite the use of *P. falciparum* cDNA as a template, short primers could not be designed due to low G+C content of the *Pf*LAP sequence.

The T_m of both primers was 53.4 °C, a temperature value close to that recommended by Innis and Gelfand (1990) (55-80 °C) and Dieffenbach *et al*. (1993) (54 °C). Li and Dahiya (2002) in their work on designing of primers for methylation PCRs encountered the problem of a low G+C content in the template and consequentially primer design difficulties. They also suggested the solution of designing longer primers as was done in the current study. The full length gene as described in section 2.3.1 was virtually cloned into the expression vector pET 28b(+). Virtual cloning was performed mainly as a step to verify that the cloning procedure would be feasible in practice using the designed primers. The software pDraw32 allows the entry of primers into its oligonucleotide database so that these can be used for any cloning procedure. A database of restriction endonucleases is built into the software and one is able to choose a pair relevant to their procedure.

The main property to look out for in the product was the expression of the His-tag in frame. This property would be essential for arguably the most important purification step downstream as shall be discussed in the next chapter. The plasmid map which resulted from virtual cloning of the full length *Pf*LAP into pET 28b(+) as described in sections 2.3.1 and 2.3.5 is shown in figure 2.3 for *Pf*LAP. The open reading frame of the expressed polypeptide was read to verify the in-

frame presence of the His-tag. The insert in figure 2.3 shows the open reading frame of the expressed protein, *Pf*LAP.

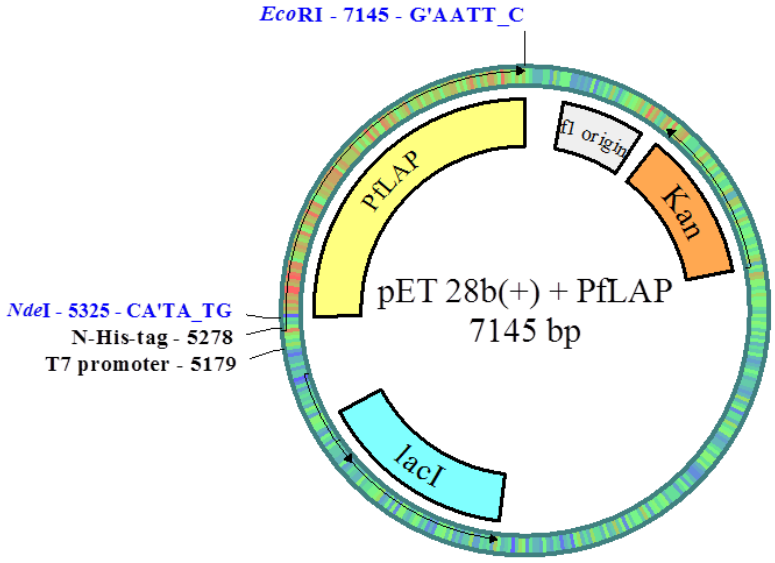


```
MGSSHHHHHHSSGLVPRGSHMYFSSLCKFLPISEKEKIYLNIVKKRFCKS 50
NIYYNNNNNNIINYNKRGLKFYPFCNNLKKNINFVNINNKKGINFHSINK 100
ERKMASEVPQVVSLDPTSIPIEYNTPIHDIKVQVYDIKGGCNVEEGLTIF 150
LVNNPGKENGPVKISSKVNDKNVSEFLKDENMEKFNVKLGTSKHFYMFND 200
NKNSVAVGYVGCGSVADLSEADMKRVVLSLVTMLHDNKLSKLTVVFEINV 250
DKNLFRFFLETLFYEYMTDERFKSTDKNVNMEYIKHLGVYINNADTYKEE 300
VEKARVYYFGTYYASQLIAAPSNYCNPVSLSNAAVELAQKLNLEYKILGV 350
KELEELKMGAYLSVGKGSMYPNKFIHLTYKSKGDVKKKIALVGKGITFDS 400
GGYNLKAAPGSMIDLMKFDMSGCAAVLGCAYCVGTLKPENVEIHFLSAVC 450
ENMVSKNSYRPGDIITASNGKTIEVGNTDAEGRLTLADALVYAEKLGVDY 500
IVDIATLTGAMLYSLGTSYAGVFGNNEELINKILNSSKTSNEPVWWLPII 550
NEYRATLNSKYADINNISSSVKASSIVASLFLKEFVQNTAWAHIDIAGVS 600
WNFKARKPKGFGVRLLTEFVLNDAL*
```

Figure 2.3 Plasmid map showing full length *Pf*LAP cloned into pET 28b(+) and *Pf*LAP open reading frame showing the N-terminal His-tag (adapted from Novagen).

2.4.2. PCR amplification

Successful PCR reactions which produce clean and specific products do not only result from meeting all primer design criteria as discussed in section 2.4.1. The standard PCR conditions can be customised to make up for whatever deficiencies exist in a set of primers (Rychlik, 2000). The components of the PCR reaction mixture and the length of the PCR steps are other factors that influence the efficiency of primers. It is also worth stating that the theoretical parameters which one obtains from using design software are not always true in practice as was observed in this study (Su *et al*., 1996). In order to design an optimised PCR reaction, gradient PCR was performed. Gradient PCR enables the assessment of the usability and efficiency of designed

primers in amplifying the desired template using concurrently running PCR reactions with ascending annealing temperatures (Crowe and Weitkamp, 2001). This method is important in identifying the specificity of primers and enables researchers to ascertain the usability of primers. In the current study a gradient of 15 °C between 50 and 65 °C was used to select the annealing temperature that gave the best PCR product as described in section 2.3.2. Almost all temperatures gave a fairly good PCR product at the expected size of approximately 1,8 kb corresponding to the size from NCBI as shown in figure 2.4.

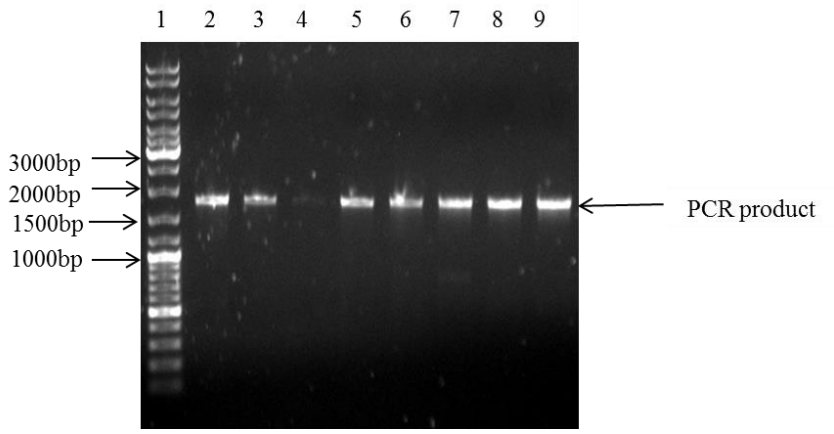

Figure 2.4 An agarose gel electrophoresis image showing the experimental determination of annealing temperature using gradient PCR. Lane 1; DNA ladder, Lanes 2-9; annealing temperatures of 50 °C, 51 °C, 52.9 °C, 55.7 °C, 59.1 °C, 62 °C, 63.8 °C and 65 °C respectively.

Prezioso and Jahns (2000) reported that the lowest annealing temperature should be 5 °C below the T_m of primers. However they concede that in practice the optimal annealing temperature is usually much higher than this lower limit by at least 12 °C. The current study seems to concur with these findings with the lower limit of 50 °C being 3.4 °C lower than the T_m of both primers and the optimal annealing temperature of choice being 15 °C above this temperature. Although figure 2.4 shows a significant amount of PCR product across the gradient, the bands between 62 °C and 65 °C had the best results in terms of the band quality and product quantity hence the choice was narrowed to these. Lopez and Prezioso (2001) state that higher annealing temperatures enhance the specificity of primers as this creates strict conditions for the process to occur thereby minimising the formation of non-specific products hence an optimal annealing temperature of 65 °C was selected. The optimised PCR reaction was performed as described in section 2.3.2 and the results (shown in figure 2.5.) indicated a good yield of the PCR product.

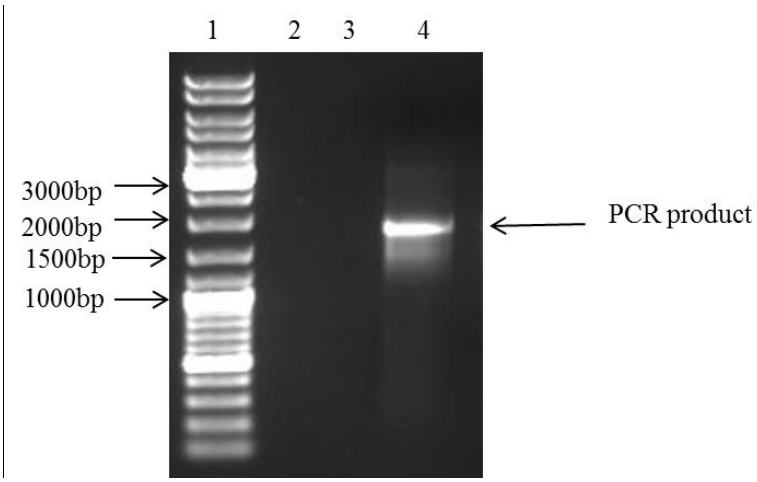

Figure 2.5 Agarose gel electrophoresis image showing the results of the optimised PCR reaction. The DNA ladder was run in lane 1 while the PCR product was run in lane 4 giving a product of ~1,800 bp. Lanes 2 and 3 were left empty to allow easy visualisation of the product.

The PCR program was initiated with a denaturation step of 3 minutes at 98 °C as recommended by the manufacturer (Finnzymes). This recommendation is echoed by Prezioso and Jahns (2000) who state that between a 1 to 5 minute denaturation step is necessary at the start of the PCR reaction. They claim this could serve to further optimise the reaction as it allows for the inactivation of any nucleases, while ensuring the complete denaturation of templates of higher complexity. Caution should however be taken regarding the length of the denaturation step to prevent the denaturation of the polymerase enzyme which would compromise the integrity of the amplification reactions. The polymerase used in the present study was Phusion hot start II DNA polymerase which is claimed to withstand denaturation temperatures greater than 98 °C and produces a blunt ended PCR product. Phusion *Taq* is only activated at high temperatures, which allows preparation at room temperatures and not on ice, without possibilities of unspecific binding of primers before the reaction has been initiated.

The elongation temperature used was 60 °C, a temperature 12 °C lower than the standard reaction temperature of 72 °C due to the high A+T content of the *P. falciparum* genome (Pollack *et al.*, 1981; Webber, 1987; Su *et al.*, 1996). Findings by Su and co-workers (1996) indicate that this reduction in elongation temperature is vital for the successful elongation of the high A+T content of *P. falciparum*. Webber (1987) reported that the *P. falciparum* genome has the highest

A+T content (82 %) reported for any organism and the coding regions of the genome have 69 % A+T content.

2.4.3. Cloning and sequencing

The gel purified PCR product (sections 2.3.2) was ligated into CloneJet® vector (section 2.3.5) where further proliferation in *E. coli* was achieved. After agarose gel electrophoresis (section 2.3.3), the PCR product was excised and cleaned from the agarose gel as described in section (2.3.4) and cloned into the CloneJet® vector as described in section 2.3.5. CloneJet® is a linearized cloning vector which accepts blunt end PCR products such as the one generated by Phusion hot start II DNA polymerase used in the current study. Figure 2.6 shows the *Pf*LAP gene cloned into CloneJet®.

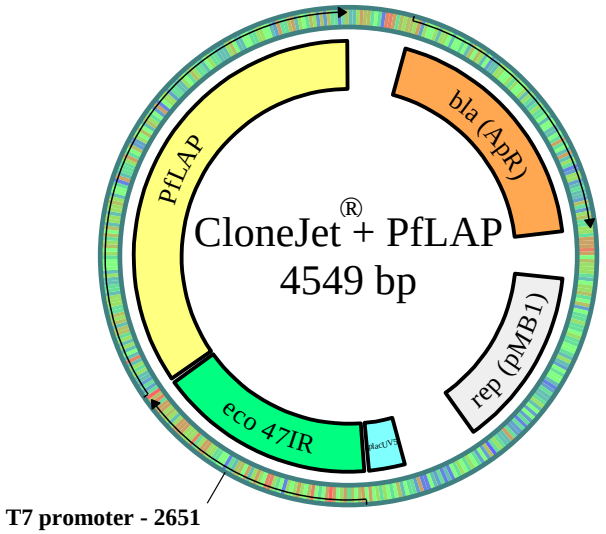

Figure 2.6 CloneJet® plasmid maps showing *Pf*LAP ligated into the cloning vector (adapted from Thermo Scientific).

Struhl (1987) reported that T4 DNA ligase is able to join blunt ended DNA fragments, though this process occurs with less efficiency than the joining of sticky ends. This therefore results in the requirements for higher concentrations of insert DNA and ligase. The blunt end cloning ratio of insert to plasmid in the current study was 3:1 compared to the 1:1 in the sticky end cloning of insert into pET 28b(+). This confirms Struhl's claims on the need for a higher insert concentration when conducting blunt end cloning. However the amount of ligase used in this study remained the same for both blunt and sticky end ligations, which yielded satisfactory

results. Once the PCR product had been ligated to the cloning vector (section 2.3.5), transformation into *E. coli* JM109 cells and propagation was done (section 2.3.7).

CloneJet® contains a lethal gene (eco 47I^R on the plasmid map in figure 2.1) which is disrupted by the PCR product when it is ligated to the vector as shown in figures 2.6. However if the vector ligates onto itself this gene is expressed and the cells that would have taken up such plasmids do not grow. Ampicillin resistance is another selectable marker which is present in CloneJet® (bla Ap^R on the plasmid map on figure 2.1) and this was used to enhance the selection pressure for positive transformants. The positive transformants were harvested and the cloned plasmids were extracted and double digested using the restriction enzymes *Eco*RI and *Nde*I (section 2.3.8). Figure 2.7 shows the restriction digest profiles of different colonies grown in LB broth. These plasmids were extracted and digested as described in section 2.3.8 and then run on agarose gel as described in section 2.3.3.

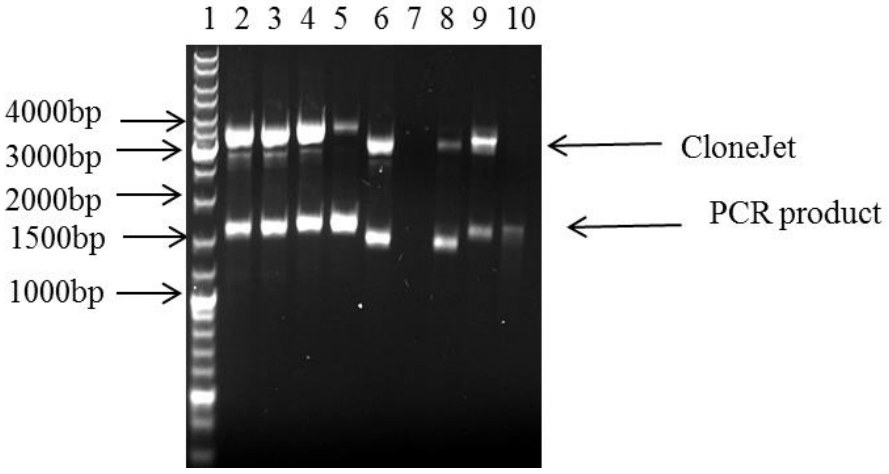

Figure 2.7 Agarose gel electrophoresis image showing the results of the double digestion of CloneJet® housing *Pf*LAP. Plasmids were extracted from positive clones and subjected to an overnight digestion by *Eco*RI and *Nde*I. Lane 1: DNA ladder; lanes 2-9: DNA fragments after double digestion of plasmids. The PCR product was run in lane 10.

A DNA band representative of the CloneJet® backbone (2.974 kb) was observed in wells 2-4, 6 and 8-9. The PCR product previously obtained from the amplification of the *Pf*LAP coding sequence was run in lane 10 as a control to help identify the insert band. Samples in lanes 2-6 and 8-9 all showed a band at the position representative of the insert. However the sample in lane

9 was selected and sent for sequencing (section 2.3.9) as it showed two distinct bands, the plasmid backbone and the insert.

2.4.4. Sequence analysis

Sequence analysis was done as described in section 2.3.9. The resulting nucleotide sequence was analysed and the result indicated the absence of the insert in the CloneJet® plasmid. This was contrary to the results seen on the gel image. The whole procedure from PCR to cloning into the cloning vector was repeated using Roche *Taq* polymerase which facilitates sticky end cloning and pGEMTeasy. Various trouble shooting techniques were employed with no success. These included PCR using the plasmid sent for sequencing as a template to prove that the insert was indeed present. The double digestion results all confirmed the presence of the insert. However the sequencing results still reflected no insert in the plasmid despite its appearance on gel images. There was no logical explanation for these results and alternative avenues were explored to facilitate the cloning of the *Pf*LAP gene into the expression vector. It was opted to have both the *P. falciparum* and human LAP genes synthesized as outlined in section 2.3.10.

2.4.5. Artificial gene synthesis

The *Hs*LAP and *Pf*LAP sequences were analysed before being sent for the final synthesis at GenScript. The *Pf*LAP sequence was truncated as outlined in section 2.3.10 as previously done by Stack *et al*. (2007) and Cunningham *et al*. (2007). The *Pf*LAP catalytic domain is located at the C-terminal of the polypeptide and the enzyme still folds correctly and maintains catalysis despite the removal of the asparagine rich region on the N-terminal of the polypeptide (Stack *et al*., 2007). Stack *et al.* (2007) reported that the expression of the full length *Pf*LAP in *E. coli* and in the yeast *Pichia pastoris* gave an inactive protein. McGowan *et al.* (2009) however managed to express the truncated version of the enzyme in *E. coli* BL21(DE3) cells. Given the expression system available for use in the current study [*E. coli* BL21(DE3)], it was decided to follow suit. One of the major drawbacks of using the *E. coli* expression system is the lack of post translational modification machinery in the *E. coli* cells (Sudhir *et al*., 2007). For this reason all possible glycosylation sites on both coding sequences were removed after analysis using the post translational modification prediction tool from the ExPASy Bioinformatics Resource Portal website. The *Hs*LAP coding sequence was analysed and checked for glycosylation sites and

these were removed as described in section 2.3.10. Different species and groups of living organisms make use of the genetic code in ways that vary one organism to another (Grosjean and Fiers, 1982). Sorensen *et al.* (1989) reported that the rate of translation of mRNA is codon specific. This means that a codon systematically selected by one organism to code for a particular amino acid may not be the codon of choice for efficient translation in another organism. Due to this phenomenon, both sequences were codon optimised for expression in *E. coli* by GenScript before synthesis. The genes were supplied in the pUC57 vector as illustrated in figure 2.8. Figure 2.9 (a) shows the amino acid sequence alignment of the *Pf*LAP complete polypeptide and the truncated, optimised version of the polypeptide.

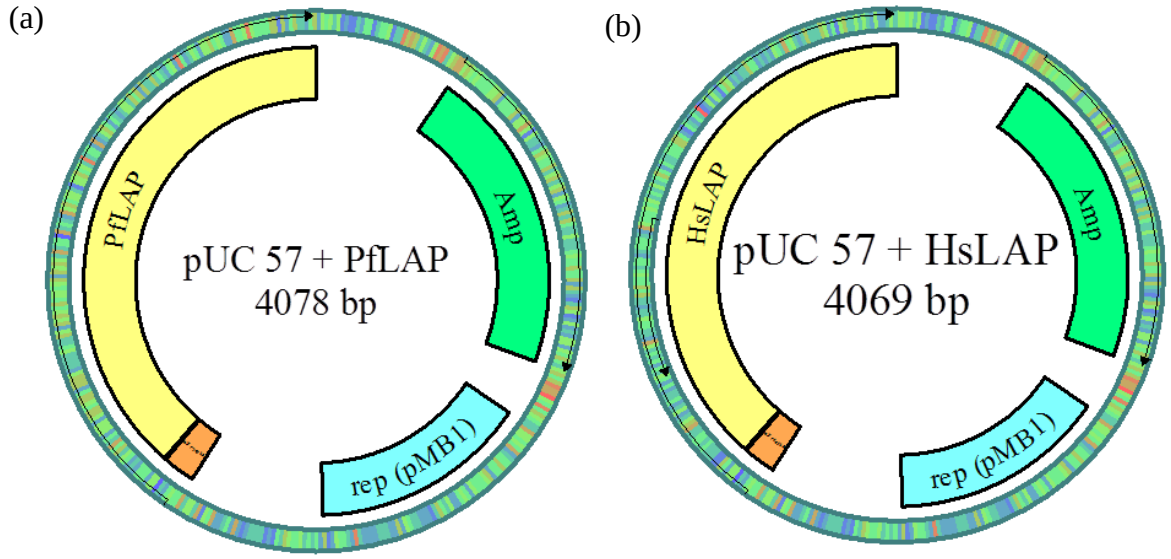

Figure 2.8 The *Pf*LAP (truncated) (a) and *Hs*LAP (b) genes optimized for expression in *E. coli* were supplied in the pUC57 plasmid (adapted from GenScript).

The truncation and editing as described in section 2.3.10 facilitated the removal of the first 82 amino acid residues and the replacement of asparagine residues at positions 152, 515, and 546 with glutamines on the *Pf*LAP polypeptide. The N-terminal asparagine rich region is responsible for the presence of N-linked glycosylation sites in *Pf*LAP hence its removal from the polypeptide. Asparagine residues at positions 152, 515, and 546 (illustrated by green background in figure 2.9(a) were all part of Asn-*X*-(Thr/Ser) motifs which are glycosylation sites (Stack *et al*., 2007). There was only one glycosylation site in *Hs*LAP as illustrated by the green background in figure 2.9(b) and the rest of the sequence remained unchanged. Many differences

still existed in the nucleotide sequences coding for these two proteins due to the codon optimization process which takes advantage of the degeneracy of the genetic code.

(a)

```
 Full PfLAP      MYFSSLCKFLPISEKEKIYLNIVKKRFCKSNIYYNNNNNNIINYNKRGLKFYPFCNNLKKNI 62
Truncated PfLAP                                                               0

Full PfLAP      NFVNINNKKGINFHSINKERKMASEVPQVVSLDPTSIPIEYNTPIHDIKVQVYDIKGGCNVE 124
Truncated PfLAP                     KMASEVPQVVSLDPTSIPIEYNTPIHDIKVQVYDIKGGCNVE  42

Full PfLAP      EGLTIFLVNNPGKENGPVKISSKVNDKNVSEFLKDENMEKFNVKLGTSKHFYMFNDNKNSVA 186
Truncated PfLAP EGLTIFLVNNPGKENGPVKISSKVNDKQVSEFLKDENMEKFNVKLGTSKHFYMFNDNKNSVA 104

Full PfLAP      VGYVGCGSVADLSEADMKRVVLSLVTMLHDNKLSKLTVVFEINVDKNLFRFFLETLFYEYMT 248
Truncated PfLAP VGYVGCGSVADLSEADMKRVVLSLVTMLHDNKLSKLTVVFEINVDKNLFRFFLETLFYEYMT 166

Full PfLAP      DERFKSTDKNVNMEYIKHLGVYINNADTYKEEVEKARVYYFGTYYASQLIAAPSNYCNPVSL 310
Truncated PfLAP DERFKSTDKNVNMEYIKHLGVYINNADTYKEEVEKARVYYFGTYYASQLIAAPSNYCNPVSL 228

Full PfLAP      SNAAVELAQKLNLEYKILGVKELEELKMGAYLSVGKGSMYPNKFIHLTYKSKGDVKKKIALV 372
Truncated PfLAP SNAAVELAQKLNLEYKILGVKELEELKMGAYLSVGKGSMYPNKFIHLTYKSKGDVKKKIALV 290

Full PfLAP      GKGITFDSGGYNLKAAPGSMIDLMKFDMSGCAAVLGCAYCVGTLKPENVEIHFLSAVCENMV 434
Truncated PfLAP GKGITFDSGGYNLKAAPGSMIDLMKFDMSGCAAVLGCAYCVGTLKPENVEIHFLSAVCENMV 352

Full PfLAP      SKNSYRPGDIITASNGKTIEVGNTDAEGRLTLADALVYAEKLGVDYIVDIATLTGAMLYSLG 496
Truncated PfLAP SKNSYRPGDIITASNGKTIEVGNTDAEGRLTLADALVYAEKLGVDYIVDIATLTGAMLYSLG 414

Full PfLAP      TSYAGVFGNNEELINKILNSSKTSNEPVWWLPIINEYRATLNSKYADINNISSSVKASSIVA 558
Truncated PfLAP TSYAGVFGNNEELINKILQSSKTSNEPVWWLPIINEYRATLNSKYADINQISSSVKASSIVA 476

Full PfLAP      SLFLKEFVQNTAWAHIDIAGVSWNFKARKPKGFGVRLLTEFVLNDAL 605
Truncated PfLAP SLFLKEFVQNTAWAHIDIAGVSWNFKARKPKGFGVRLLTEFVLNDAL 523
```

(b)

```
HsLAP            MFLLPLPAAGRVVVRRLAVRRFGSRSLSTADMTKGLVLGIYSKEKEDDVPQFTSAGENFDK  61
Opt HsLAP       HMFLLPLPAAGRVVVRRLAVRRFGSRSLSTADMTKGLVLGIYSKEKEDDVPQFTSAGENFDK  62

HsLAP           LLAGKLRETLNISGPPLKAGKTRTFYGLHQDFPSVVLVGLGKKAAGIDEQENWHEGKENIRA 123
Opt HsLAP       LLAGKLRETLQISGPPLKAGKTRTFYGLHQDFPSVVLVGLGKKAAGIDEQENWHEGKENIRA 124

HsLAP           AVAAGCRQIQDLELSSVEVDPCGDAQAAAEGAVLGLYEYDDLKQKKKMAVSAKLYGSGDQEA 185
Opt HsLAP       AVAAGCRQIQDLELSSVEVDPCGDAQAAAEGAVLGLYEYDDLKQKKKMAVSAKLYGSGDQEA 186

HsLAP           WQKGVLFASGQNLARQLMETPANEMTPTRFAEIIEKNLKSASSKTEVHIRPKSWIEEQAMGS 247
Opt HsLAP       WQKGVLFASGQNLARQLMETPANEMTPTRFAEIIEKNLKSASSKTEVHIRPKSWIEEQAMGS 248

HsLAP           FLSVAKGSDEPPVFLEIHYKGSPNANEPPLVFVGKGITFDSGGISIKASANMDLMRADMGGA 309
Opt HsLAP       FLSVAKGSDEPPVFLEIHYKGSPNANEPPLVFVGKGITFDSGGISIKASANMDLMRADMGGA 310

HsLAP           ATICSAIVSAAKLNLPINIIGLAPLCENMPSGKANKPGDVVRAKNGKTIQVDNTDAEGRLIL 371
Opt HsLAP       ATICSAIVSAAKLNLPINIIGLAPLCENMPSGKANKPGDVVRAKNGKTIQVDNTDAEGRLIL 372

HsLAP           ADALCYAHTFNPKVILNAATLTGAMDVALGSGATGVFTNSSWLWNKLFEASIETGDRVWRMP 433
Opt HsLAP       ADALCYAHTFNPKVILNAATLTGAMDVALGSGATGVFTNSSWLWNKLFEASIETGDRVWRMP 434

HsLAP           LFEHYTRQVVDCQLADVNNIGKYRSAGACTAAAFLKEFVTHPKWAHLDIAGVMTNKDEVPYL 495
Opt HsLAP       LFEHYTRQVVDCQLADVNNIGKYRSAGACTAAAFLKEFVTHPKWAHLDIAGVMTNKDEVPYL 496

HsLAP           RKGMTGRPTRTLIEFLLRFSQDNA  519
Opt HsLAP       RKGMTGRPTRTLIEFLLRFSQDNAE 521
```

Figure 2.9 Alignment of (a) truncated and optimised *Pf*LAP amino acid sequence with that of the full length amino acid sequence (b) optimised *Hs*LAP amino acid sequence with that of the native amino acid sequence.

2.4.6. Sub-cloning

The synthesized genes (sections 2.3.10) were digested from the pUC 57 (section 2.3.8) cloning vectors and sub-cloned into the pET 28b(+) expression vector as described in sections 2.3.5 and as shown in figure 2.10.

(a)

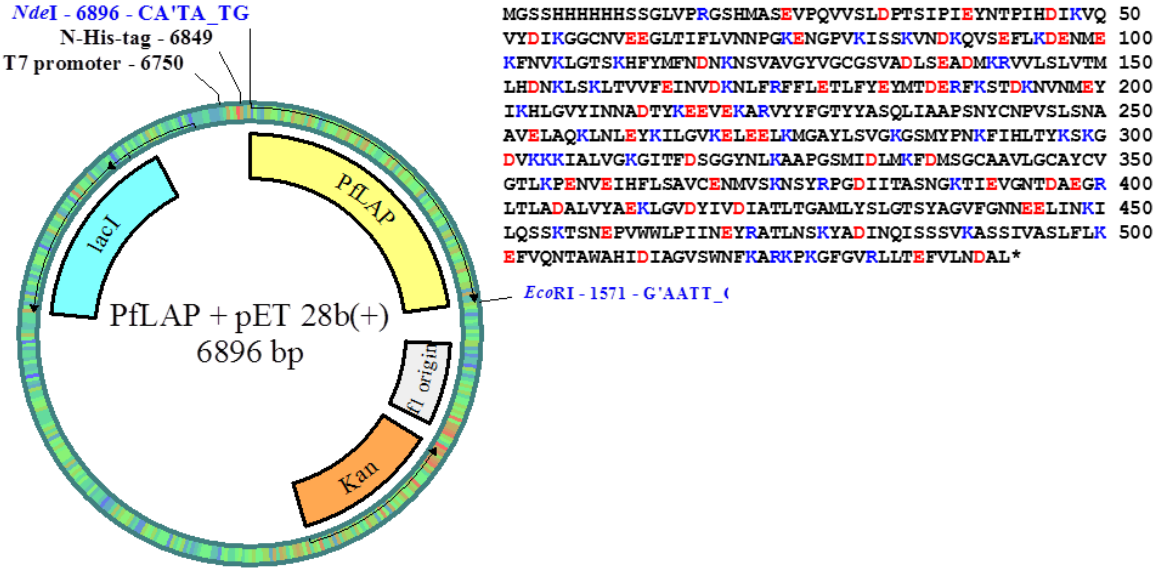

(b)

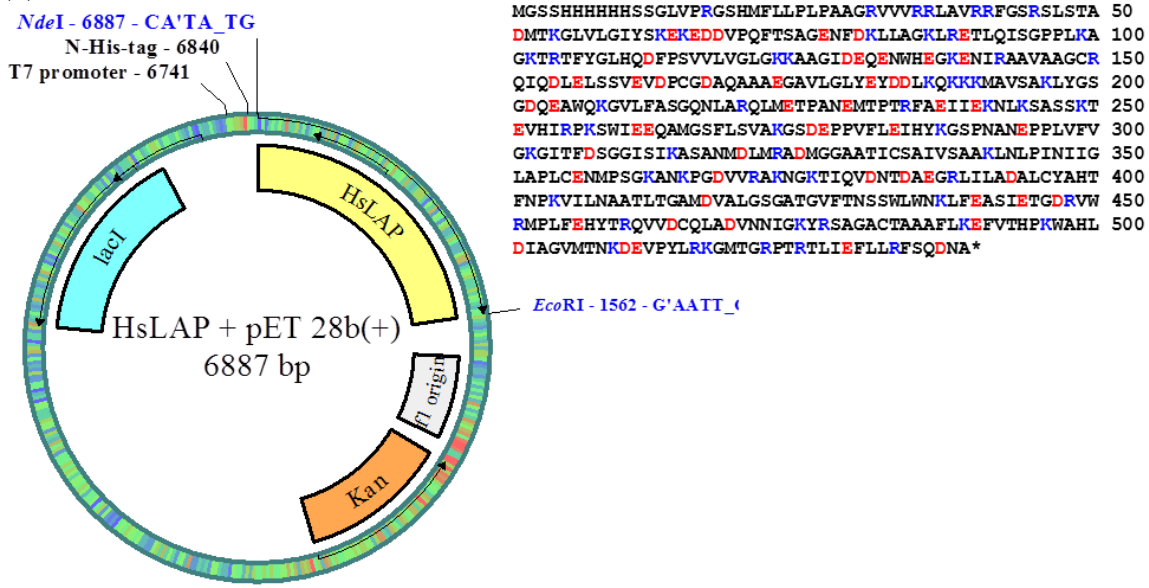

Figure 2.10 Plasmid maps of (a) *Pf*LAP and (b) *Hs*LAP cloned into pET 28b(+) and the open reading frames of the expressed enzymes. The inserts show that the genes were cloned in frame with the His-tag (adapted from Novagen).

The insertion of the genes into the vector was verified by screening reactions as described in section 2.3.8. The results of the double digestion reactions are shown in figure 2.11.

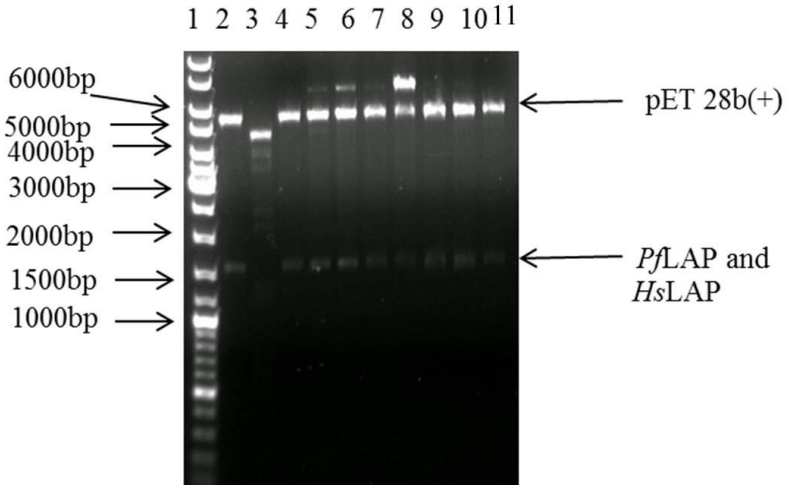

Figure 2.11 Agarose gel electrophoresis image showing the results of the double digestion of pET 28b(+) housing *Pf*LAP (lanes 2-6) and *Hs*LAP (lanes 7-11). DNA ladder was loaded into the first lane. Inserts were observed at ~1.5 kb for both *Pf*LAP and *Hs*LAP samples and a PET 28b(+) band was observed at ~5.4 kb.

Figure 2.11 shows that the sub-cloning of both *Pf*LAP and *Hs*LAP into pET 28b(+) was successful as insert and plasmid backbone DNA bands were observed on most samples run on the agarose gel. Samples from lane 2 (*Pf*LAP) and lane 11 (*Hs*LAP) were selected and sent for sequencing as these profiles reflected clean samples. The gel pattern was mainly as expected and showed predominant 2 bands, one plasmid backbone and one insert. Lanes 5-8 however exhibited another band above the plasmid backbone band and this is indicative of undigested plasmid. Sequencing (section 2.3.9) confirmed the inserts to be *Pf*LAP and *Hs*LAP. Confirmation was done through aligning the obtained sequences to the known sequences (section 2.3.9).

2.4.7. Expression constructs

Following sequence confirmation of the inserts of the desired genes in the expression vectors (section 2.4.6) the constructs were transformed into the expression cell lines to transcribe and translate the genetic information into a protein as described in section 2.3.7.

2.5. Conclusions

Primer design, virtual cloning and PCR were successfully performed and yielded a 1.8 kb *Pf*LAP gene as confirmed by agarose gel electrophoresis and the use of a DNA ladder. The PCR product was ligated using blunt end ligation into the cloning vector (CloneJet®) and propagated in *E. coli* JM109 cells before screening and sequencing. Positive transformants were confirmed using selectable markers and further by double digestion of the plasmids extracted from the cells. Despite the appearance of the *Pf*LAP PCR product on the agarose gels on which the double digestion samples of CloneJet® were run, sequencing results gave only the presence of the plasmid backbone without the insert. After a number of repetitions and obtaining the same results, gene synthesis was opted for as a method of obtaining the LAP genes.

The reasons for the failure of sequencing to identify the *Pf*LAP which appeared on the gel images remain ambiguous and cannot be explained. To date we could not find any reports on the expression and/or characterisation of the human cytosolic LAP. Because a DNA template for the PCR amplification of the *Hs*LAP gene was not available, it had been originally planned to have this gene synthesised and cloned into an expression vector. The two genes were synthesised and jumped into the expression vector. Gel images of double digestion reactions followed by sequencing confirmed positive inserts. Competent *E.coli* BL21(DE3) were chemically prepared and successfully transformed with the expression vector housing each of the LAP genes using the heat shock method. Once transformed, the BL21(DE3) cells were ready for protein expression, which will be discussed in chapter 3.

Chapter 3: Expression and purification of LAP

3.1. Introduction

Twentieth century advances in biotechnology and a better understanding of genetics have resulted in a large number of gene sequencing projects which have availed coding sequences of many proteins across all living organisms (Kunst *et al*., 1997; Venter *et al*., 2001; Gardner *et al*., 2002; Giaever *et al*., 2002). Recombinant DNA technology has made it possible to clone these coding sequences into expression vectors that are tailored to direct the over-expression of the analogous proteins in the appropriate expression system (Johnson, 1983). Small and large scale production of virtually any protein can now be accomplished through the fermentation of cells housing the expression vector.

3.1.1. Expression systems

There are various expression systems that can be used for the over-expression of proteins, namely; (i) bacteria such as *E. coli* (Miroux and Walker, 1996), *Bacillus subtilis* (Kabisch *et al*., 2013) and *Pseudomonas putida* (Timmis, 2002), (ii) yeast such as *Sacharomyces cerevisiae* (Bitter and Egan, 1984; Mellor *et al*., 1984) and *Pichia pastoris* (Cereghino and Cregg, 2000), (iii) insect cell cultures (Stack *et al*., 2007), (iv) plant cell cultures (Hellwig *et al*., 2004), (v) transgenic plants (Giddings *et al*., 2000; Ma *et al*., 2003), (vi) mammalian cell cultures (Wurm, 2004) and (vii) transgenic animals (Pollock *et al*., 1999; Houdebine, 2008). Of these systems, expression in *E. coli* remains the favourite choice of researchers because of factors such as (i) the affordable carbon source growth requirements, (ii) the relatively high protein yields obtained, (iii) the ability to grow in high density cultures and (iv) the vast knowledge available and understanding of the physiology, genetics and the biochemistry of *E. coli* which makes its manipulation fairly easy (Studier, 2005; Sahdev *et al*., 2008). However the inability to secrete proteins extracellularly, the formation of insoluble inclusion bodies and the lack of post-translational modification machinery, among other factors, limit the usability of the *E. coli* expression system (Palomares *et al*., 2004; Hannig and Makrides, 1998).

Advances in biochemistry have helped circumvent some of these problems by developing strategies to make the *E. coli* expression system able to accommodate the successful production of proteins which can be further modified to induce activity (Hannig and Makrides, 1998). The most widely used expression vectors for protein expression in *E. coli* are the pET system vectors. Protein expression, in these vector systems is driven by the T7 promoter which facilitates the production of T7 RNA polymerase which in turn facilitates the transcription of coding sequences and the consequent expression of the desired protein. Proteins produced this way are called recombinant proteins (Studier and Moffatt, 1986; Studier, 1991).

3.1.2. Purification strategies

Once a protein has been expressed, it can be extracted from the host cells by treatment with lysozyme or subjecting the cells to ultrasonic treatment and further purified by various downstream methods. The cell-free lysate is a mixture of the host cell proteins, nucleic acids and polysaccharides among other cell components. The recombinant proteins must be separated from the host cell proteins as pure protein is needed for the characterisation experiments. Vectors such as pET 28a-c(+) carry a sequence coding for 6 histidine residues on either the N-terminal or the C-terminal of the protein to be expressed. This facilitates downstream purification using immobilized metal affinity chromatography (IMAC). In this method separation is through the binding of the His-tagged protein to metal ions which are immobilized onto the supporting material (e.g. silica beads) via a chelating ligand such as nitroloacetic acid (NTA). The metal ions known to have an affinity for histidine include Ni^{2+}, Cu^{2+}, Zn^{2+} and Co^{2+} (Hochuli *et al*., 1987; Block *et al*., 2009).

Other chelating ligands that have been used for IMAC include iminodiacetic acid (IDA) and N,N,N´-tris(carboxymethyl)ethylenediamine (TED) (Hochuli *et al*., 1987). The chelating ligands differ in the way they coordinate with metal ions. NTA is a tetradentate ligand which means that it coordinates with four binding sites on the metal ion while leaving the rest for protein binding (Gaberc-Porekar and Menart, 2001). IDA and TED differ from NTA in that while NTA is tetradentate, they are tridentate and pentadentate, respectively (Hochuli *et al*., 1987; Gaberc-Porekar and Menart, 2001). Figure 3.1 shows a model of the interaction of the chelating ligands with the supporting material and His-tagged proteins. The His-tagged proteins can be batch

absorbed onto the chelating ligand beads by mixing the sample with beads and then pouring the mixture into a column where low affinity binding proteins can be eluted using low imidazole concentrations while His-tagged proteins are eluted using higher imidazole concentrations. Alternatively the sample can be run through a column packed with agarose beads bound to NTA and nickel ions. His-tagged proteins can be eluted competitively by running a linear gradient of increasing imidazole concentrations or through the protonation of histidine residues which is done by decreasing the pH (Bolanos-Garcia and Davies, 2006).

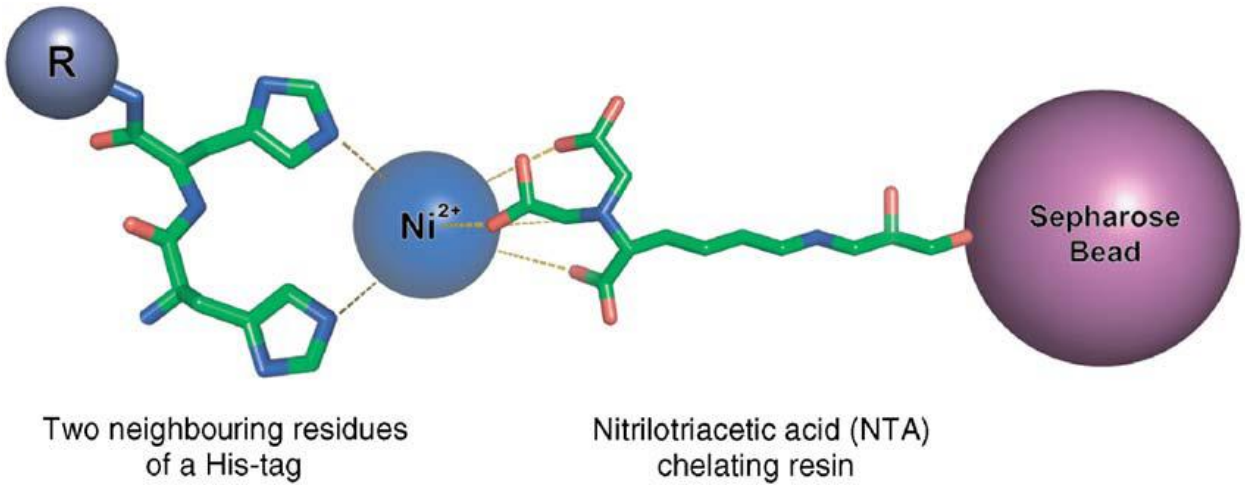

Figure 3.1 IMAC mechanism. Ni^{2+} is coordinated to NTA which in turn is attached to the sepharose resin. Attachment of the Ni^{2+} with NTA is via four of six coordination sites present on Ni^{2+}. This leaves two sites which are available for coordination with histidine residues on His-tagged proteins (taken from Bolanos-Garcia and Davies, 2006).

The protein sample post IMAC contains high concentrations of imidazole and may also contain contaminating proteins. Further purification can be accomplished through size exclusion chromatography (SEC), dialysis or desalting methods. SEC separates molecules according to variations in sizes. The medium is a porous gel through which the sample is applied and separates due to size differences, some molecules make their way through the pores in the gel beads and hence elute later than the ones that run through the spaces between gel beads (void volume). Gels used for SEC are composed of cross-linked hydrophilic chains, which although inert, are highly polar owing to the hydroxyl groups in their structure (Porath and Flodin, 1959). Commonly used gels include (i) sephadex and sephacryl which are cross-linked dextran gels (ii) sepharose which is made from agarose (Andrew, 1964; Romanowska, 1970). There are other

gels made from other materials such as polyacrylamide, agar and starch which also have good separation properties (Laurent and Killander, 1963). Unlike IMAC, SEC does not involve the binding of the protein to the matrix and the protein can be collected in any buffer (GE healthcare, 2010).

Dialysis involves separating molecules based on their molecular size using a semi-permeable membrane to allow passage of smaller molecules while retaining larger ones. The semi-permeable membrane is made from cellulose fibres and has a pre-determined pore size (Dennison, 1999). Dialysis can be used as a method of removing salts or smaller proteins from recombinant protein samples. The principle behind desalting is the same as SEC and the two processes use the same type of medium for separation. Compared to dialysis, desalting has several advantages such as rapidity, the absence of buffer change steps and the re-usability of gels. Once the desalted protein has been isolated, sodium dodecyl sulphate polyacrylamide gel electrophoresis (SDS-PAGE) can be used to estimate its purity and to check if it is of the expected size (Graslund *et al*., 2008).

3.1.3. Enzyme kinetics

Enzyme kinetics involves the investigation of the catalytic behaviour of enzymes and the factors affecting the rates of enzyme catalysed reactions (Bisswanger, 2008). These factors include enzyme concentration, substrate concentration, the presence of inhibitors or activators, the pH, temperature and ionic strength of the reaction mixture (Segel, 1951). Enzyme kinetics is important in elucidating mechanisms by which enzymes catalyse reactions and their regulation. Most enzyme catalysed reactions that have been studied exhibit a rectangular hyperbolic relationship between the reaction velocity (v) and the substrate concentration [S] (Eisenthal and Cornish-Bowden, 1973). This relationship is best explained by the Michaelis-Menten equation (equation 1).

Equation 1: $$v = V_{max}\,[S]/(K_m + [S])$$

The Michaelis-Menten equation is an important equation of enzyme kinetics and it describes the dependence of an enzyme reaction on substrate concentration. The characterisation of an enzyme

catalysed reaction involves the determination of two constants, namely V_{max} and K_m. V_{max} is the reaction velocity approached when the substrate concentration is at saturation and points to a point in the reaction where the rate of the reaction no longer depends on the [S] (Copeland, 2000). K_m is the substrate concentration at half V_{max} and reflects the affinity of the enzyme for a particular substrate and the catalytic efficiency of the enzyme. Low values of K_m indicate high affinity while high values indicate poor affinity (Gilbert, 2000). Another way of expressing V_{max} is k_{cat}, which is a measure of the turnover rate of an enzyme (Bisswanger, 2008). The ratio k_{cat} /K_m is a reflection of the catalytic efficiency or the specificity of an enzyme and high values depict high efficiency and specificity (Bisswanger, 2008).

The characterisation of an enzyme catalysed reaction involves the experimental determination of V_{max} and K_m. This is done by conducting enzyme assays under varying substrate concentrations and plotting *v* against [S]. Subsequent characterisation steps may involve the investigation of the role of cofactors, inhibitors or activators. The determination of accurate values of V_{max} and K_m from the plot of *v* against [S] is a complicated feat since V_{max} can only be "approached" and not reached (Eisenthal and Cornish-Bowden, 1973). Methods for the determination of constants V_{max} and K_m are vital to enzyme kinetics and substantial efforts have been implemented in generating mathematically robust methods for getting the most credible estimates of these constants (Ritchie and Prvan, 1996). Three linear transformations of equation 1 have been adopted to derive the kinetic constants V_{max} and K_m. These linearization methods include the Lineweaver-Burke plot, the Eadie-Hofstee plot and the Hanes-Woolf plot and they are represented by the equations 2, 3 and 4, respectively (Ritchie and Prvan, 1996).

Equation 2: $$\mathbf{1/v = K_m/V_{max}[S] + 1/V_{max}}$$

Equation 3: $$\mathbf{v = K_m v/[S] + V_{max}}$$

Equation 4: $$\mathbf{[S]/v = 1/V_{max}\,([S]) + K_m/V_{max}}$$

Using these transformations, the exact values of kinetic constants can be derived from the intercepts of the axes as shown in figure 3.2.

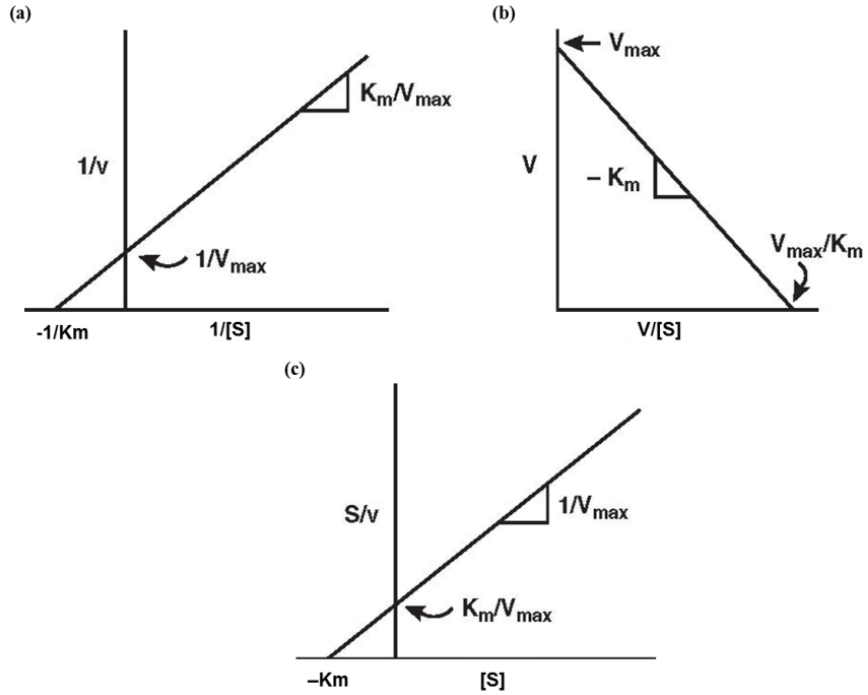

Figure 3.2 Linear transformation graphs showing the derivation of K_m and V_{max} or values from which K_m and V_{max} can be calculated using the slopes or the intercepts. (a) Lineweaver-Burke plot, (b) Eadie-Hofstee plot and (c) Hanes-Woolf plot (taken from Gilbert, 2000).

The plots in figure 3.2 all have margins of error and therefore each has a bias to some extent. The Lineweaver-Burke plot is the most widely used plot even though it is known to be the least credible (Ritchie and Prvan, 1996). Figure 3.3 shows error limits in the various transformations of the Michaelis-Menten equation. Error bars show that velocities at low substrate concentrations are heavily biased when using the Lineweaver-Burke transformation. The Eadie-Hofstee transformation has (*v*) on both axes, making it liable to errors as neither of the axes is independent of velocity. Error bars also indicate that at high substrate concentrations the transformation is significantly biased. From figure 3.3 it is clear that the transformation most credible as far as its depiction of the Michaelis-Menten data is concerned is the Hanes-Woolf plot (Bisswanger, 2008).

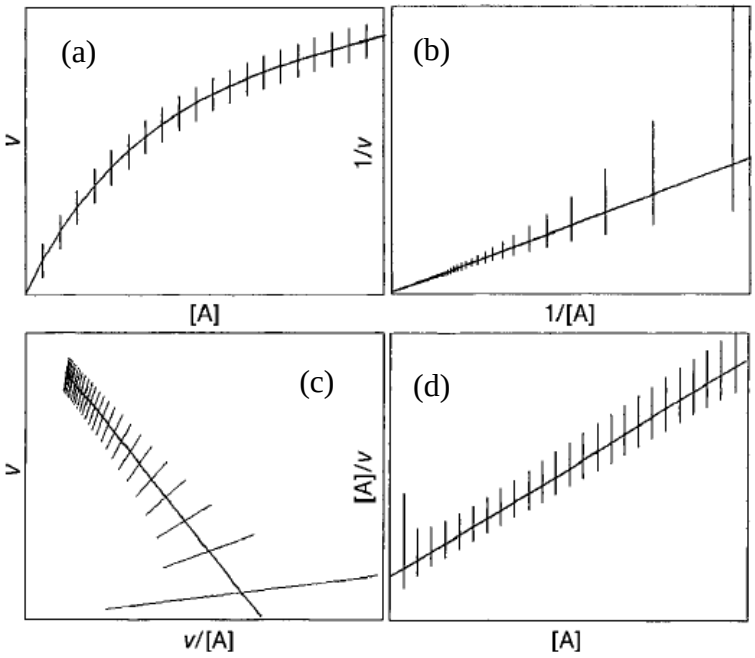

Figure 3.3 Margins of error associated with the different transformations of the Michaelis-Menten equation assuming an absolute constant error. (a) Direct plot of *v* against [S], (b) Lineweaver-Burke plot, (c) Eadie-Hofstee plot, (d) Hanes-Woolf plot (taken from Bisswanger, 2008).

3.2. Aims and objectives

The aims of this section included the over-expression of both the *Pf*LAP and *Hs*LAP in *E. coli* BL21(DE3) cells using the expression vectors obtained in the previous chapter, lysis of the cells, and the purification of the enzymes from the crude cell extracts. Purification methods used included centrifugation, IMAC, SEC and desalting. After each of these steps, SDS-PAGE was used to confirm the presence of the desired proteins in the sample and to evaluate its purity. Once the pure protein was obtained, characterisation was performed using an optimized enzyme assay. The parameters on which the enzymes were characterised included the effects of divalent metal ions on enzyme activity, temperature stability, pH stability, and the determination of the constants of each enzyme. The purpose of all these steps was to obtain the optimal conditions of stability for each of the enzymes and their reaction kinetics so as to use these as a standard against which the effects on metallic nanoparticles would be compared.

3.3. Methods and materials

3.3.1. Protein concentration determination

Protein concentration determinations were conducted using the bicinchoninic acid (BCA) (4,4'-dicarboxy-2,2'-biquinoline) method (Smith *et al.,* 1985). The assay is sensitive between 10 μg.ml^{-1} and several mg.ml^{-1}. A Thermo Scientific kit was used according to the manufacturer's instructions. Bovine serum albumin (BSA) was used for the construction of the standard curves. A set of protein standards was prepared with bovine BSA and 50 μl of each standard / unknown sample was mixed with 1 ml of the working reagent and swiftly vortexed prior to incubation at 37 °C or 60 °C for 30 minutes. After incubation absorbance values were read at 562 nm using a Spectroquant® Pharo 300 (Merck) spectrophotometer. In the present study protein concentrations of up to 1 000 μg.ml^{-1} fell within the linear range and could be detected using the incubation at 37 °C, while protein concentrations between 25 and 250 μg.ml^{-1} could be detected using the 60 °C incubation. The standard curves obtained are shown in figure 3.4.

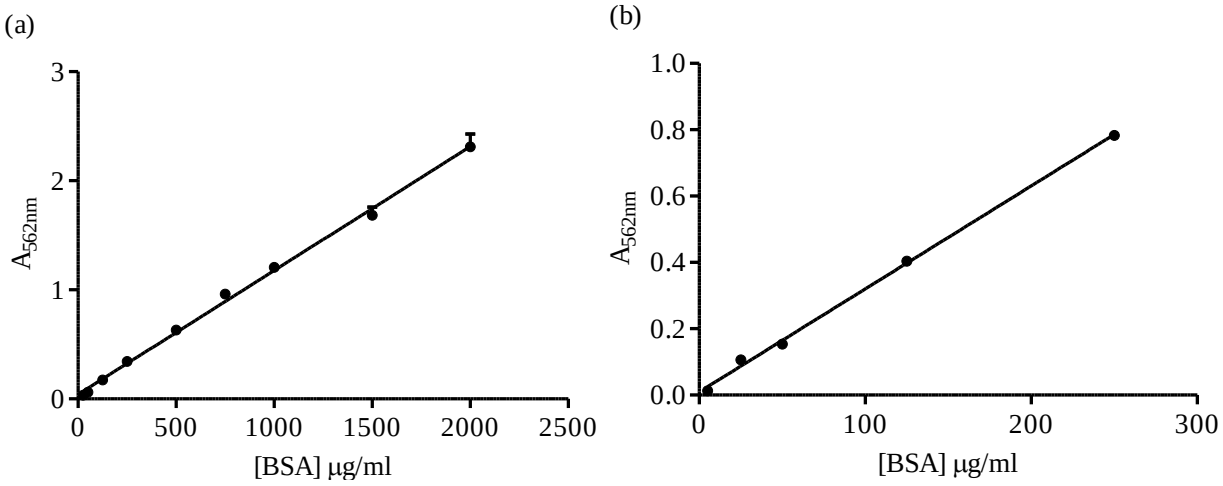

Figure 3.4 Standard curves constructed to determine unknown protein concentrations using the BCA protein assay with BSA as the protein standard (a) 37 °C and (b) 60 °C. Error bars represent the standard deviation among results.

3.3.2. Polyacrylamide gel electrophoresis

3.3.2.1.SDS-PAGE analysis

SDS-PAGE was performed with 4 % polyacrylamide stacking and 10 % polyacrylamide separating gels in a Tris-Glycine buffer system using the protocol described by Laemmli (1970). Samples were mixed in a 1:1 ratio with loading dye (50 μl TD + 200 μl TS), heated at 100 °C for

10 minutes on a BIO-RAD Digital Dry Bath heating block and loaded onto the gel. For each gel electrophoresis run, 10 µl of molecular weight marker (PageRuler™ Prestained Protein Ladder, size range 10-170 kDa; Thermo Scientific) was run alongside the samples. Electrophoresis was performed using the BioRad Mini-PROTEAN® Tetra Cell and a BioRad PowerPac™ power supply at 100 constant volts for 2 hours. A modification of the Fairbanks *et al*. (1971) method was used to stain and de-stain SDS-PAGE gels to enable visualization of the proteins. This method involves staining the gels with Coomassie Brilliant Blue R250 overnight on a BioRad UltraRocker rocking platform at 50 rpm. De-staining was done by a series of heating and cooling cycles in solutions of descending concentrations of Coomassie Brilliant Blue R250 (Fairbanks solutions A, B, C, and D). Once de-stained, bands of proteins equal to or greater than 5 ng could be visualized with the naked eye.

3.3.2.2.Native PAGE

Native PAGE was performed with 4 % polyacrylamide stacking and 10% polyacrylamide separating gels in a Tris-Glycine buffer system. Samples were mixed in a 1:1 ratio with native TS loading dye. Electrophoresis was performed using the BioRad Mini-PROTEAN® Tetra Cell and a BioRad PowerPac™ power supply at 100 constant volts for 6 hours at room temperature. Staining and de-staining of the native gels was done as described in section 3.3.2.1.

3.3.3. Induction studies

Induction studies were done to verify the over-expression of the LAPs and to determine optimum incubation time during expression. This was done by using a negative control which involved transforming BL21(DE3) cells with empty pET 28b(+). These cultures were grown alongside the cells containing the plasmid housing the LAP gene and samples from both cultures were taken at regular time intervals, centrifuged and the pellet kept for SDS-PAGE analysis to check for protein expression. The pellet was re-suspended in 1 ml 50 mM Tris, pH 8.0 and sonicated for 30 seconds using a Vibra Cell™ Sonics and Materials Inc. USA at 60 % output. The concentration of protein in each of the samples was determined using the BCA method described in section 3.3.1. The samples were adjusted to equal protein concentrations and subjected to SDS-PAGE as described in section 3.3.2.1.

3.3.4. Over-expression of LAP

The enzyme-pET 28b(+) constructs (section 2.3.5) were transformed into *E. coli* BL21(DE3) chemically competent cells for expression as described in section 2.3.7. Transformed cultures were grown overnight at 37 °C on LB agar plates containing 30 μg.ml^{-1} kanamycin. Bacterial colonies were sub-cultured into 50 ml LB media and grown over night at 37 °C. Cells were sub-cultured in auto-induction media (1 % N-Z-amine, 0.5 % yeast extract, 50 mM Na_2HPO_4, 50 mM KH_2PO_4, 25 mM $(NH_4)_2SO_4$, 2 mM $MgSO_4$, 0.5 % glycerol, 0.05 % glucose, 0.2 % lactose) (Sturdier, 2005) on a Labcon shaker at 140 rpm for 36 hours at 20 °C.

3.3.5. LAP purification

3.3.5.1.Harvesting and cell lysis

Biomass obtained from protein expression (section 3.3.4) was collected by centrifugation and washed thrice (5 000 ×*g*, 15 minutes, 4 °C) using 50 mM Tris pH 8.0. All centrifugation steps were performed using an Avanti JE centrifuge (Coulter Beckman, USA). Washed biomass was re-suspended in 50 mM Tris pH 8.0 in a cell:buffer ratio of 1:20 wet weight. Cell lysis was performed by adding lysozyme (1 mg.ml^{-1}) to the cell suspension followed by incubation at 37 °C (160 rpm, 1 hour). Lysozyme activity was halted by the immediate freezing of the sample at -80 °C for a minimum of 2 hours. This step also served to create ice crystals in the cells which aid in the rupturing of the cell membranes and the subsequent release of the cell contents upon defrosting. Cell suspensions were removed from -80 °C and allowed to thaw at 4 °C for downstream purification.

Cell debris was removed from the suspension through centrifugation (2900 ×*g*, 30 minutes, 4 °C) and the resulting supernatant was subjected to ultracentrifugation (100 000 ×*g*, 90 minutes, 4 °C) using an Optima L-90K (Coulter Beckman) ultracentrifuge to separate the cytoplasmic fraction from the membrane fraction. Samples of the centrifuged and ultracentrifuged supernatants were stored for SDS-PAGE analysis, protein concentration determination and for enzyme assays in order to construct a purification table. Caution was exercised throughout all purification steps to ensure solutions were always at 4 °C. This was achieved by using pre-chilled equipment where applicable.

3.3.5.2.Immobilized metal affinity chromatography

The soluble fraction obtained after ultracentrifugation (section 3.3.5.1) was mixed with 4× binding buffer to a final concentration of 1× binding buffer (20 mM Tris pH 7.4; 0.5 M NaCl; 20 mM imidazole). The resulting protein solution was loaded into a Superloop™ 150 ml (GE Healthcare) sample loop connected to a HisTrap FF column (5 ml, GE Healthcare) which was in turn connected to an AKTA fast protein liquid chromatography (FPLC) machine (GE Healthcare). The HisTrap FF column had been equilibrated with 1× binding buffer. Unbound proteins were eluted from the column with 50 ml binding buffer at a flow rate of 1 $ml.min^{-1}$. Bound proteins were eluted from the column using a linear gradient from 0-100% elution buffer (20 mM Tris pH 7.4; 500 mM NaCl; 500 mM imidazole) over 100 ml. Fractions of 5 ml were collected for the volume used to create the linear gradient. A sample of the eluent was stored for SDS-PAGE analysis, protein concentration determination and for enzyme assays in order to construct a purification table. The sample collection test tubes, binding and elution buffers were chilled prior to IMAC and kept on ice throughout the whole process.

3.3.5.3.Size exclusion chromatography

IMAC samples corresponding to the UV absorbance peak and confirmed by SDS-PAGE results were pooled and concentrated down to < 2 ml using Vivaspin6 columns (Sartorius Stedim Biotech) in an Eppendorf 5810R Centrifuge (4000 ×*g*; 4 °C). Two drops of glycerol were added to the sample before loading it onto a Sephacryl S100HR (GE Healthcare XK16/100) (1000 mm height, 16 mm internal diameter) column at a flow rate of 1 $ml.min^{-1}$ pre-equilibrated with 50 mM Tris buffer, pH 8.0, containing 50 mM NaCl. The proteins were eluted in the same buffer. However the duration (~6 hours) and the ambient temperatures at which SEC was carried out led to the total loss of enzyme activity, resulting in the adaptation of the desalting method (section 3.3.5.4).

3.3.5.4.Desalting

IMAC samples corresponding to the UV absorbance peak and confirmed by SDS-PAGE results were pooled and concentrated down to 2.5 ml using Vivaspin6 columns (Sartorius Stedim Biotech) in an Eppendorf 5810R Centrifuge (4 000 ×*g*; 4 °C). The 2.5 ml concentrated sample

was loaded onto an 8.3 ml Sephadex™ G-25 PD-10 desalting column (GE Healthcare) equilibrated with 25 ml of 50 mM Tris pH 8.0 at 4 °C. LAP was eluted with 3.5 ml of the same buffer under gravity according manufacturer's instructions. After elution glycerol was added to the enzyme to a final concentration of 10 % to help maintain stability. A sample of the eluent was stored for SDS-PAGE analysis, protein concentration determination and for enzyme assays in order to construct a purification table.

3.3.6. LAP assay

For the determination of LAP activity, 130 µl of 50 mM Tris pH 8.0 containing 2 mM $MnCl_2$ and10 µl of L-leucine *p*-nitroanilide (L*p*NA) were incubated at 37 °C in a Synergy MX (BioTek®) thermostated spectrophotometer and the absorbance monitored at 405 nm until constant. The reaction was initiated by adding 10 µl of LAP. The mixture was immediately shaken for 5 seconds to allow mixing. Absorbance readings at 405 nm were recorded for 5 minutes at 15 second intervals. A blank reaction was run alongside the test reaction in which the 10 µl enzyme solution was substituted with 10 µl Tris buffer pH 8.0. For the activity determination of *Pf*LAP, an extra control was incorporated in which the 10 µl substrate solution was substituted with 10 µl Tris buffer pH 8.0. This was done after observing that the enzyme and the buffer cross-reacted and produced an increase of absorbance which was independent of the enzyme activity on the substrate. The enzyme rate (ΔA_{405nm}/minute) was calculated using the maximum linear rate for both the test and blank reactions. One unit is defined as the amount of enzyme that will hydrolyze 1.0 µmole of L*p*NA to L-leucine and *p*-nitroaniline per minute. The final assay mixture contained 47 mM Tris buffer, 1.3 mM of L-leucine-*p*-nitroanilide and varying concentrations of enzyme which depended on the purification batch used (Tuppy *et al*., 1962). Enzyme activity was calculated using equation 5:

Equation 5*:*

$$\text{Units/ml enzyme} = \frac{(\Delta A405\ \text{nm/min Test} - \Delta A405\ \text{nm/min blank})(0.15)}{0.0099 \times 0.01}$$

Where:

0.15 = total volume of assay (in ml)

0.0099 = micromolar extinction coefficient of *p*-nitroaniline at 405 nm (Tuppy *et al*., 1962)

0.01 = Volume of enzyme used (in ml).

3.3.7. LAP zymogram

Two native PAGE gels were prepared as described in section 3.3.2.2 and 20 µl of protein were loaded into a well on each of the 2 gels. After native PAGE (section 3.3.2.2), one of the gels was washed twice with distilled water for 10 minutes and equilibrated with 50 mM Tris buffer, pH 8.0, twice for 5 minutes. Equilibration was followed by incubating the gel in a 0.0015 % w/v L*p*NA solution for 10 minutes at 37 °C. Diazotization of liberated *p*-nitroaniline was done at room temperature by immersing the gel into freshly made 0.1 % w/v sodium nitrite solution in 1 M HCl for 2 minutes. Excess sodium nitrite was removed with 1 % w/v urea, and the reaction was continued for 30 seconds by gentle shaking of the gel. The diazotized gel was then immersed into a 0.025 % w/v 1-naphthylamine solution in 22 % v/v ethanol with gentle agitation until a distinct pink azo dye formed (5 minutes) (Bozic and Vujcic, 2005). The duplicate gel was stained with Coomassie Brilliant Blue R250 (section 3.3.2.1) to show that the pink azo dye band corresponded to the Coomassie stained band.

3.3.8. Western blotting

Purified LAPs separated using SDS-PAGE (section 3.3.2.1) were transferred to nitrocellulose membrane, pre-soaked in ddH_20 and transfer buffer [13 mM Tris-HCL, 100 mM glycine and 20 % (v/v) methanol] for 10 minutes each, using a semi-dry Transblot (LASEC, USA) at a constant amplitude of 400 mA for 50 minutes. Protein transfer onto nitrocellulose was confirmed by Ponceau staining [0.5 % (w/v) Ponceau S in 1 % (v/v) glacial acetic acid]. Nitrocellulose membranes with transferred proteins were blocked with 1 % Blotto [non-fat dry milk (Santa Cruz Biotechnology) in Tris-buffered saline-Tween (TBST; 50 mM Tris, pH 7.5, 150 mM NaCl, 1 % {v/v} Tween20)] for 30 minutes and incubated with His-probe [Rabbit polyclonal; Santa Cruz Biotechnology (sc-8040)] overnight at 4 °C with agitation, diluted 1 in 1000 in 1 % Blotto. The membrane was rinsed four times in TBST for 15 minutes replacing the TBST each rinse. The membrane was incubated with species-specific anti-Rabbit IgG conjugated to horseradish peroxidase [HRP] (AbCAM, ab6802) at 1:5000 dilution in 1 % Blotto for 45 minutes with agitation at room temperature. After secondary antibody incubation, the membrane was rinsed four times with TBST for 15 minutes each, replacing the TBST at each rinse. Detection of

protein bands was performed using the Clarity Western ECL Substrate kit (Biorad; UK) with visualization of chemi-illuminescence on x-ray film (AGFA, USA).

3.3.9. Enzyme characterization

3.3.9.1. LAP metal ion dependence

The effects of divalent metal ions on the activity of both *Pf*LAP and *Hs*LAP were evaluated using the metal chloride salts of five metals, namely Zn, Mg, Co, Ca and Mn. Each of the metal chlorides was incorporated in the assay buffer to the final concentration of 0.01 μM, 0.1 μM, 1 μM and 2 μM. For each assay, a control in which the enzyme sample was substituted with 50 mM Tris pH 8.0 was run. Assays were performed as described in section 3.3.6. The percentage activity increase was calculated by using the enzyme reaction in the absence of metal ions as the baseline activity.

3.3.9.2. Temperature stability studies

The stability of each of the LAPs at different temperatures was studied over a period of 3 hours. Prior to each stability study, serial dilutions followed by enzyme assays were performed to obtain the enzyme concentration giving optimum activity. BioRad Digital Dry Bath heating blocks were set to the desired temperatures 30 minutes prior to experimental start time. The enzyme samples at different test temperatures were used for assays as described in section 3.3.6 at times 0, 15, 30, 45, 60, 75, 90, 120 and 180 minutes. Controls were run alongside each of these experiments with each temperature having its own control which consisted of 50 mM Tris pH 8.0. Percentage relative activity was calculated using the highest activity at a given time across the temperature range as the 100 % activity.

3.3.9.3. pH stability studies

pH stability studies were conducted at the temperature of optimum stability obtained from the study described in section 3.3.9.2 which was 25 °C for *Pf*LAP and 37 °C for *Hs*LAP. Prior to each stability study, serial dilutions followed by enzyme assays were performed to obtain the enzyme concentration giving optimum activity (section 3.3.9.2). An equimolar cocktail of

different buffer salts covering a pH range between 4 and 10 was used to conduct pH studies. The buffer salt composition and the pH range covered by each salt are shown in table 3.1.

Table 3.1 Components of the cocktail buffer covering a pH range of 3-10.

Buffer salt	pH range covered
Sodium acetate	3 – 5.5
2(N-morpholino)ethane sulfonic acid (MES)	5.5 – 7
Tris	7–9
2(cyclohexylamino)ethane sulfonic acid (CHES)	8.6–10

The initial enzyme concentration was 2× that of the enzyme concentration giving optimal activity (section 3.3.9.2) before being mixed with the relevant test buffer in a 1:1 ratio. After dilution of the enzyme with the buffer, samples were immediately taken for enzyme assays that represented the 0 minutes sample. The rest of the samples were incubated at the temperature of optimum stability for subsequent assays at 15, 30, 45, 60, 75, 90, 120 and 180 minutes. Controls were run alongside the assays at each pH. Each control consisted of one part 50 mM Tris pH 8.0 and one part of the relevant test buffer, all mixed to the same volume as the enzyme – test buffer mixture. Percentage relative activity was calculated using the highest activity at a given time across the temperature range as the 100 % activity.

3.3.10. Kinetic studies

The determination of the kinetic parameters (K_m and V_{max}) of *Pf*LAP and *Hs*LAP was performed by running the enzyme assays as described in section 3.3.6 with a few parameters changed as per enzyme characterization results. Serial dilutions were performed where necessary in order to have a constant enzyme concentration for all studies on one enzyme. For the kinetic studies of *Pf*LAP, the enzyme was incubated at 25 °C in Tris pH 8.0 for 15 minutes prior to its addition to the assay reaction; the control sample in which the enzyme was substituted by 50 mM Tris pH 8.0 was also treated the same way. *Hs*LAP kinetic studies were similar to those of *Pf*LAP with variations in temperature and pH of 37 °C and 7, respectively. Guided by literature, substrate concentration range finding was performed by monitoring the trend in enzyme activity at various substrate concentrations (Kohno *et al*., 1985; Chi *et al*., 2007; Pokharel and Rathaur, 2007).

Eventually a range between 1 mM and 100 mM was selected, with the specific concentrations being 1, 2, 5, 10, 20, 30, 50, 75 and 100 mM L*p*NA. Velocity was plotted against substrate concentration to obtain the Michaelis-Menten kinetic graph. To aid in obtaining accurate values of K_m and V_{max}, the Hanes-Woolf transformation of the Michaelis-Menten equation was used by plotting [S]/*v* against [S]. From the Hanes-Woolf graph, K_m and V_{max} were obtained as described in section 3.1.3. The turnover number k_{cat} was obtained by dividing V_{max} by the total enzyme concentration. k_{cat}/K_m was also calculated to determine the catalytic efficiency of the LAP enzymes.

3.4. Results and discussions

3.4.1. Over-expression of LAP

The over-expression of LAP enzymes was achieved using the *E. coli* – T7 RNA polymerase expression system. This system is arguably the mostly used expression system for the production of recombinant proteins and its advantages are stated in section 3.1.1 (Miroux and Walker, 1996). In the current study both *Pf*LAP and *Hs*LAP were expressed in *E. coli* BL21(DE3) using auto-induction media as described in section 3.3.4. Induction study results are shown in figures 3.5 and 3.6. The figures clearly show the over-expression of both the *Plasmodium* and the *Homo sapiens* forms of LAP as evidenced by the prominent protein bands at ~58 kDa. The level of expression as shown by these figures is high and confirms the reports by Studier and Moffat (1986) that when induced, *E. coli* cells can redirect its cell machinery to produce the target protein to levels as high as 50 % of the total cell protein.

Stack *et al.* (2007) expressed *Pf*LAP as a 320 kDa homo-hexamer with 60 kDa subunits from a truncated sequence similar to the one used in the current study. The size of *Pf*LAP in the present study was 58.231 kDa as calculated using the online Protein Calculator version 3.3. This size is in the same region with the results obtained by Stack *et al.* (2007) and the protein band on the SDS PAGE is slightly below the theoretical size. No published records on the expression and purification of cytosolic *Hs*LAP could be found hence records on its size were unavailable. However Kohno *et al.* (1986) characterised LAP purified from the human liver and found it to be a hexamer consisting of three hetero-dimers with subunits of 53 kDa and 65kDa per dimer. In the

present study the size of *Hs*LAP, as calculated using online Protein Calculator version 3.3, was 56.594 kDa. A band was observed at about 55 kDa and this was believed to be *Hs*LAP.

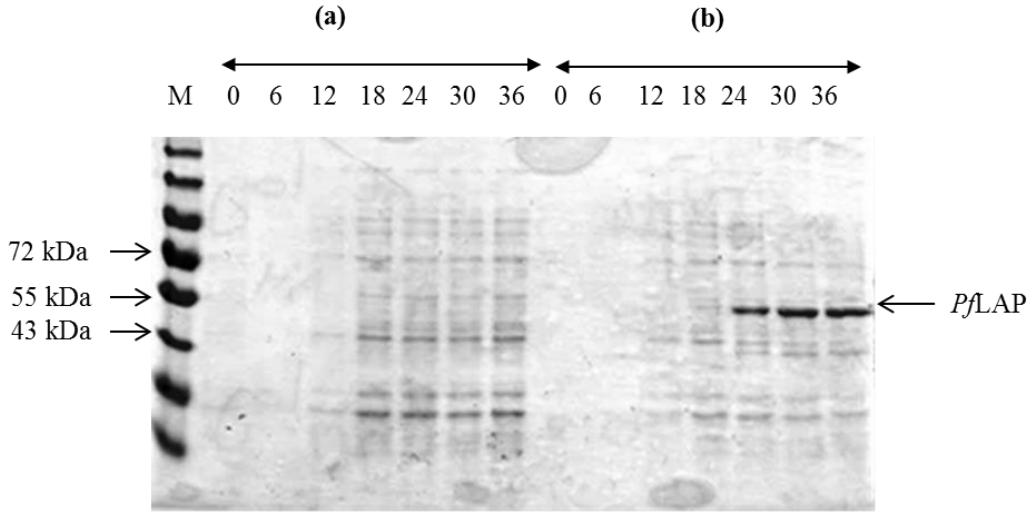

Figure 3.5 SDS-PAGE analysis (10% under reducing conditions) of samples collected for *Pf*LAP induction study. (a) Samples collected from the negative control culture (section 3.3.3) over 36 hours, (b) samples collected from the culture expressing *Pf*LAP over 36 hours.

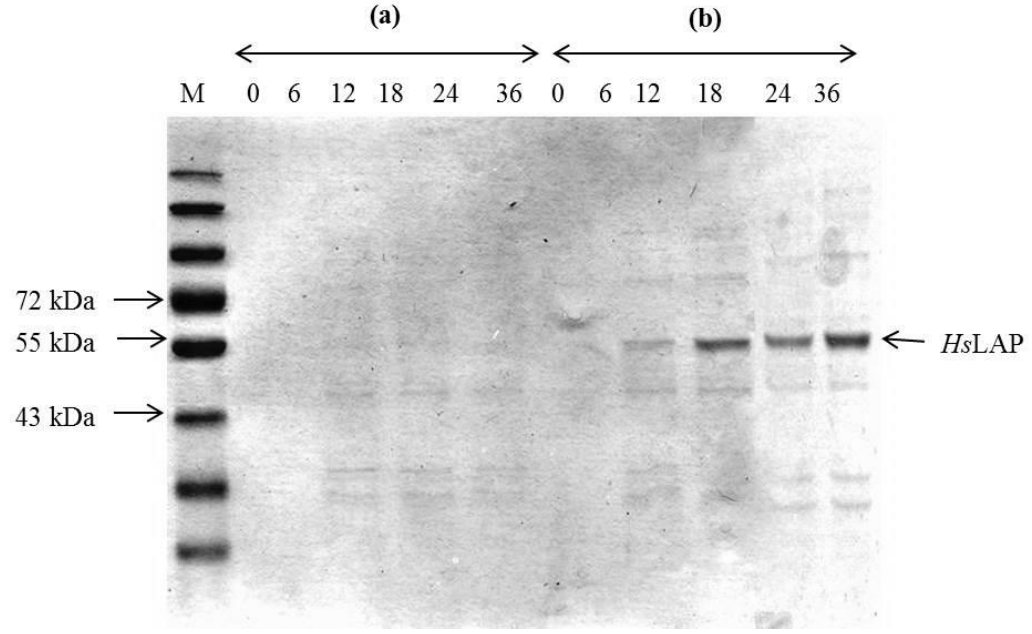

Figure 3.6 SDS-PAGE analysis (10%, under reducing conditions) of samples collected for *Hs*LAP induction study. (a) Samples collected from the negative control culture (section 3.3.3) over 36 hours, (b) samples collected from the culture expressing *Hs*LAP over 36 hours.

Detectable levels of *Hs*LAP were observed after 12 hours incubation (figure 3.6) compared to *Pf*LAP (figure 3.5) where detectable levels were only observed after 24 hours. The production of recombinant proteins in a recombinant system alters the metabolic activity of the host cells as the majority of the cell's resources are diverted into target protein production. These resources can be in the form of raw materials or energy and their diversion from the normal metabolic uses creates a "metabolic burden" in a cell (Sorensen and Mortensen, 2004; Palomares *et al*., 2004). The early induction of *Hs*LAP compared to that of *Pf*LAP means that the cell division in the *Pf*LAP media occurs more extensively prior to induction than it does in *Hs*LAP where the metabolic burden of protein expression becomes a restricting factor. At the time of induction, much more cells were involved in the expression of *Pf*LAP than *Hs*LAP hence the sharp increase of *Pf*LAP concentration between 18 and 24 hours compared to the gradual increase of *Hs*LAP between 12 and 24 hours. The data obtained from the induction studies was used to determine the length of the incubation in the final production of both LAPs. For the production of *Hs*LAP, incubation was allowed to proceed for 36 hours while *Pf*LAP production was sufficient between the 24^{th} and the 30^{th} hours. However for the purposes of standardisation, both processes were allowed to proceed for 36 hours.

3.4.2. Purification of *Pf*LAP

Purification was started with the harvesting of cells after 36 hours of incubation as concluded in section 3.4.1. The cell biomass was washed thrice in buffer before lysing using lysozyme as described in section 3.3.5.1. After enzymatic lysis the cells were resuspended in buffer and frozen at -80 °C before thawing and the subsequent removal of cellular debris using centrifugation. Enzymatic lysis alongside other traditional methods such as sonication and the French press involve the total lysis of the host cell and consequently the contamination of the target protein with all the cellular proteins naturally found in the host. This necessitates the need for robust purification procedures downstream. Johnson and Hecht (1994) presented a freeze thaw method of the whole host cells as a way of harvesting the recombinant proteins without lysing the whole cells and as a result obtaining a more pure protein than when implementing the procedure used in the current study (section 3.3.5.1). The freeze thaw cycles disrupt the membrane structure and cause pores on the membrane of the *E. coli* cells while lysozyme digests

the cell wall (Johnson and Hecht, 1994). Therefore the use of both lysozyme and the freeze thaw methods were deemed appropriate in the present study as each of the methods compromises each of the barriers holding the desired recombinant protein within the cell. The freeze thaw method alone has been demonstrated to work but it involves three cycles of freezing and thawing which may result in loss of enzyme activity. After cell lysis, the insoluble biomass is separated from the soluble matter through ultracentrifugation. The soluble matter contains the recombinant protein and native *E. coli* proteins as is the case with the total lysis of cells. Separation of the *E. coli* proteins among any other contaminating substances from the recombinant protein may be further achieved by chromatographic techniques such as IMAC which was used in the present study. IMAC was the method of choice because both LAPs were expressed with N-terminal His-tags as described in section 2.4.1.

3.4.2.1. *Pf*LAP immobilized metal affinity chromatography

In the present study, the column used contained Sepharose beads charged with Ni^{2+} (5 ml FF His Trap column, G.E Health). The soluble fraction obtained after fractionation (section 3.4.2) was loaded onto the column as described in section 3.3.5.2 and the resulting *Pf*LAP profile is shown on figure 3.7(a).

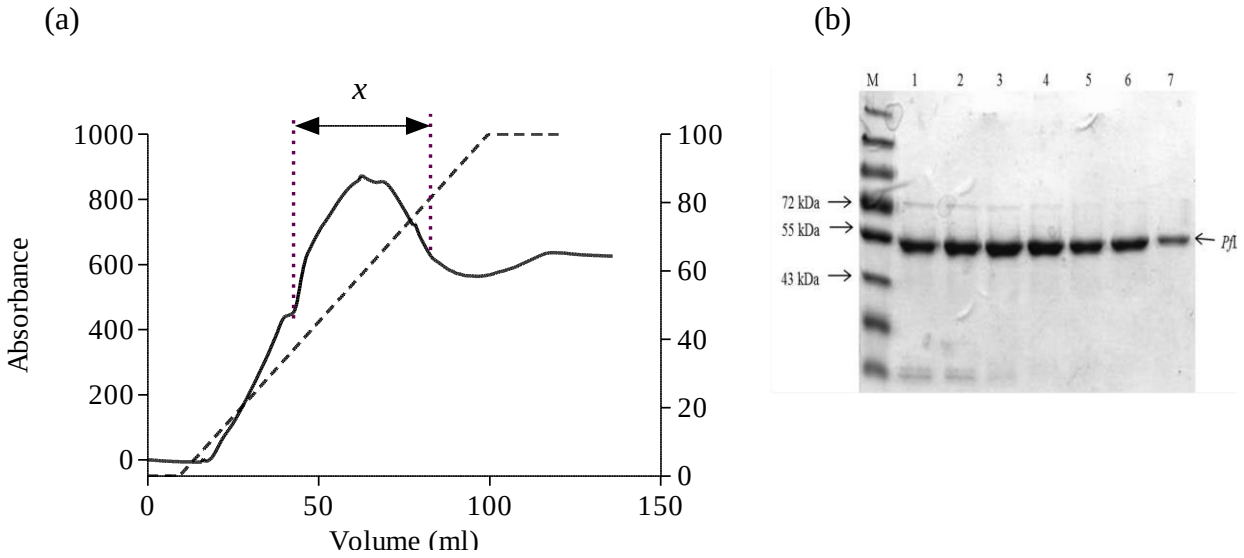

Figure 3.7 (a) Nickel affinity elution profile of *Pf*LAP performed over a gradient of 0-100% elution buffer (500 mM imidazole). *Pf*LAP eluted over 7 fractions (fractions 8-14, represented by *x*) between 50 % and 80 % elution buffer. The continuous line represents absorbance while the broken line represents the relative percentage gradient of the elution buffer, (b) 10% SDS-PAGE gel (reducing conditions) image showing the 7 selected fractions in their increasing order, with fraction 8 in lane 1..

Fractions corresponding to the peak on figure 3.7(a) were run on an SDS-PAGE and the results confirmed that the peak was as a result of *Pf*LAP elution [figure 3.7(b)]. *Pf*LAP was eluted over seven 5 ml fractions to give a final volume of 35 ml. Elution of *Pf*LAP began at about 50 % elution buffer concentration (0.25 M imidazole) and completed at about 80 % (0.4 M imidazole). *Pf*LAP eluted at high imidazole concentrations relative to *Hs*LAP which is discussed later in section 3.4.3.1. Since elution of proteins from the IMAC column is by the competitive displacement of histidine residues by imidazole, it can be concluded that *Pf*LAP was bound tighter to the resin than *Hs*LAP (Block *et al*., 2009).

3.4.2.2. *Pf*LAP size exclusion chromatography

IMAC as a method is not specific for a particular protein but for histidine residues which can be found in virtually any protein. This leaves room for contamination of the desired protein with *E. coli* proteins which have exposed histidine residues. Due to these limitations of IMAC, which were evident through extra protein bands on the SDS-PAGE gels [figure 3.7(b)]. Further protein purification was attempted through SEC which also acts as a desalting method by removing imidazole from the recombinant protein sample. This was done as described in section 3.3.5.3 and the resulting elution profile for *Pf*LAP is shown in figure 3.8(a). The corresponding SDS-PAGE analysis is shown in figure 3.8(b).

SEC was successfully performed and gave a good yield of *Pf*LAP as evidenced by both the peak and the SDS-PAGE image (figure 3.8). Though SEC has relatively low resolving power, it is sufficient for purification after IMAC, especially if the target protein is in abundance in the sample. Advantages of SEC include its ability to be performed in almost any buffer and its usefulness in resolving proteins that oligomerize in the sample, removal of small molecules such as imidazole. In the present study, the eluate collected had very minimal impurities as evidenced by the SDS-PAGE gel image (figure 3.8b). However the enzyme was inactive at the end of purification and it was discovered that it had lost its activity during purification, especially the IMAC and SEC steps. It was suspected that the enzyme could be heat labile as the cystine aminopeptidase observed by (Oya *et al*., 1974), and since IMAC and SEC were performed at ambient temperatures, it resulted in the loss of activity.

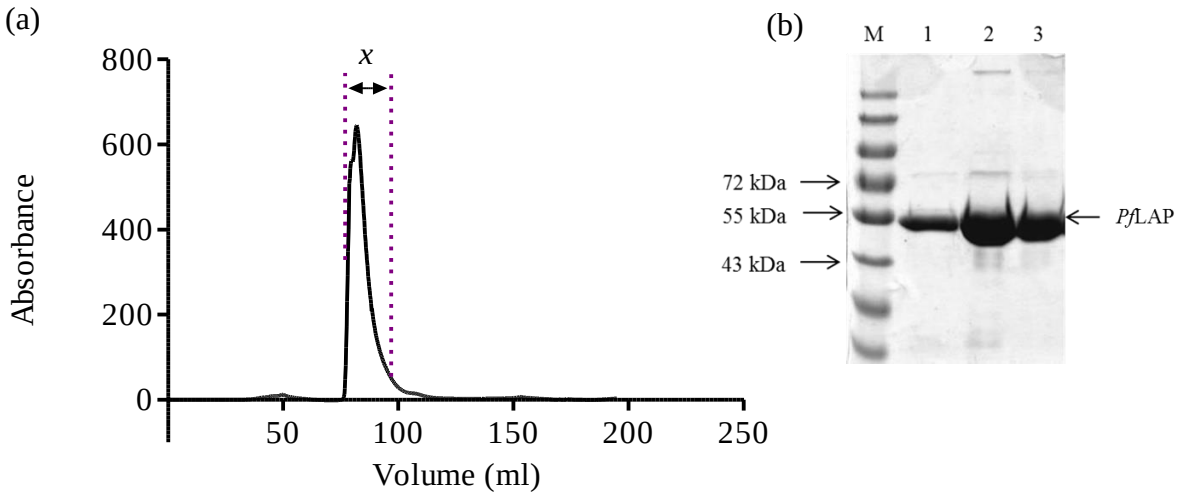

Figure 3.8 (a) Elution profile obtained after the SEC purification of *Pf*LAP using Sephacryl S100HR resin. Fractions corresponding to the only peak were pooled for further purification. (b) The gel image on the insert shows 10% SDS-PAGE (under reducing conditions) of samples taken from each of the selected fractions.

To verify this suspicion, a sample of the soluble fraction of the lysate collected after centrifugation was divided into 2; one was kept at 4 °C and the other at ambient temperatures for an hour. Following the incubation period the sample kept at ambient temperatures had lost 60 % while the sample at 4 °C had only lost 5 %. Due to this setback, the SEC step was substituted with a desalting step (section 3.3.5.4).

3.4.2.3. *Pf*LAP Desalting

Desalting was performed mainly to remove the imidazole, salt (NaCl) and any other small protein molecules from the LAP sample. The principle of desalting is the same as that of SEC and these two procedures generally use the same resin as the stationary phase. Desalting was performed in a cold room at 4 °C using a desalting column as described in section 3.3.5.4. Being able to carry out the desalting procedure at 4 °C was one of the main factors in choosing the method, as the main goal was preventing loss of activity associated with purification at ambient temperatures. Another available alternative to desalting was dialysis. Dialysis achieves the same goal as desalting albeit with much less rapidity and with more demanding preparatory and

operational steps involved. On the other hand desalting columns are re-usable and require much less effort to set up (Porath and Flodin, 1959).

3.4.3. Purification of *Hs*LAP

Purification was started with the harvesting of cells after 36 hours of incubation as concluded in section 3.4.1. The cell biomass was washed thrice in buffer before lysing using lysozyme as described in section 3.3.5.1. After enzymatic lysis the cells were resuspended in buffer and frozen at -80 °C before thawing. The principles, advantages and disadvantages of the freeze thaw method implemented in the present study are discussed in section 3.4.2. After thawing, the cell debris was removed from the soluble matter using ultracentrifugation.

3.4.3.1. *Hs*LAP immobilized metal affinity chromatography

The purification of *Hs*LAP was done in the same way as that of *Pf*LAP. The procedure was performed as described in section 3.3.5.2 and the resulting *Hs*LAP profile is shown on figure 3.9.

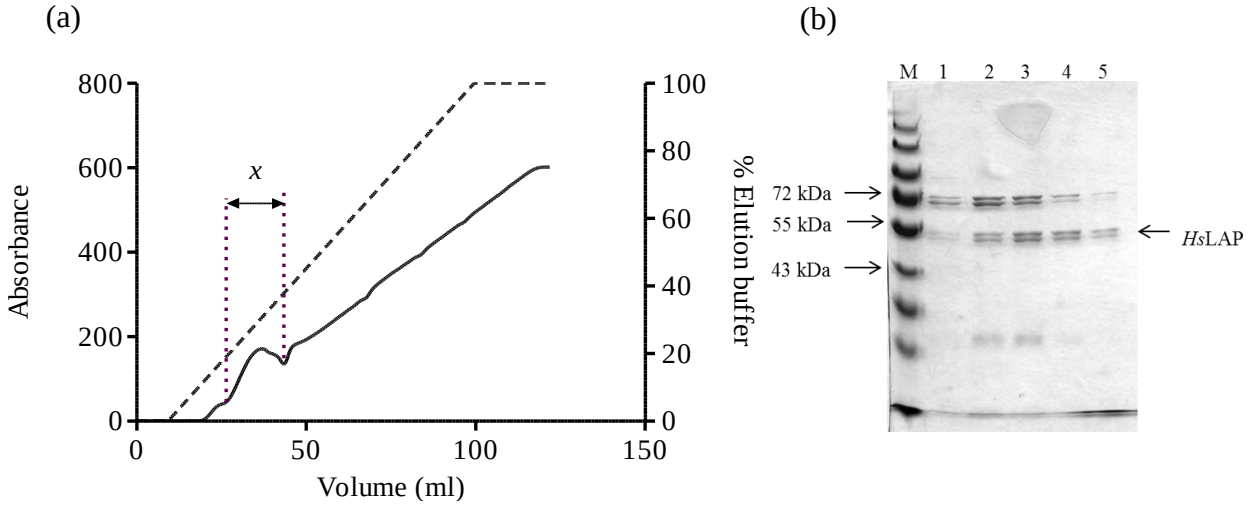

Figure 3.9 (a) Nickel affinity elution profile of *Hs*LAP performed over a gradient of 0-100 % elution buffer (500 mM imidazole). *Hs*LAP eluted over 5 fractions between 20 % and 35 % elution buffer. The continuous line represents absorbance while the broken line represents the relative percentage gradient of the elution buffer. *x* represents the selected fractions. (b) 10% SDS-PAGE (under reducing conditions) gel image showing the 5 selected fractions (fractions 3-7) in ascending order from lane 1 to 5.

From the elution profile and the SDS-PAGE gel image [figure 3.9(a)], it is observed that the *Hs*LAP eluted over 5 fractions and had a maximum absorbance of 171.5 mAU, much less than

the 872.6 mAU of *Pf*LAP [figure 3.7(a)]. Elution initiated at about 20 % elution buffer (0.1 M imidazole) and was completed at 35 % elution buffer (0.175 M imidazole). This early elution of *Hs*LAP compared to *Pf*LAP (section 3.4.2.1) indicated that *Pf*LAP bound more strongly to the Ni^{2+} and may suggest the presence of more exposed histidine residues in *Pf*LAP apart from the His-tag (Block *et al*., 2009). The intensity and the thickness of the protein bands on an SDS-PAGE gel is directly proportional to the amount of protein in the sample. The protein bands observed for the *Hs*LAP expression [figure 3.9(b)] are less pronounced than in the *Pf*LAP [figure 3.7(b)]. This alongside the absorbance values of both IMAC profiles suggest that far more *Pf*LAP was expressed as compared to *Hs*LAP. This supports the suggestion that late induction in *Pf*LAP expression (section 3.4.1) allowed more *E. coli* cell division and consequently a higher yield than in the *Hs*LAP expressing cells.

Besides the histidine residues of a His-tag, there are other chelating residues on a polypeptide structure such as histidine, cysteine, aspartate and glutamate that are able to bind to metal ions, albeit with weaker interactions (Jensen *et al.,* 2004; Block *et al*., 2009). If these residues are exposed and available for interaction with the metal ions, they enhance the binding stability of a protein to the resin. Bolanos-Garcia and Davies (2004) also stated that the inter/intra-molecular interactions in a recombinant protein may limit the accessibility of the His-tag to the metal ions and thereby reduce the binding affinity of the protein. These factors could explain the differences in the elution profiles of *Pf*LAP [figure 3.7(a)] and *Hs*LAP [figure 3.9 (a)].

The SDS-PAGE gels of both samples show other protein bands apart from the desired proteins, though much fainter in the *Pf*LAP sample but strongly present in the *Hs*LAP sample, especially at 26 kDa, 55 kDa and at 70 kDa on figure 3.9(b). Grasslund *et al.* (2008) reported that this co-purification of *E. coli* proteins is a common problem especially if the target protein is expressed in low quantities. Table 3.1 shows some proteins that have been reported to co-purify with recombinant proteins when using IMAC (Bolanos-Garcia and Davies, 2004; Howell *et al*., 2006; Grasslund *et al*., 2008). From this list it is postulated that the contaminating proteins seen on the SDS-PAGE image [figure 3.9(b)] are the 25.10 kDa CA, the 57.35 kDa GroEL and the 69.11 kDa DnaK.

Table 3.2 List of *E.coli* proteins that co-purify with his-tagged proteins in IMAC (Grasslund *et al.*, 2008).

Protein	Accession code	Monomer mass (kDa)
GroES	NP_418566	10.39
Fur	NP_415209	16.79
Sly D	NP_755987	20.85
CA	NP_414668	25.10
RplB	P60422	29.86
DnaJ	NP_414556	41.10
GroEL	AAS75782	57.35
DnaK	NP_414555	69.11

These contaminating proteins are stress response proteins which are highly expressed by *E. coli* in response to the over-expression of heterologous proteins in the cells (Bolanos-Garcia and Davies, 2004). The proteins have high affinity for the metal ions used in IMAC due to clusters of histidine residues present on their surface structure and one such protein on the list in table 3.1 is Sly D. Molecular chaperones such as GroES and GroEL are able to bind directly to the resin or to the recombinant protein and are often found in the eluent after IMAC (Grasslund *et al*., 2008).

In the present study, the low expression level of *Hs*LAP coupled with its relatively low affinity for Ni-NTA resin (compared to *Pf*LAP) allowed contaminating proteins to be eluted along with the *Hs*LAP in higher amounts than in the *Pf*LAP sample. Since the IMAC columns can only bind a limited amount of protein, loading a saturating amount of recombinant protein greatly reduces the amount of contaminants. This phenomenon may be what accounts for very low levels of contaminating proteins in the *Pf*LAP sample. Despite the drawbacks of IMAC such as its limited specificity, it is still a very useful tool in protein purification due to its low cost, rapidity and mild elution conditions compared to other affinity chromatographic techniques. However if greater purity is a necessity, other chromatographic techniques such as ion-exchange or adsorption chromatography may be used. Another technique which may be used to remove contaminants found in the IMAC eluate is using a protease that specifically removes the histidine tag from the recombinant protein and re-using IMAC. This way the cleaved recombinant protein in the solution can be eluted and collected as the unbound sample (Grasslund *et al*., 2008).

3.4.3.2.*Hs*LAP Desalting

The desalting of pooled *Hs*LAP sample obtained from the IMAC step (section 3.4.3.1) was performed as previously done for *Pf*LAP (section 3.4.2.3). SEC as conducted for *Pf*LAP (section 3.4.2.2) was not performed for *Hs*LAP due to protein instability encountered with *Pf*LAP. Since the desalting procedure removed small size impurities in the protein sample, the 57.35 kDa GroEL and the 69.11 kDa DnaK (table 3.2) eluted with the recombinant proteins as these are not very different from *Hs*LAP which is 56.594 kDa.

3.4.4. Progression of purity: *Pf*LAP vs *Hs*LAP

BCA protein concentration determination and enzyme activity assays were performed on samples taken after each purification step. The results from the protein concentration determination (section 3.3.1) were used to load equal amounts of protein on SDS-PAGE gels for resolution. The results for both *Pf*LAP and *Hs*LAP purification are shown in figure 3.10.

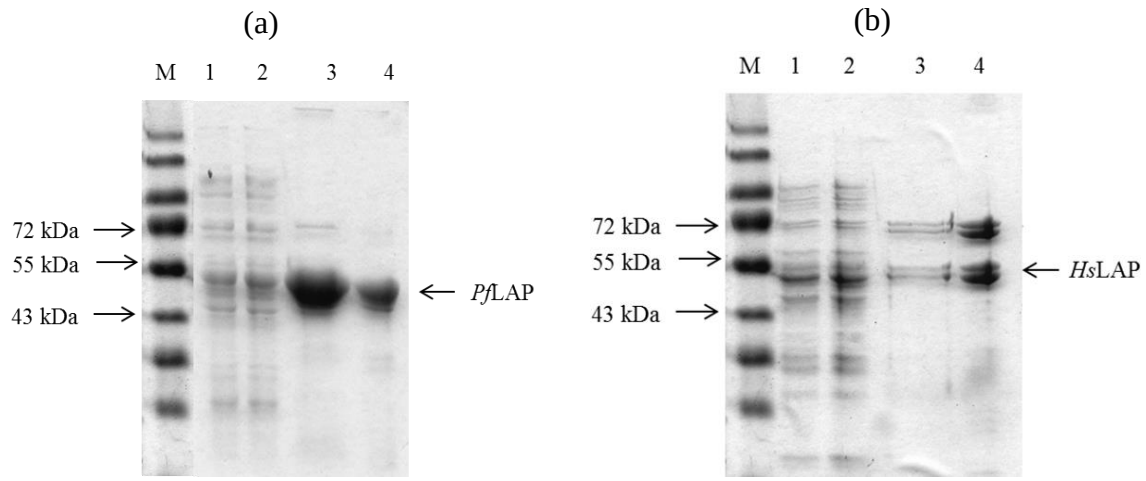

Figure 3.10 10% SDS-PAGE (under reducing conditions) of samples collected after each purification stage. (M) Protein marker (1) Crude lysate sample, (2) Soluble fraction obtained after ultracentrifugation, (3) IMAC sample and (4) Desalted sample. (a) *Pf*LAP and (b) *Hs*LAP.

The gels in figure 3.10 indicate an increase in the purity of the recombinant proteins as purification progresses, especially after IMAC where the bulk of the *E.coli* proteins are removed from the sample. This confirms the importance of IMAC as a rapid method for substantial purification and its use as the principal purification step in most protein purifications strategies

(Zeng *et al*., 2001). However its limitations as discussed in section 3.4.3.1 are easily observed in the contaminating bands especially in the *Hs*LAP sample [figure 3.10(b)].

The IMAC sample obtained during *Pf*LAP purification shows a denser band on the IMAC sample than the desalted sample [figure 3.10(a)]. This irregularity is most probably due to the interference by imidazole in the BCA protein assay method. The permissible limit of imidazole in the assay sample according to the Thermo Scientific manual is 50 mM imidazole. However the imidazole content in the post IMAC *Pf*LAP sample was greater than 250 mM. Though greater than the limit, the concentration of imidazole in the *Hs*LAP was substantially lower than that of *Pf*LAP hence the regularity of the *Hs*LAP SDS-PAGE gel [figure 3.10(b)]. The progression of purity as shown in figure 3.10(a) or (b) was further clarified by running enzyme assays and generating purification tables to show the protein yield and increase in specific activity of the enzyme as purification progresses. The values obtained for *Pf*LAP and *Hs*LAP purification are displayed in tables 3.3 and 3.4, respectively.

Table 3.3 Purification table of recombinant *Pf*LAP.

Fraction	**Vol (ml)**	**[Protein] ($mg.ml^{-1}$)**	**Total Protein (mg)**	**Activity ($U.ml^{-1}$)**	**Total Activity (U)**	**Specific Activity ($U.mg^{-1}$)**	**Fold Purification**	**% Yield**
Crude lysate	89	1.99	176.8	24.2	2 157.6	0.14	1	100
Soluble Fraction	85	2	170.1	23.7	2 017.7	0.14	1.02	93.5
IMAC	35	0.44	15.5	13.6	477. 3	0.88	6.4	22.1
Desalting	3.8	3.69	14	48.5	184. 2	3.46	25.2	8.5

Table 3.4 Purification table of recombinant *Hs*LAP.

Fraction	**Vol (ml)**	**[Protein] ($mg.ml^{-1}$)**	**Total Protein (mg)**	**Activity ($U.ml^{-1}$)**	**Total Activity (U)**	**Specific Activity ($U.mg^{-1}$)**	**Fold Purification**	**% Yield**
Crude lysate	103	1.65	169.7	48. 99	5 046	0.29	1	100
Soluble Fraction	95	1.45	137.4	31. 31	2 974. 8	0.23	0.79	59
IMAC	25	0.063	1.6	1 5.15	37 8.8	9.65	3.3	0.75
Desalting	3.8	0.474	1.8	20.2	76.8	11. 23	38.9	1.52

*Pf*LAP was expressed in substantial amounts in *E. coli* with a range of 30-40 mg of protein being obtained per litre of expression media. This represented a yield of approximately 10 % (table 3.3). Even though all cells were lysed and frozen after 36 hours, only a third of the lysed cells volume was purified at a time and the information on table 3.2 is a representation of this volume. Stack *et al.* (2007) expressed the enzyme in insect cells and obtained a yield of 15-25 mg protein per litre. From these results it is clear that *E. coli* expression gives a relatively superior protein yield when compared to using insect cells.

However it is worth noting that the enzyme expressed by Stack *et al.* (2007) in insect cells was stable for up to a month, whilst the enzyme in the current study exhibited stability for 2 weeks. Stack *et al.* (2007) also expressed *Pf*LAP in *E.coli* BL21(DE3) cells and found that that the enzyme was only stable for 48 hours at 4 °C. McGowan *et al.* (2010) also expressed *Pf*LAP in *E. coli* using the same protocol as Stack *et al.* (2007), but did not publish the stability or protein yield from this expression system. The yield obtained in the current study is an indicator of high level expression of *Pf*LAP. For a strong promoter such as the T7 promoter, protein concentrations ranging from 10-30 % of the total cellular protein are expected, as was observed in the present study (Hannig and Makrides, 1998).

*Hs*LAP expression produced 3-4 mg of protein per litre with an average yield of 2 % (table 3.4). This yield was very low compared to *Pf*LAP and reflected on the IMAC profile and the protein bands on SDS-PAGE in section 3.4.3.1. From the induction studies conducted on both LAPs (section 3.3.3), initiation of *Hs*LAP expression occured much earlier than *Pf*LAP induction, and without considering possible toxicity to host cells, one would think that *Hs*LAP would be expressed in larger amounts than *Pf*LAP. However, once induced, the concentration of *Pf*LAP in the culture increased and surpassed that of *Hs*LAP. Studier and Moffat (1986) found the same phenomenon when they expressed two different proteins in the same system. Even though there was sufficient indication that there were comparable levels of transcription and stability of both mRNAs, they postulated that the difference in the level of expression of these proteins was due to discrepancies in translation efficiency. In the present study it's postulated that this possibly could have been the case in the expression of *Hs*LAP and *Pf*LAP.

The coding sequences for both LAP enzymes were codon optimised for expression in *E. coli*, which should imply that the efficiency of translation would be the same for both proteins. Contrary to this idea are Sorensen and Mortensen's (2004) findings that some genes even though codon optimised for expression in a recombinant system were poorly transcribed and the mRNA lacked stability. Despite the low *Hs*LAP expression, it is worth noting that the specific activity of the purified *Hs*LAP is almost four times that of *Pf*LAP. Because specific activity can be used as a measure of purity of the enzyme sample, it is clear that *Hs*LAP was the purer of the two enzymes after desalting. This notion was confirmed by the activity of *Hs*LAP which produced a higher intensity reaction than an equal concentration of *Pf*LAP.

In conclusion, both enzymes were expressed in sufficient yields for use in characterisation and kinetic studies. The *Pf*LAP was the more stable of the two enzymes when stored at 4 °C as *Hs*LAP lost all its activity in only 3 days. This low stability of *Hs*LAP may also explain the substantial loss of activity between the crude lysate and the soluble fraction which may have come about as a result of both temperature and other factors resulting from enzyme handling. Worth noting is that the protein determination assays, enzyme activity assays and volume measurements all have a margin of error which should not be ignored when considering the values presented in the purification tables (table 3.3 and 3.4). Such errors may arise from substances which interfere with assays such as imidazole in the IMAC samples.

3.4.5. Western blotting

Western blotting was performed as described in section 3.3.8. The results for both *Pf*LAP and *Hs*LAP are shown in figure 3.11. The LAP zymogram (section 3.3.7) could not yield desired results hence the resolution to resort to western blotting. The anti-polyHistidine antibodies used in the western blot were for the identification of His-tagged proteins in the sample. Bands which are believed to be representative of both *Hs*LAP and *Pf*LAP were observed above the 50 kDa position as expected. This confirmed that the activity observed in the samples is due to His-tagged LAP enzymes as identified in the virtual cloning processes (section 2.3.1). However there were contaminating bands on the *Pf*LAP sample at positions above 35 kDa and at position 25 kDa. It follows that these proteins may have had poly-histidine residues for them to be

detected in the western blot. As discussed in section 3.4.3.1 and as shown in table 3.2, there are proteins in *E. coli* which are co-purified with His-tagged proteins due to their possession of poly-histidine residues in their structure. Among these proteins shown in table 3.2, there are proteins DnaJ and CA which are 41.10 kDa and 25.10 kDa, respectively, and are possibly the proteins observed on the western blot.

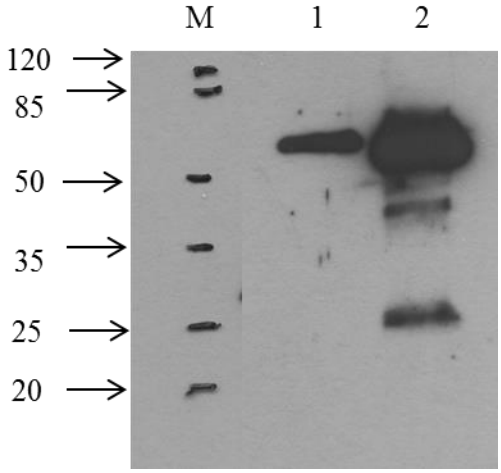

Figure 3.11 10 % Western blot gel image of His-tagged LAP proteins. (M) Marker, (1) *Hs*LAP, (2) *Pf*LAP

It is however a surprise that these contaminating bands were not observed in the *Hs*LAP sample as they had been observed on the SDS-PAGE gels and this could not be explained. In figure 3.10 (b), the *Hs*LAP gel desalted sample has prominent bands at the LAP position and at 70 kDa, but almost undetectable bands at the smaller range compared to the *Pf*LAP gel. The co-purified protein might be Hsp70 or DnaK (table 3.2). It is a possibility that the extra bands in the *Pf*LAP sample are a product of the cleavage or proteolysis of the *Pf*LAP protein itself due to unknown circumstances (Corning Inc., 2012). If that is the case then it would explain the absence of the bands in the *Hs*LAP sample, a property which is otherwise inexplicable.

3.4.6. *Pf*LAP characterisation

3.4.6.1. Metal ion dependence

LAPs are metallopeptidases and therefore require metal ions for their functionality (Smith and Spackman, 1954; Sanderink *et al*., 1988; Taylor, 1993). The effect of divalent metal cations on

the activity of LAPs was investigated using metal chloride salts of the metals as described in section 3.3.9.1. The results of the effects of the five chosen metal ions on *Pf*LAP are shown in figure 3.12.

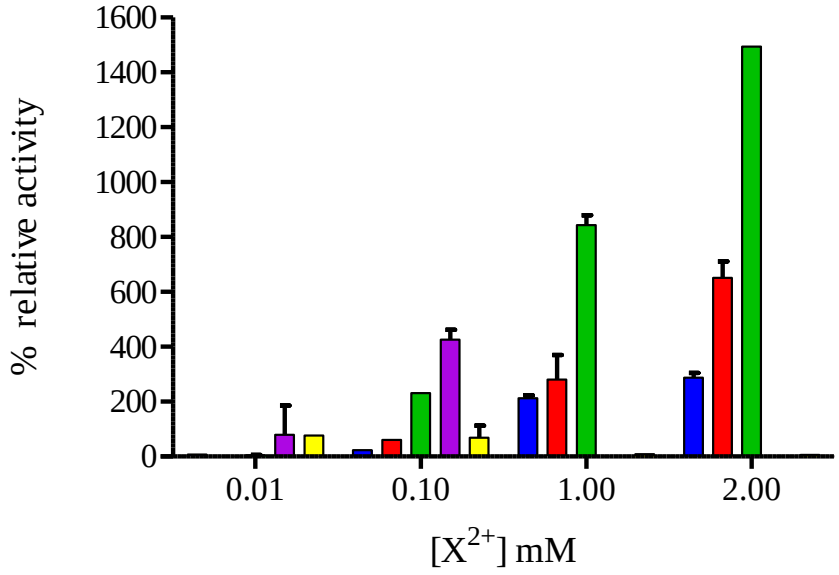

Figure 3.12 The effect of divalent metal cations on the activity of *Pf*LAP as assayed using the chloride salts of the metals. Green –$MnCl_2$, Purple – $CoCl_2$, Blue – $MgCl_2$, Red – $CaCl_2$ and Yellow – $ZnCl_2$. Error bars represent standard deviation.

From the results in figure 3.12, it is evident that almost all of the metal ions tested in this study had an enhancing effect on the activity of *Pf*LAP albeit to varying extents. Relative activity was calculated with reference to activity without metal ions as the baseline. Zn^{2+} had the least effect at the low concentrations of 0.01 and 0.1 mM while Mn^{2+} had the highest effects, increasing activity by up to 15 fold. Co^{2+} increased activity about 5 fold at 0.1 mM after which it had no effect on the enzyme activity. On the contrary, Mg^{2+} and Ca^{2+} increased activity at 1 and 2 mM concentrations but showed no effects below 1 mM. Mg^{2+} doubled *Pf*LAP activity at 1 mM and almost tripled it at 2 mM, while under the influence of Ca^{2+}, a 3 fold increase in activity was observed at 1 mM and 6.5 fold at 2 mM.

Stack *et al*. (2007) reported that *Pf*LAP expressed in insect cells was activated up to 24 fold by 1 mM Mn^{2+} and Co^{2+}, while Mg^{2+}, Zn^{2+} and Ca^{2+} each had an 8, 4, and 1.5 fold increase respectively. These results differ quite significantly in the magnitudes by which each metal ion affected the enzyme. The general trend is that there is activation that results from the inclusion of divalent metal ions in the enzyme reaction. The discrepancies observed are likely due to the

difference in enzyme purity and the expression system used by Stack *et al.* (2007). These differences, mainly in enzyme stability, have been observed between *Pf*LAP expressed in insect cells and that expressed in *E. coli* (Stack *et al*., 2007). *Pf*LAP along with other LAPs such as the bovine lens LAP and the porcine kidney LAP are known to be homo-hexamers with two metal binding sites per subunit. Site 1 is known to be a loosely binding site and can exchange the native metal ion which is usually Zn^{2+} for other metal ions such as Mn^{2+}, Co^{2+} and Mg^{2+} with a subsequent increase in activity. Site 2 is known to be a tight binding site occupied by Zn^{2+} which cannot be replaced by other ions under normal physiological conditions (Van Wart and Lin, 1981; Allen *et al*., 1983; Maric *et al*., 2009). Therefore in the present study it is believed that the binding of the test ions to site 1 resulted in increased activity of the enzyme. Based on these considerations it was decided to continue characterization studies using the addition of 2 mM Mn^{2+} ions.

3.4.6.2. Temperature stability study

The temperature at which *Pf*LAP is most stable was investigated as described in section 3.3.9.2 and the results obtained after 15 minutes of incubation are presented in figure 3.13.

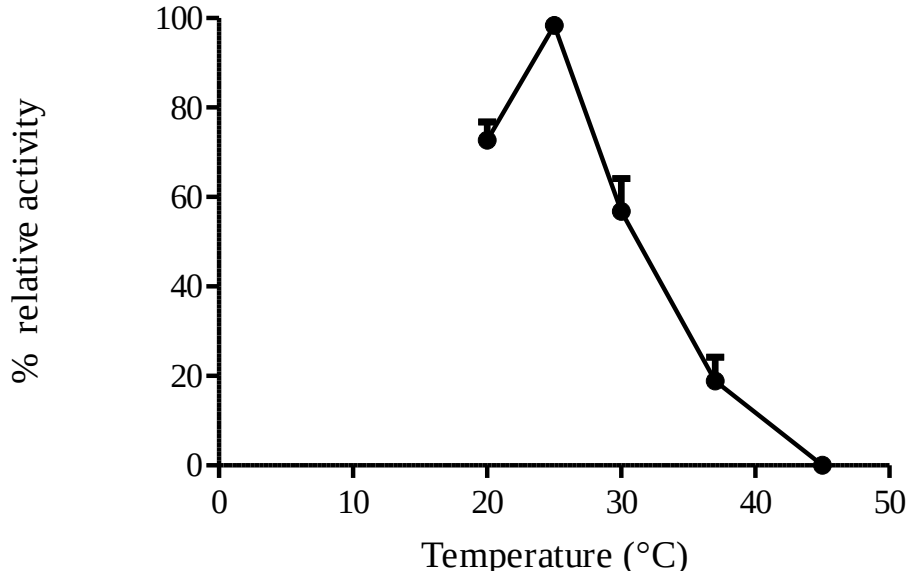

Figure 3.13 Temperature stability of *Pf*LAP tested at temperatures ranging from 20-45 °C. Data was obtained from 3 data sets each in triplicates collected on different days. Error bars represent standard deviation among data sets.

The enzyme was incubated at each temperature for a maximum of 3 hours, but the common incubation time for maximum activity at each temperature was 15 minutes. The relative percentage activity calculated for 15 minutes incubation (figure 3.13) was expressed with reference to the temperature with the maximum activity (100 % relative activity). Increase in temperature was directly proportional to a decrease in the stability of *Pf*LAP with the exception of activity observed below 25 °C. At 20 °C, relative activity was low, which was expected as lower temperatures are known to slow down chemical reactions in nature. At temperatures above 25 °C there was a rapid decrease in activity with only 60 % of the initial activity remaining at 30 °C. Incubation of the enzyme mixture at 45 °C resulted in a total loss of activity.

*Pf*LAP expressed in the present study was very heat labile during purification as previously stated in section 3.4.2.2. Results given in figure 3.13 confirm this observation as the activity decreases rapidly when the temperature increases above 25 °C. This may be attributed to the life cycle of *P. falciparum* which occurs within two different hosts which differ vastly from each other. Mosquitoes, like all insects, are cold blooded creatures and do not have temperature regulation in their bodies (Handel, 1965) and *P. falciparum* may have evolved to survive where body temperatures may drop with environmental temperatures hence the low optimal stability temperature. However *P. falciparum* also survives in the human host whose temperature is 37 °C, yet in the present study 20 % activity remained at that temperature. This discrepancy cannot be explained though it is postulated that the heat labile *Pf*LAP expressed in the present study is as a result of the expression system used and its stability may vary with the enzyme expressed in *P. falciparum* itself (Gardiner *et al*., 2005).

It is worth mentioning that the same version of *Pf*LAP expressed in different expression systems did not yield a protein with properties consistent with those of the present study; the enzyme expressed in *Pichia pastoris* was totally inactive while the *Pf*LAP expressed in *E. coli* had activity for only 48 hours at 4 °C and the *Pf*LAP expressed in insect cells had activity for up to 30 days (Stack *et al*., 2007). This shows that the sensitivity and biochemical properties of expressed enzymes can be influenced by the expression system used to produce the enzyme.

3.4.6.3. pH stability study

The pH stability of *Pf*LAP was investigated at 25 °C over a period of 3 hours as described in section 3.3.9.3 and the results obtained after 15 minutes of incubation are presented in figure 3.14. Percentage activity was calculated relative to the highest activity at 15 minutes.

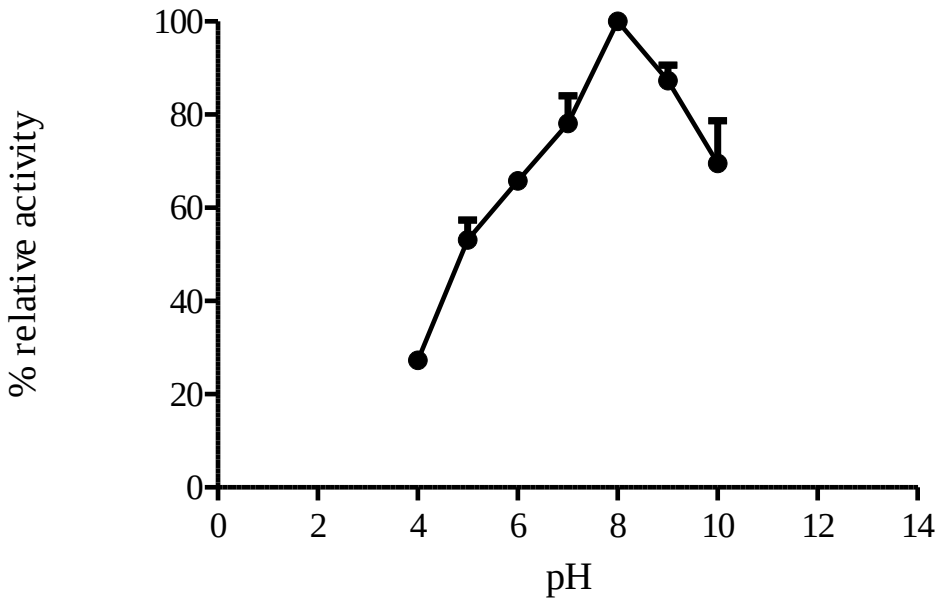

Figure 3.14 pH stability of *Pf*LAP tested at 25 °C over a period of 3 hours. Test pH ranged from 4 to 10. Data was obtained from 3 data sets each in triplicates collected on different days. Error bars represent standard deviation among data sets.

The enzyme exhibited good stability between pH 5 and 10, with the optimum stability observed at pH 8.0. These findings agree with the findings of Stack *et al*. (2007) where *Pf*LAP was most stable at neutral to alkaline pH. In the same study conducted by Stack *et al*. (2007), they also found that the enzyme exhibited its optimal activity at pH 8.2. *Pf*LAP has been found to exist in the *P. falciparum* cytosol, which has a pH of 7.4 (Gardiner *et al*., 2005; Skinner-Adams *et al*., 2009). Studies on other related LAPs namely *Setaria cervi*, *P. vivax* and *Cryptosporidium parvum* show similar results (Pokharel and Rathaur, 2007; Lee *et al*., 2009; Kang *et al*., 2011). At pH 10 there was still an excess of 60 % residual activity and this suggests that the enzyme is fairly stable at even higher pH levels.

3.4.7. *Hs*LAP characterisation

3.4.7.1.Metal ion dependence

The effect of divalent metal cations on the activity of *Hs*LAP was investigated using metal chlorides as described in section 3.3.9.1. The results of the effects of five metal ions on *Hs*LAP are shown in figure 3.15.

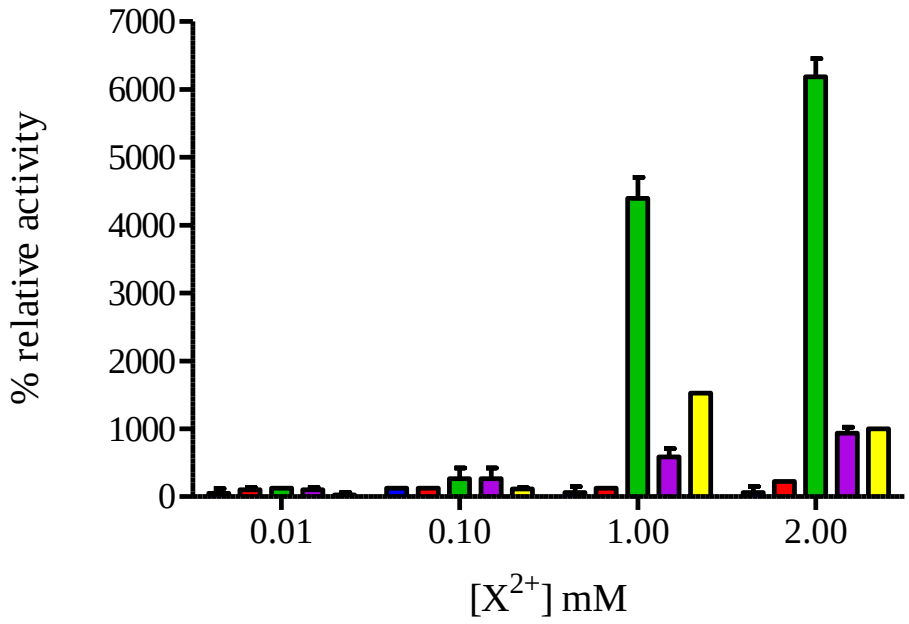

Figure 3.15 The effect of divalent metal cations on the activity of *Hs*LAP as assayed using the chloride salts of the metals. Green –$MnCl_2$, Purple – $CoCl_2$, Blue – $MgCl_2$, Red – $CaCl_2$ and Yellow – $ZnCl_2$. Error bars represent standard deviation.

*Hs*LAP exhibited extremely low to no activity increase in the presence of low concentrations of the metal chloride salts (figure 3.15), unlike *Pf*LAP which showed a considerable increase in activity at low concentrations of the metal chloride salts. Mn^{2+} was the only ion which displayed extensive influence on the activity of *Hs*LAP with increases of 43 fold and 65 fold after inclusion of 1 mM and 2 mM Mn^{2+} respectively. Zn^{2+} and Co^{2+} were the only other ions to significantly activate *Hs*LAP. Zn^{2+} had its highest activity at 1 mM while Co^{2+} had its highest activity at 2 mM. Kohno *et al*. (1985) reported that Mn^{2+} had the best activating effects on human liver LAP, a result which is consistent with the findings of the present study. Ledeme *et al*. (1983) also reported that Mn^{2+} and Mg^{2+} activated human liver LAP. When compared to *Pf*LAP, *Hs*LAP had a more restricted preference of the metal ions which influence its activity. This

difference is possibly a reflection of structural differences between these two enzymes which may be exploited in designing specific targeting agents. Thus Mn^{2+} was selected as the metal chloride salt to be incorporated in the subsequent assays to determine stability (temperature and pH) and to obtain the kinetic parameters.

3.4.7.2. Temperature stability study

The temperature at which *Hs*LAP is most stable was investigated as described in section 3.3.9.2 and the results obtained after 15 minutes of incubation are presented in figure 3.16.

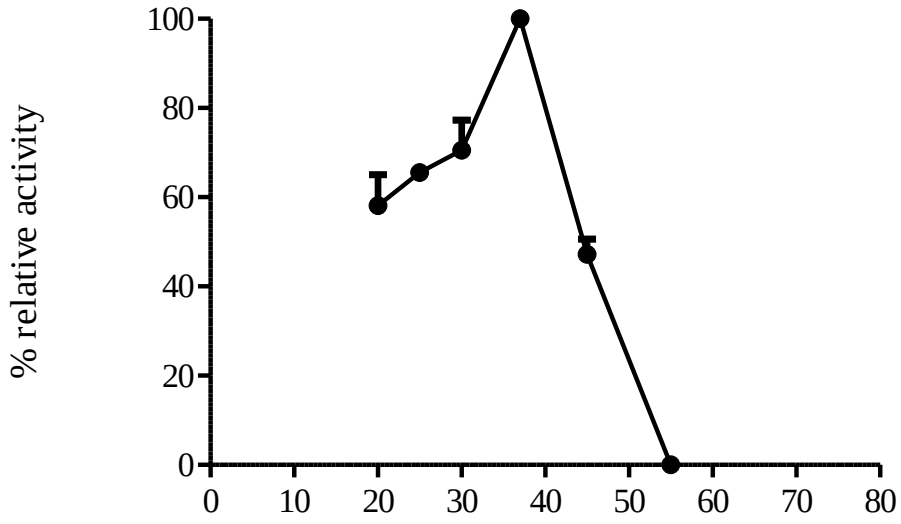

Figure 3.16 Temperature stability of *Hs*LAP tested at temperatures ranging from 20-55 °C. Data was obtained from 3 data sets, each in triplicates collected on different days. Error bars represent standard deviation among data sets.

Percentage activity was calculated relative to the highest activity at 15 minutes. Optimum stability was observed at 37 °C where the enzyme was most stable over the test period of 3 hours. *Hs*LAP exhibited some stability at low temperatures with temperatures from 20-30 °C maintaining stability between 60 % and 70 %. After 37 °C there was a sharp decrease in activity with a total loss of activity at 55 °C and above after 15 minutes of incubation. This effect is most likely a result of denaturation and is synonymous with extreme fever which results in death in humans. Being a human cytosolic enzyme it was expected that *Hs*LAP would have an optimum stability temperature of 37 °C, the physiological temperature at which most biochemical processes take place within the human body. The narrow temperature range at which *Hs*LAP

exhibits its highest activity is a reflection of the narrow homeostatic control of the human body temperature which ensures integrity of biochemical processes. When compared to *Pf*LAP, *Hs*LAP is more stable and more active at higher temperatures.

3.4.7.3. pH stability study

The pH stability of *Hs*LAP was investigated at 37 °C over a period of 3 hours as described in section 3.3.9.3 and the results obtained after 15 minutes of incubation are presented in figure 3.17.

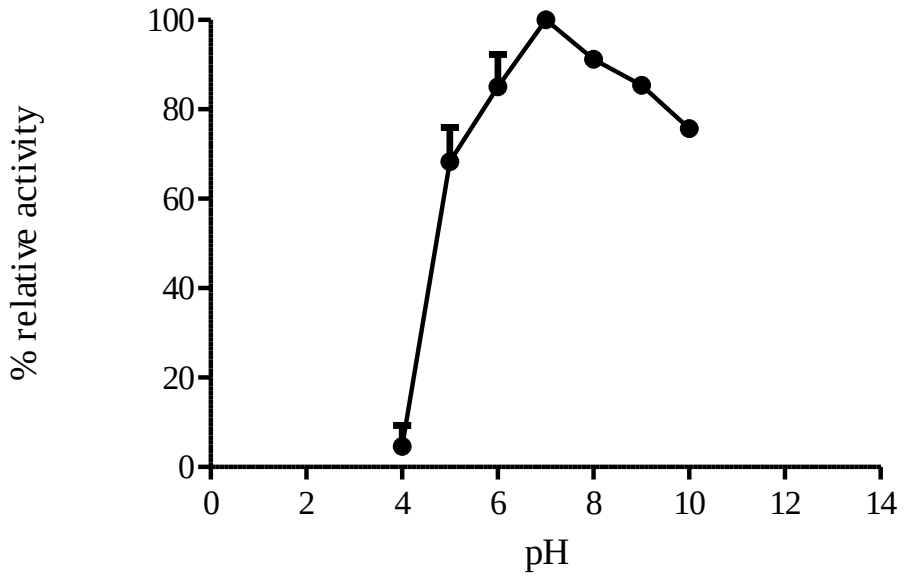

Figure 3.17 pH stability of *Hs*LAP tested at 37 °C over a period of 3 hours. Test pH ranged from 4 to 10. Data was obtained from 3 data sets each in triplicates collected on different days. Error bars represent standard deviation among data sets.

Optimal activity was obtained after 15 minutes of incubation as represented in figure 3.17. Percentage activity was calculated relative to the highest activity at 15 minutes. *Hs*LAP unlike *Pf*LAP seemed to have higher stability over a broad range of pH with an excess of 70 % activity maintained between the pH 5 and 10. Kohno *et al*. (1985) found the human liver LAP to be most stable between pH 7.5 and 8.5. The results obtained in the present study exhibit optimal stability at pH 7 and up to 85 % is retained at pH 9; these results concur with the findings of Kohno *et al*. (1985). There was only low activity below pH 5, and considerable stability at alkaline pH. The

human cytosolic pH is neutral and therefore it was expected that the stability of *Hs*LAP would be close to this region.

3.5. Kinetic studies

Kinetic studies were conducted as described in section 3.3.10. Each set of experiments were performed in triplicate and repeated on three different days to give a total of nine repeats. The results were analysed using the software GraphPad Prism 5 which enabled non-linear regression analysis.

3.5.1. *Pf*LAP kinetic studies

*Pf*LAP followed Michaelis-Menten kinetics; this is synonymous with other recombinant LAPs from other organisms (Liu *et al*., 2007; Pokharel and Rathaur, 2007; McGowan *et al*., 2010). The resulting Michaelis-Menten kinetics graph is shown in figure 3.18. The kinetic parameters K_m and V_{max} were automatically calculated by GraphPad Prism 5 and are given in table 3.5. The complications of obtaining accurate values for K_m and V_{max} from a Michaelis-Menten plot have compelled researchers to use linear transformations of the Michaelis-Menten equation. The most widely used linear transformation of the Michaelis-Menten equation is the Lineweaver-Burke plot; this is also the most unsatisfactory linear plot for determining K_m (Ritchie and Prvan, 1996). The Hanes-Woolf plot, albeit rarely used, has the advantage that it is not biased by velocities at low concentrations of substrate. Therefore the transformation of choice in the present study was the Hanes-Woolf plot and the resulting graph is shown in figure 3.19. A line of best fit was drawn and the line equation was used to calculate K_m and V_{max} which are given in table 3.5.

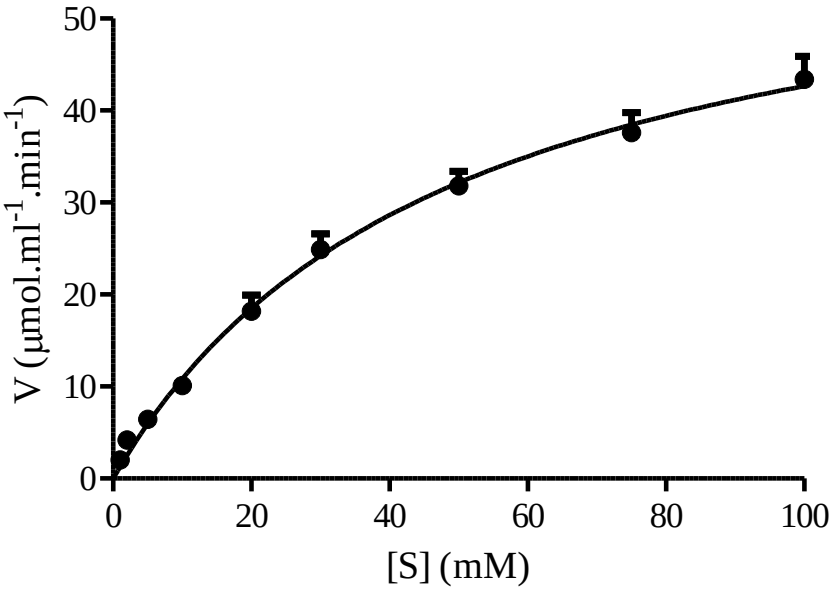

Figure 3.18 The Michaelis-Menten graph of *Pf*LAP activity on L*p*NA. Data was obtained from 3 data sets each in triplicates collected on different days. Error bars represent standard deviation among data sets.

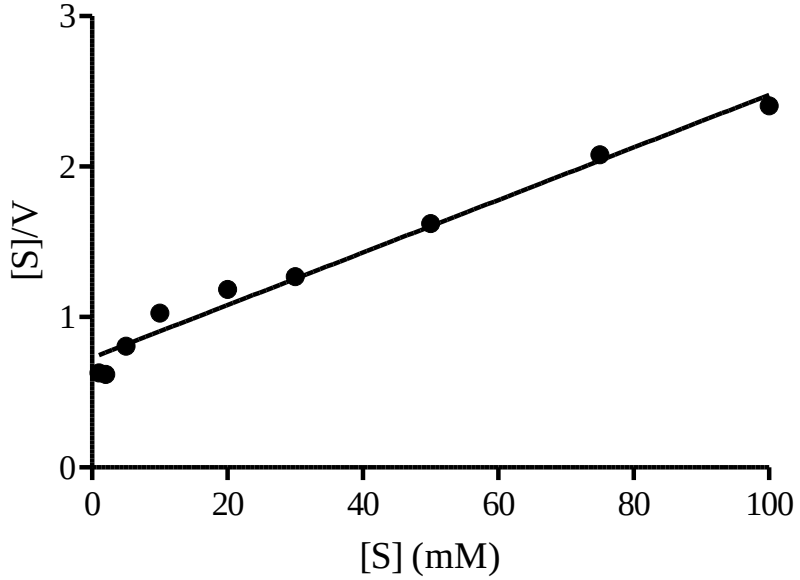

Figure 3.19 The Hanes-Woolf transformation of the kinetic study data represented in the Michaelis-Menten curve in figure 3.18. Error bars represent standard deviation. K_m and V_{max} were calculated using the linear equation y = 0.0167x + 0.7123. R^2 value = 0.9783.

Table 3.5 The reaction kinetics parameters of *Pf*LAP obtained using the non-linear regression and the Hanes-Woolf linear transformation of the Michaelis-Menten kinetics.

Plot	Variables			
	K_m (mM)	V_{max} (μmol.ml^{-1}.min^{-1})	k_{cat} (min^{-1})	k_{cat} / K_m (M^{-1}.min^{-1})
Non-linear regression	48.52±6.772	63.34±4.133	7.24×10^2 ±47.24	1.49×10^4
Hanes-Woolf	42.7	59.9	6.85×10^2	1.6×10^4

The values in table 3.5 show the usefulness of linear transformations of the Michaelis-Menten kinetics when compared to the non-linear regression in giving more accurate kinetic data. The enzyme kinetics of *Pf*LAP revealed a poor affinity and efficiency of *Pf*LAP towards the substrate L*p*NA as reflected by a K_m of 42.7 mM and a k_{cat} /K_m of 1.6×10^4 M^{-1}.min^{-1}. Stack *et al*. (2007) purified *Pf*LAP from insect cells and using L-leucine-4-methylcoumarinyl-7-amide as a substrate and obtained a K_m of 12.12 μM, a k_{cat} of 3.9×10^4 sec^{-1} and a $k_{cat\ t}$/K_m of 3.22×10^9 M^{-1}.sec^{-1}. When compared to these figures, the *Pf*LAP in the present study had relatively poor affinity and efficiency towards L*p*NA. This phenomenon is not a surprise as the group to which a leucine residue is attached also affects the efficiency of the breakage of the amide bond by LAP (Ledeme *et al*., 1983; Kohno *et al*., 1985). Since k_{cat} is a direct reflection of specific activity which in turn reflects the purity of the enzyme, it may be speculated that the differences observed in the *Pf*LAP used in the present study and the one expressed by Stack *et al*. (2007) may partly be because of differences in enzyme purity. Substrate purity is another factor known to cause an increase in K_m (Segel, 1951). However the possibility of this being the cause of a high K_m in the present study is unlikely as the substrate is of high purity (98 %).

3.5.2. *Hs*LAP kinetic studies

Similar to *Pf*LAP, *Hs*LAP was observed to follow Michaelis-Menten kinetics. The graph obtained from the experimental determination of initial velocities is shown in figure 3.20. The kinetic parameters K_m and V_{max} were automatically calculated by GraphPad Prism 5 and are given in table 3.6.

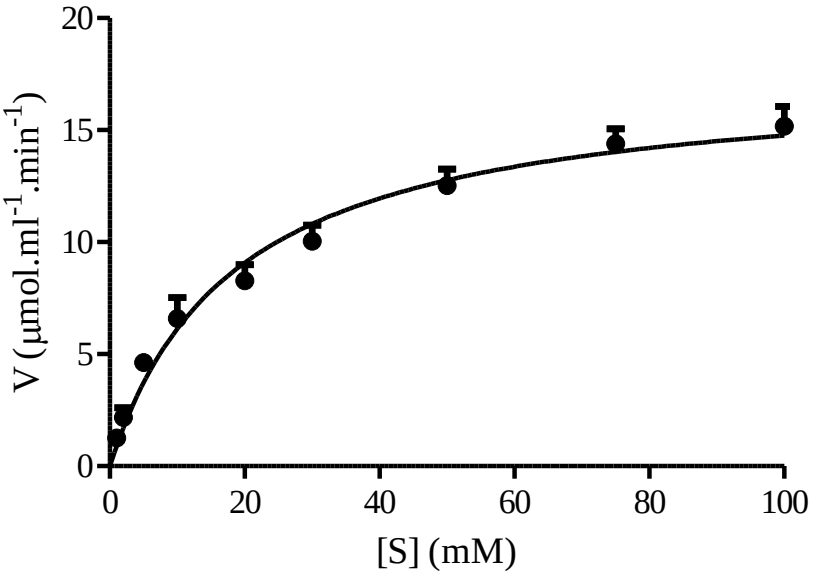

Figure 3.20 The Michaelis-Menten graph of *Hs*LAP activity on L*p*NA. Data was obtained from 3 data sets each in triplicates collected on different days. Error bars represent standard deviation among data sets.

The Hanes-Woolf plot was used as the linear transformation of the Michaelis-Menten graph and the resulting graph is shown in figure 3.21.

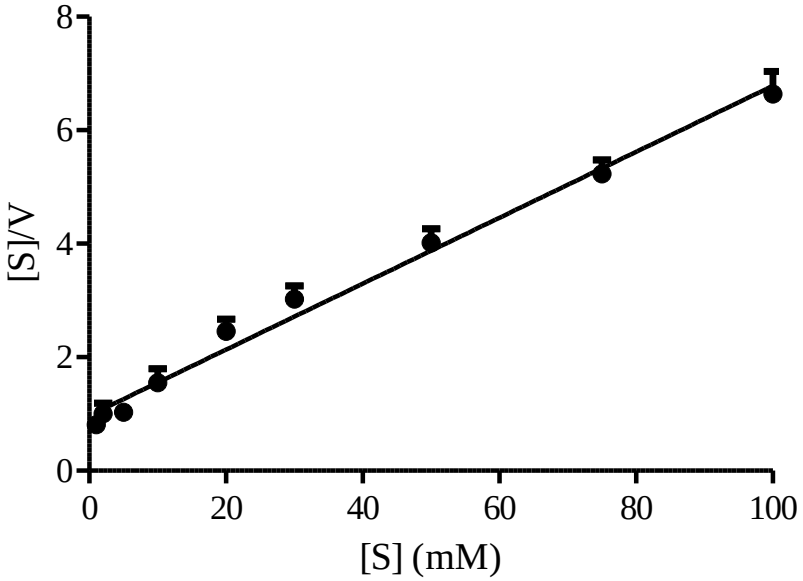

Figure 3.21 The Hanes-Woolf transformation of the kinetic study data represented in the Michaelis-Menten curve in figure 3.20. Error bars represent standard deviation. K_m and V_{max} were calculated using the linear equation y = 0.0581x + 0.9712. R^2 = 0.9895.

Table 3.6 The reaction kinetics parameters of *Hs*LAP obtained using the non-linear regression and the Hanes-Woolf linear transformation of the Michaelis-Menten kinetics.

Plot	Variables			
	K_m (mM)	V_{max} (μmol.ml^{-1}.min^{-1})	k_{cat} (min^{-1})	k_{cat} / K_m (M^{-1}.min^{-1})
Non-linear regression	18.55±2.819	17.5±0.8677	1.75×10^3 ±86.77	9.43×10^4
Hanes-Woolf	16.72	17.21	1.72×10^3	1.03×10^5

The human liver LAP purified by Kohno *et al*. (1985) had a K_m of 4.42 mM and V_{max} of 0.04 μmol.ml^{-1}.min^{-1} towards L*p*NA. The low K_m of this enzyme is perhaps an indication of its high fold of purification of 1 538.6 compared to 38.9 obtained in this study (table 3.4). The enzyme purified by Kohno *et al*. (1985) was from human liver tissue and had its full native state unlike the enzyme expressed in *E. coli* which may be defective to a certain extent as a result of the absence of post-translational modification equipment in *E .coli* (Palomares *et al*., 2004; Hannig and Makrides, 1998). The catalytic efficiency of the human liver enzyme purified by Kohno *et al*. (1985) was not calculated hence the significance of the V_{max} value could not be validated as low or high since the total enzyme concentration was not known.

When compared to *Pf*LAP, *Hs*LAP has a much greater affinity for L*p*NA as evidenced by the low K_m of 16.72 mM compared to the 42.7 mM of *Pf*LAP. The turnover rate of *Hs*LAP was 251.4 % that of *Pf*LAP; this superior efficiency of *Hs*LAP was further confirmed by the k_{cat} /K_m value of 1.03×10^5 M^{-1}.min^{-1} which was 642 % that of *Pf*LAP. This data suggest the stronger affinity of *Hs*LAP for L*p*NA and a higher purity of *Hs*LAP compared to *Pf*LAP. Indeed, as seen in tables 3.3 and 3.4, the specific activity of *Hs*LAP, which translates to its purity, was 324.8 % that of *Pf*LAP, and the fold purification was 154.5 % that of *Pf*LAP.

3.6. Conclusions

The aims and objectives of this section comprised the over-expression, purification and characterisation of both *Pf*LAP and *Hs*LAP. Both enzymes were expressed in *E. coli* BL21(DE3) cells as confirmed by induction studies conducted on both enzyme expressions. The enzymes were purified using ultracentrifugation, IMAC and desalting, and 25.2 and 38.9 fold purifications were achieved for *Pf*LAP and *Hs*LAP, respectively. The specific activity of *Hs*LAP was more

than 3 fold that of *Pf*LAP suggesting that even though *Hs*LAP was expressed in much lower quantities than *Pf*LAP, a more pure protein was produced. *Pf*LAP was most stable at 25 °C under slightly alkaline conditions with a pH optimum of 8. *Hs*LAP had a temperature optimum of 37 °C and pH optimum of 7. Both enzymes exhibited optimal stability within narrow temperature and pH ranges with the exception that *Hs*LAP showed wide pH range. As expected, divalent metal ions had activating effects, with Mn^{2+} increasing activity of both LAPs, but more so on *Hs*LAP.

The kinetic parameters of both LAPs were experimentally determined and both enzymes followed Michaelis-Menten kinetics. Both the non-linear regression analysis and the Hanes-Woolf linear transformation were used to obtain K_m and V_{max}. The enzyme turnover rate and the catalytic efficiency were calculated. For *Pf*LAP, the parameters were: K_m 42.7 mM; V_{max} 59.9 μmol.ml^{-1}.min^{-1}; k_{cat} 684.57 min^{-1} and a k_{cat} /K_m of 1.6×10^4 M^{-1}.min^{-1}. *Hs*LAP gave a K_m of 16.72 mM; V_{max} 17.21 μmol.ml^{-1}.min^{-1}; k_{cat} 1.72×10^3 min^{-1} and a k_{cat} /K_m 1.03×10^5 M^{-1}.min^{-1}. From these parameters it can be seen that *Hs*LAP has a higher affinity and a higher catalytic efficiency towards L*p*NA than *Pf*LAP. With the characterisation of the enzymes completed, the next step was to observe the effect of silver nanoparticles on enzyme activity upon incubation at optimum parameters, which is covered in the next chapter.

Chapter 4: AgNPs: Synthesis, characterisation and LAP-nanoparticle interactions

4.1. Introduction

Nanotechnology is the production and use of materials at nanoscale, typically in the range between 1-100 nm, although materials with dimensions that are a few hundred nanometres may be involved (Farokhzad and Langer, 2009). The application of nanotechnology in medicine presents a confluence between physical sciences and biological sciences which can be exploited to improve the fight against medical conditions such as cancer, HIV and bacterial infections (Elechiguerra *et al*., 2005; Morones *et al*., 2005; Ghosh *et al*., 2008). There has been considerable enthusiasm in the world of science towards the field of nanobiotechnology as it shows great promise of breakthroughs in medical research (Whitesides, 2003). Biological systems consist of cells which have a characteristic size of about 10 μm diameter and nanoparticles present ways of investigating and "spying" on cellular processes without much interference in their functioning (Salata, 2004; Zhang *et al*., 2008). Singh *et al*. (2008) reported that among the nanomaterials currently in use, metallic nanoparticles exhibit the best antimicrobial properties. Various metallic nanoparticles have been synthesised, characterised and their effects on biological processes investigated. Among these, GNPs and AgNPs have emerged as very strong candidates for applications in medicine (Huang *et al*., 2007; Chen *et al*., 2008; Ghosh *et al*., 2008; Singh *et al*., 2008; Lara *et al*., 2009; Lara *et al*., 2010).

Toshima and Yonezawa (1998) reported two ways in which metallic nanoparticles can be synthesised; (i) the breakdown of bulk metals, otherwise known as the top down approach, and (ii) the growth of nanoparticles from small building blocks such as atoms otherwise known as the bottom up approach (Feyman, 1959, Farokhzad and Langer, 2009). The latter has been the most widely used of the two methods. Typically, metal salts are reduced in the presence of a stabilising agent such as polyvinylpyrrolidone (PVP) to yield inert metallic nanoparticles (Pal *et al*., 2008; Ghosh *et al.*, 2008). Such nanoparticles have a very high surface area to volume ratio, making them ideal for interacting with biomolecules. Stabilising agents play an important role in

determining the morphology and distribution of nanoparticles while protecting them from undesirable processes such as agglomeration and corrosion (Dominiguez-Vera *et al*., 2007).

4.2. Aims and objectives

The aims of the current chapter were to synthesise and characterise AgNPs in order to assess and verify their properties. This was followed by interaction of the AgNPs with both LAP enzymes and performing enzyme kinetics as described in section 3.3.10 in order to evaluate the effects of the nanoparticles on enzyme activity.

4.3. Materials and methods

4.3.1 AgNPs synthesis

Silver nanoparticles were synthesized using the method described by Pal *et al*. (2008). In a typical procedure, 10 ml of 1 % (w/v) ethanolic solution of PVP and 0.2 ml of 0.1 M $AgNO_3$ were placed in a 25 ml cotton wool plugged conical flask and microwaved for 5 seconds (700 W; 2 450 MHz). The colourless solution instantaneously turned to the characteristic pale yellow colour, indicating the formation of AgNPs (Solomon *et al*., 2007; Pal *et al*., 2008).

4.3.2. Characterisation of AgNPs

The optical characteristics of AgNPs were measured and recorded using an Epoch Biotek plate reader. Wave scans were performed between 300-800 nm using a 96 well microtiter plate. A wave scan of the ethanolic PVP solution prior to the addition of $AgNO_3$ was performed as a control. For the determination of size, shape and nanoparticle distribution, a Zeiss Libra 120 TEM coupled to an Olympus Soft Imaging Solutions digital camera was used to capture the images. An $AgNO_3$ sample was viewed under the TEM as a control. Grids for TEM analysis were prepared by carefully placing a drop of the solution onto a formvar carbon film on a 200 mesh *c*opper grid held in suspension using high precision forceps. Excess liquid was removed after one minute using filter paper and the grid was air dried overnight. The consistency and integrity of the nanoparticles were assessed over time by storing the nanoparticles under different conditions and following their stability by viewing them under the TEM after a fortnight. The conditions under which the particles were stored included (i) dark conditions at room

temperature, (ii) dark conditions at 4 °C and (iii) light conditions at room temperature. Size distributions of the nanoparticles were determined by physically counting the nanoparticles in the TEM images using the Image J version1.42I software (Wayne Rasband, National Institutes of Health, USA). The nanoparticles were synthesised and stored in glass containers.

4.3.3. Effective nanoparticle concentration

Before nanoparticles could be interacted with the LAP enzymes, a suitable nanoparticle concentration had to be attained. This concentration had to have a significant effect on enzyme activity while allowing the enzyme reaction to proceed in a way that could allow kinetic studies to be performed. Firstly the nanoparticles stock solution was diluted to a concentration which was double the various test concentrations of nanoparticles (1, 2.5, 5 and 10 μM) using Tris buffer, pH 8.0. The enzyme solution (3.7 $mg.ml^{-1}$) at optimal pH (Tris buffer, pH 8.0) was mixed with double the desired AgNP concentration in a 1:1 ratio. The effect of the ethanolic PVP solution on enzyme activity in the absence of silver nitrate was also investigated. This was done by running regular LAP assays as described in section 3.3.6 after incubating LAP with the corresponding concentration of ethanolic PVP as that present in the nanoparticle concentrations (1, 2.5, 5 and 10 μM). The effect of nanoparticles and ethanolic PVP on enzyme activity were determined at times 0 and 15 minutes of incubation of the enzyme-nanoparticle mixture at 25 °C; pH 8.0 and 2 mM Mn^{2+} for *Pf*LAP, and 37 °C; pH 7.0 and 2 mM Mn^{2+} for *Hs*LAP as determined in sections 3.4.6 and 3.4.7.

4.3.4. LAP kinetics in the presence of AgNPs

The effects of AgNPs on the kinetic parameters of the purified recombinant LAPs were investigated by setting up full set of kinetic experiments as described in section 3.3.10 with the addition of 10 μM AgNPs. The enzyme solutions 3.7 $mg.ml^{-1}$ in Tris buffer pH 8.0 for *Pf*LAP and 0.48 $mg.ml^{-1}$ in Tris buffer pH 7.0 for *Hs*LAP were mixed with double the desired AgNP concentration in a 1:1 ratio. This enzyme-AgNP mixture was incubated at the respective temperature (25 °C for *Pf*LAP and 37 °C for *Hs*LAP) as discussed in sections 3.4.6.2 and 3.4.7.2 for 15 minutes before assaying for activity as described in section 3.3.6. Enzyme kinetic experiments were also conducted without the AgNPs as described in section 3.3.10 for

comparison and to elucidate the effects caused by the AgNPs. Assays to determine the effects of nanoparticles were run in tandem with ethanolic PVP negative controls, in addition to the negative controls described in section 3.3.6.

4.4. Results and Discussions

4.4.1. AgNP synthesis

The synthesis of AgNPs was conducted using microwave induced reduction of silver ions as described in section 4.3.1. After 5 seconds of microwave irradiation, there was a visible colour change from clear to yellow in the solution as shown in figure 4.1. The colour change from clear to yellow is confirmation that silver nanoparticles were produced (Pal *et al.*, 2008).

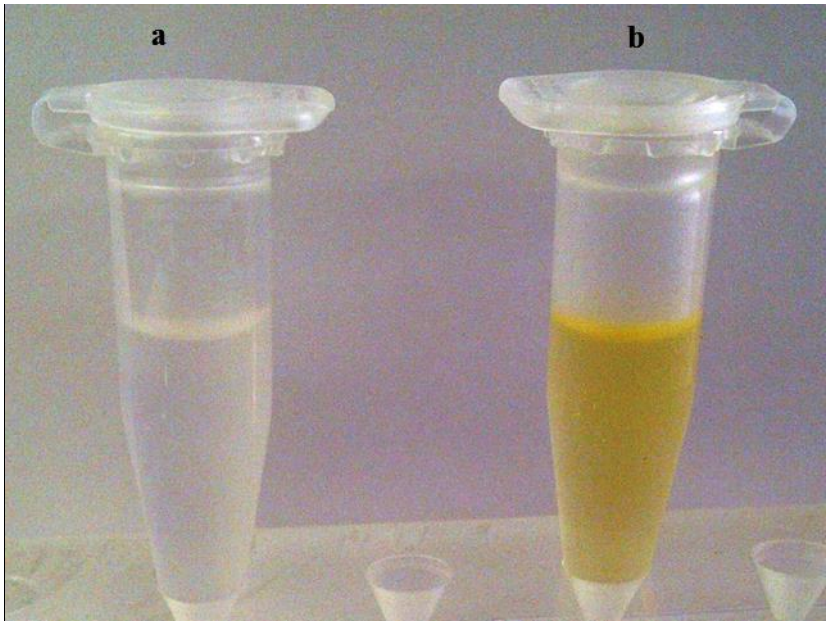

Figure 4.1 Digital photograph showing the colour change observed after 5 seconds of microwave irradiation of a 1 % (w/v) ethanolic PVP solution containing 0.002 M $AgNO_3$. (a) $AgNO_3$ solution before microwave irradiation, (b) $AgNO_3$ solution after microwave irradiation.

Microwave assisted formation of silver nanoparticles from a silver salt has also been reported by Pastoriza-Santos and Liz-Marzan (2002). They stated that the reduction of silver ions by reducing agents is a temperature dependent process which can occur at room temperature albeit at very slow rates. It would then follow that the use of microwave irradiation serves to speed up

the formation of nanoparticles (Pal *et al.,* 2008). This was observed when a duplicate sample to the mixture heated in the microwave, was left at room temperature slowly changed colour to yellow over a period of about 30 minutes. The colour intensity increased with time to a brown colour, an indication of continuous formation of AgNPs.

Microwave irradiation is preferred to other heating methods due to its ability to uniformly distribute heat energy in the solution thereby producing uniformly distributed nanoparticles (Pastoriza-Santos and Liz-Marzan, 2002). Different routes exist to the synthesis of silver nanoparticles, including biological methods or methods similar to the microwave irradiation methods with the only variation being in the choice of either the reducing agent or the stabilising agent (Sun and Xia, 2002; Thakkar *et al*., 2009; Saxena *et al.,* 2010). The method described by Pal *et al.* (2008) was chosen as synthesis method not only for its yield of mono-dispersed nanoparticles but also for its rapidity.

4.4.2. Characterisation of AgNPs

4.4.2.1. UV/Vis spectrum

The UV/Vis spectrum of AgNPs 2 hours after synthesis was obtained as described in section 4.3.2 and is shown in figure 4.2. The spectrum gave a maximum absorbance peak at 420 nm, which falls within the plasmon resonance range for silver nanoparticles (He *et al*., 2002). The peak of the spectrum is dependent on the size of the particles formed in solution and the refractive index of the media in which the particles are formed (Pal *et al.,* 2007). This explains the similarity of the current results with those of Pastoriza-Santos and Liz-Marzan (2002) and the differences with other AgNPs synthesised differently (Dominguez-Vera *et al*., 2003). The $AgNO_3$ solution which was not microwaved gave no peak in the 420 nm range indicating that the formation of AgNPs had not occurred prior to the addition of the reducing and stabilising agents as indicated by the dashed line in figure 4.2. The absorption peak in figure 4.2 was generated after allowing the nanoparticle solution to stand for 2 hours after the synthesis. Readings taken soon after synthesis showed lower peaks. This is synonymous with the intensity of the colour which increases with time after microwave irradiation. This is most likely the continuous formation and the growth of nanoparticles through aggregation of smaller particles after the microwave irradiation (Pal *et al.,* 2007).

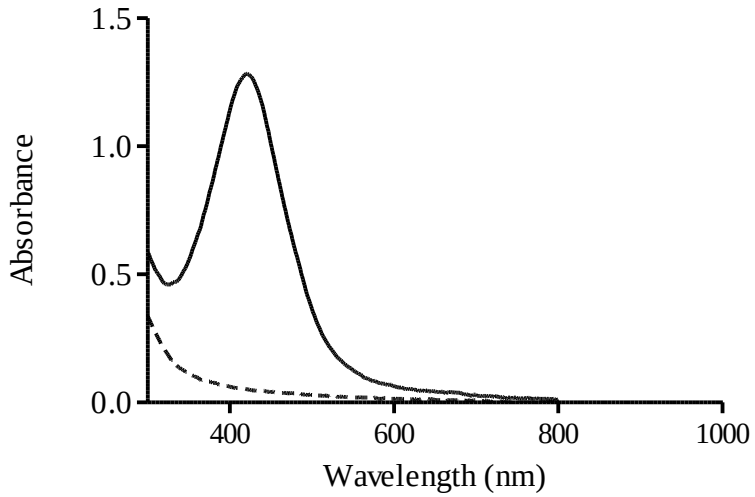

Figure 4.2 UV/Vis absorption spectrum of AgNPs. The continuous line represents the spectrum of the reduced and stabilised AgNPs subjected to microwave irradiation. The dashed line represents the control.

4.4.2.2.TEM

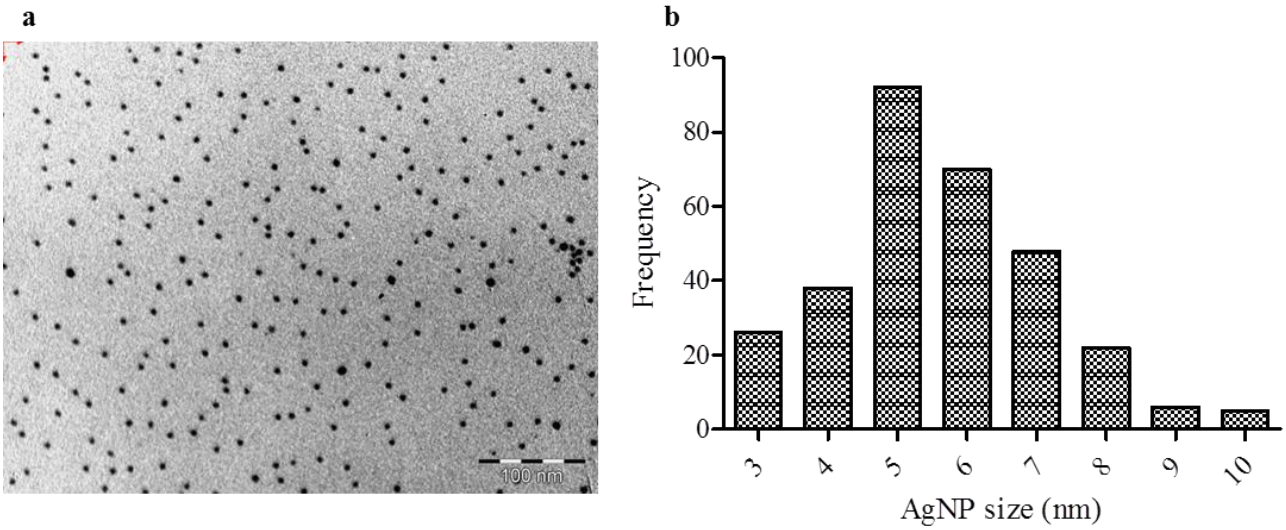

Figure 4.3 (a) TEM image of spherical monodispersed AgNPs. Scale bar equals 100 nm.(b) Size distribution graph of 300 nanoparticles counted.

The shape, size and distribution of AgNPs were visualised by TEM and counted using Image J version 1.42I (section 4.3.2), and are shown in figure 4.3. The AgNPs formed were spherical in shape and exhibited a good degree of monodispersion [figure 4.3(b)]. Monodispersion is mainly

attributed to the even distribution of heat achieved through microwave irradiation. The shape and size of the nanoparticles is influenced to a large extent by the reaction conditions and the molar ratios of the precursors (Sun and Xia, 2002). The size range of AgNPs in the present study was 3-10 nm with the predominant sizes in a narrow range of 5-6 nm [figure 4.3(b)]. This size range was considered desirable for use in the nanoparticles interaction studies, as literature suggests that nanoparticles smaller than 20 nm are more effective for interactions with proteins (Elechiguerra *et al*., 2005).

The small size of silver nanoparticles is a pivotal attribute but it can also be a major drawback. This is because the small size and large surface area of nanoparticles can easily result in their aggregation and difficulty in handling. This however can be circumvented by the use of a capping agent which forms stabilising complexes with the nanoparticles and stabilises them for long periods. In the present study, AgNP solutions were stored for a fortnight under different conditions (section 4.3.2) to evaluate the optimum storage conditions, in terms of temperature and light. Figure 4.4a-c shows that the morphology of the AgNPs stored under different light and temperature conditions remained spherical, while d-f showed a small increase in mean diameter of the nanoparticles when compared to [figure 4.2(b)].

The AgNPs exhibited a high level of stability after a fortnight of storage under different light and temperature conditions. All storage conditions maintained the monodispersion of nanoparticles during the time of storage. The major divergence from the sample taken a fortnight earlier (figure 4.2) is the increase in AgNP diameter, especially 6-7 nm. This is likely because of the continued formation of AgNPs and the controlled growth of the nanoparticles through the depositing of atoms on existing AgNPs. Aggregation of nanoparticles, though very limited, was observed in the images of samples stored at 4 °C [figure 4.4(b)] and at room temperature in the light [figure 4.4(c)]. The sample stored at room temperature in the dark [figure 4.4(a)] was chosen for use in enzyme interactions due to the level of monodispersion exhibited as compared to other samples [figures 4.4(b) and 4.4(c)]. For interaction with biomolecules, size ranges of 1-10 nm have been reported to be effective and with this consideration, the sizes obtained in the present study were considered satisfactory (Elechiguerra *et al*., 2005).

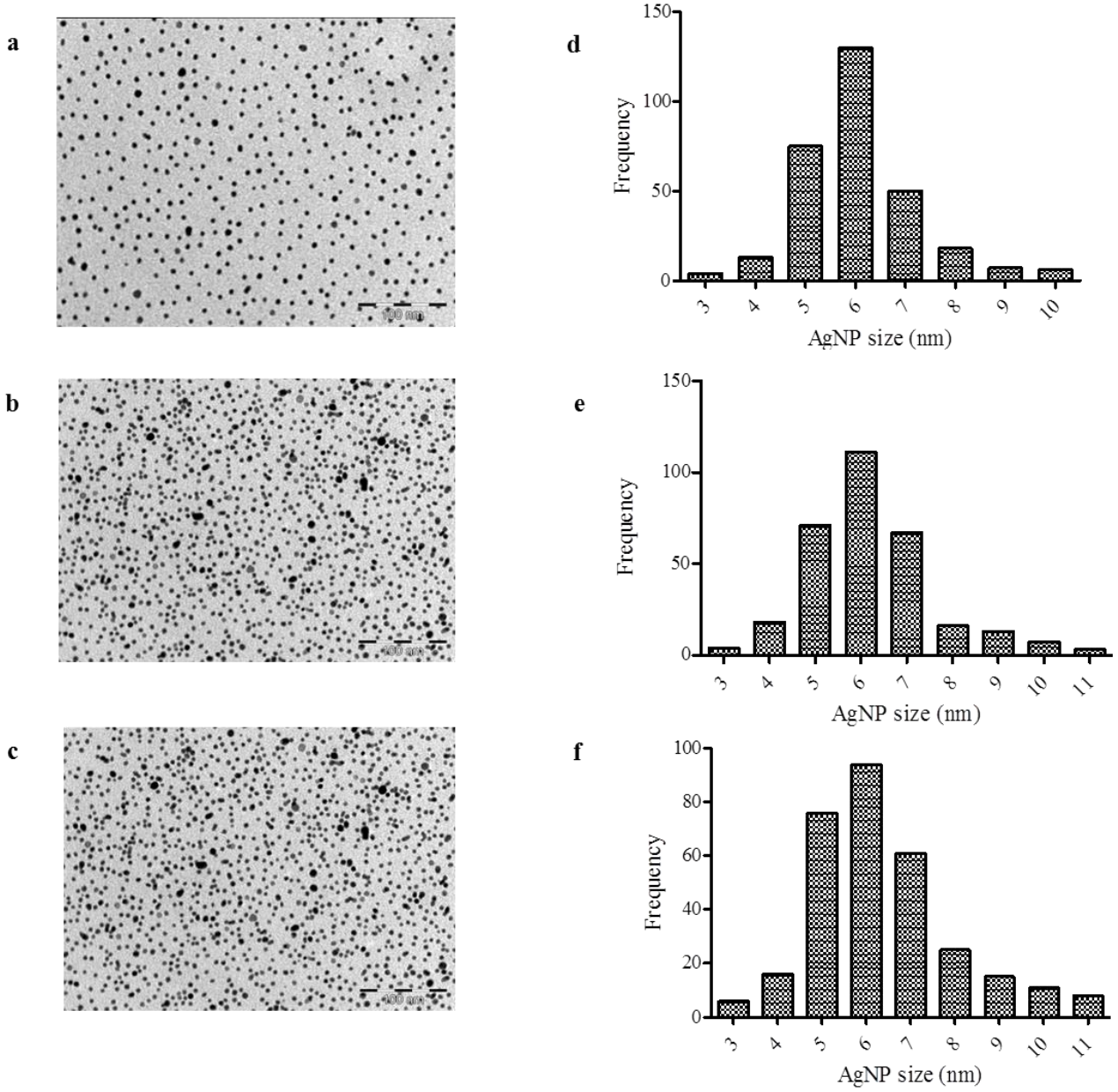

Figure 4.4 TEM images and size distribution of AgNPs stored for a fortnight. (a) Dark at room temperature (b) Dark at 4 °C and (c) Light at room temperature. The scale bar on each TEM image represents 100 nm. (d - f) Size distribution graphs corresponding to the adjacent TEM images. A total of 300 nanoparticles were counted per sample.

4.4.3. Effective nanoparticle concentration

The best suitable concentration of AgNPs to be interacted with LAPs was determined through testing a range of concentrations as described in section 4.3.3. The experiments were performed in triplicates and were conducted on two different days to give a total of six repeats. The main

aim of this study was to determine the effect of synthesized AgNPs on recombinant *Pf*LAP and *Hs*LAP activities and to draw a comparison. For this reason a single AgNP concentration had to be used for both enzyme interaction experiments. Consequently the range finding was done for one enzyme only. The results are shown in figure 4.5 and they show that the lower the nanoparticle concentration, the less the effect on the enzyme activity.

The lowest concentration (1 μM) had 96.5 % activity while the highest concentration (10 μM) had 56.6 %. Based on these result 10 μM was selected as the concentration to use in downstream experiments as it resulted in a 43 % inhibition of *Pf*LAP activity. The desired AgNP concentration should be one which would inhibit / activate enzyme activity significantly while allowing for accurate activity determination in the presence of the activator / inhibitor. It is worth mentioning that since the present study is in relation with the possible use of AgNPs in humans, the concentration of AgNPs for the interaction studies should be chosen very carefully as high concentrations of AgNPs are capable of causing cytotoxicity and genotoxicity through the generation of ROS (AshaRani *et al*., 2009). Based on this information AgNP concentration higher than 10 μM was not considered for this study.

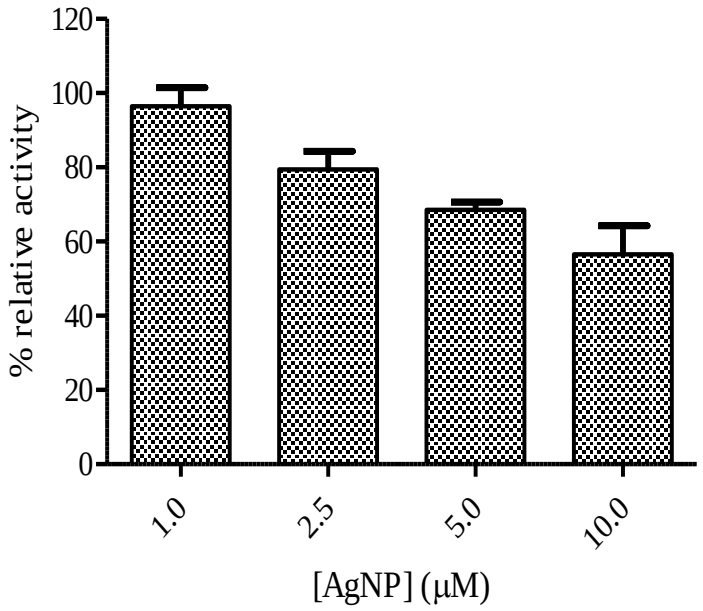

Figure 4.5 The effect of various concentrations of AgNPs on *Pf*LAP. Error bars reflect standard deviation, n = 6.

4.4.4. Effects of AgNPs on LAP activity

4.4.4.1. Interaction of AgNPs with *Pf*LAP

The interaction of *Pf*LAP with AgNPs was conducted using a concentration of 10 μM AgNP concentration based on the results obtained for the range finding experiments (section 4.3.3). The interaction experiments were conducted as described in section 4.3.4. The kinetics results were analysed as previously described in section 3.3.10 using the Michaelis-Menten non-linear regression curve and the Hanes-Woolf linear transformation. The Michaelis-Menten kinetics curve resulting from the AgNPs is given in figure 4.6 and shows the AgNP interaction kinetic curve versus the normal (no AgNP) kinetics curve. The kinetic data obtained was transformed using the Hanes-Woolf equation (equation 4, section 3.1.3) and the results are given in figure 4.7. The results for both the linear Hanes-Woolf and the non-linear regression (Michaelis-Menten) were obtained using the GraphPad Prism 5 software and were used to calculate the kinetic parameters.

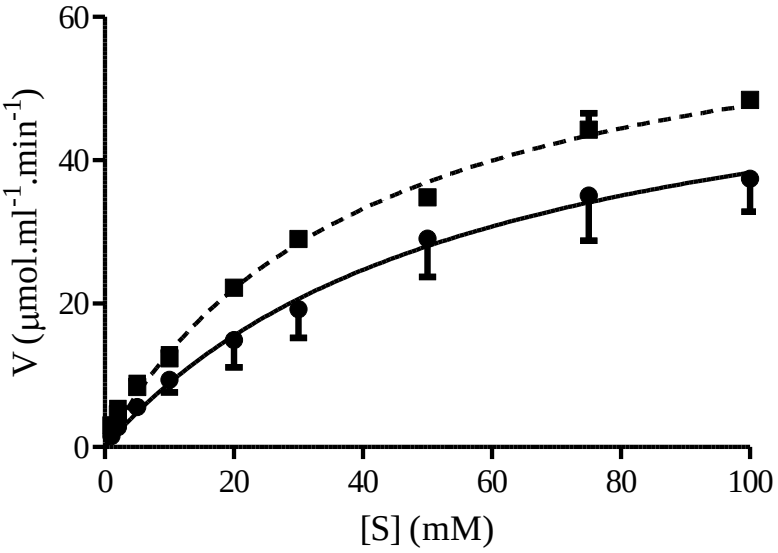

Figure 4.6 Michaelis-Menten kinetics curves showing the results from the interaction of *Pf*LAP with 10 μM AgNPs. The broken line is the control which denotes the kinetics of *Pf*LAP obtained in the absence of AgNPs; the solid line was obtained from kinetic studies incorporating the AgNPs.

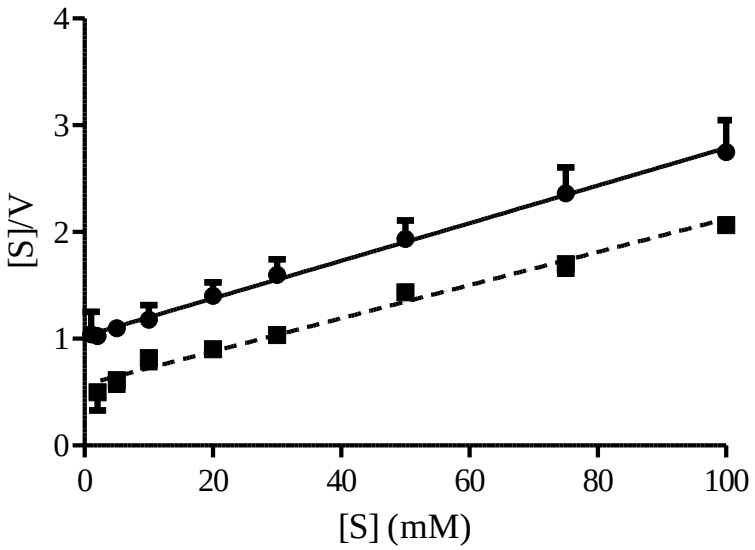

Figure 4.7 Hanes-Woolf linear transformation of the kinetic data generated using AgNPs. The broken line represents the control while the solid line represents the kinetics in the presence of 10 μM AgNPs. The equations and R^2 values for the lines are as follows: Control: $y = 0.0153x + 0.5737$, $R^2 = 0.985$. AgNps interaction: $y = 0.0176x+1.0248$, $R^2 = 0.998$. Error bars represent standard deviation.

Table 4.1 is a summary of the kinetic parameters obtained for *Pf*LAP incubated in the presence and absence of 10 μM AgNPs. Figures 4.6 and 4.7 show that the AgNPs had an inhibitory effect on *Pf*LAP activity. The effect is better illustrated by the V_{max} and K_m values. The V_{max} and K_m for the enzyme alone was 37.5 mM and 65.36 $\mu M.ml^{-1}.min^{-1}$ respectively, while the values for the nanoparticle reactions were 58.23 mM (K_m) and 56.82 $\mu mol.ml^{-1}.min^{-1}$ (V_{max}). The increase in K_m (55 %) is indicative that the enzyme has a lower affinity for the substrate in the presence on the nanoparticles. This along with the decrease in maximum velocity (13 %) implies that the inhibition is a mixed inhibition model. Consequently there was also a decrease in the enzyme turnover rate as well as a 44 % decrease in the catalytic efficiency of the enzyme.

Table 4.1 The kinetic parameters of *Pf*LAP (with / without AgNPs) obtained using the non-linear regression and the Hanes-Woolf linear transformation of the Michaelis-Menten kinetics.

Reaction	Plot	Variables			
		K_m (mM)	V_{max} (μmol.ml^{-1}.min^{-1})	k_{cat} (min^{-1})	k_{cat} / K_m (M^{-1}.min^{-1})
*Pf*LAP + 10 μM AgNPs	Non-linear regression	57.73±19.66	60.35±10.25	6.23×10^2	1.08×10^4
	Hanes-Woolf	58.23	56.82	5.87×10^2	1.0×10^4
*Pf*LAP	Non-linear regression	41.03±4.73	67.24±3.58	6.94×10^2	1.7×10^4
	Hanes-Woolf	37.5	65.36	6.75×10^2	1.8×10^4

4.4.4.2.Interaction of AgNPs with *Hs*LAP

*Hs*LAP–AgNP interaction experiments were done according to the protocols used for the *Pf*LAP-AgNP interaction studies (section 4.4.4.1), and the data analyzed as described in section 3.3.10 using the Michaelis-Menten non-linear regression and the Hanes-Woolf linear transformation. The Michaelis-Menten kinetics curve resulting from the AgNPs is given in figure 4.8 and shows the AgNP interaction kinetic curve versus the normal kinetics curve.

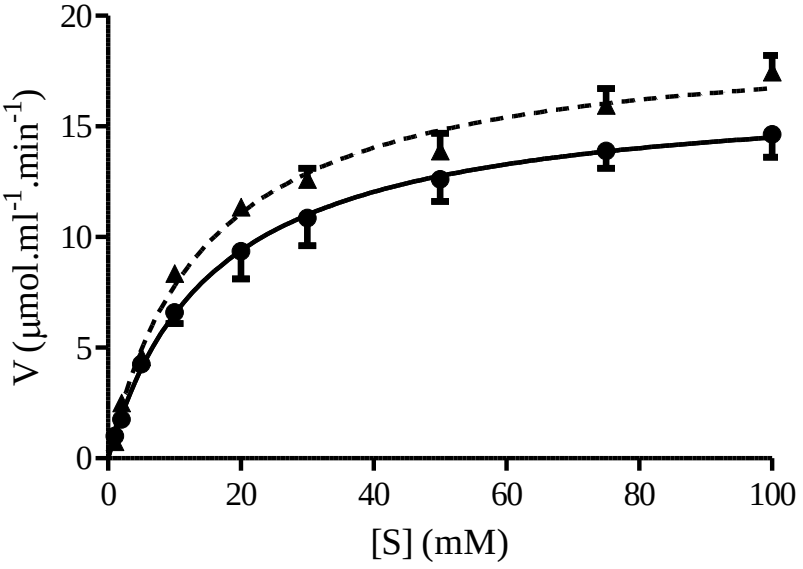

Figure 4.8 Michaelis-Menten kinetics curves showing the results from the interaction of *Hs*LAP with 10 μM AgNPs. The broken line is the control which denotes the kinetics of *Hs*LAP obtained in the absence of AgNPs; the solid line was obtained from kinetic studies incorporating the AgNPs. Error bars represent standard deviation.

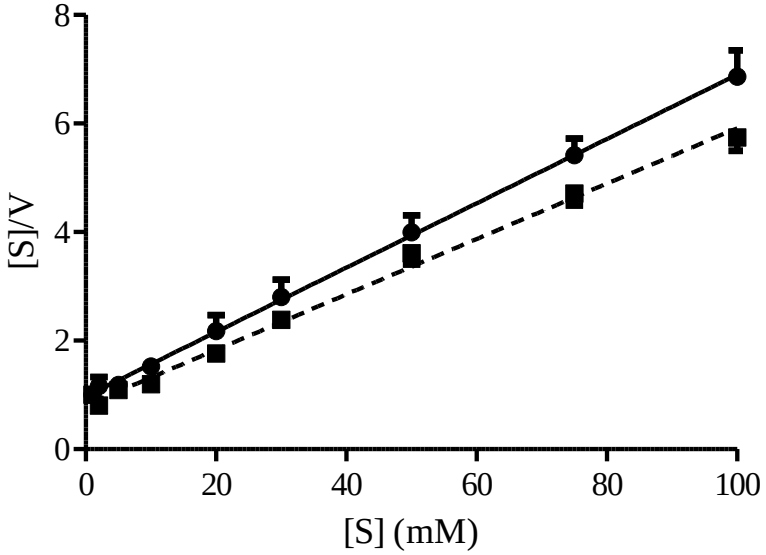

Figure 4.9 Hanes-Woolf linear transformation of the data shown in figure 4.8. The broken line represents the control while the solid line represents the kinetics in the presence of 10 μM AgNPs. The equations and R^2 values for the lines are as follows: Control: $y = 0.05104x + 0.808$, $R^2 = 0.992$. AgNps interaction: $y = 0.05926x+0.973$, $R^2 = 0.999$.

Noticeable changes were observed in the interaction of AgNPs with *Hs*LAP as presented in table 4.2, though not as apparent as the changes observed in the *Pf*LAP-AgNP interactions (table 4.1). The V_{max} and K_m for the enzyme alone was 15.83 mM and 19.59 $\mu mol.ml^{-1}.min^{-1}$ respectively, while the values for the nanoparticle reactions were 16.42 mM (K_m) and 16.88 $\mu mol.ml^{-1}.min$ (V_{max}). The increase in K_m (3.7 %) is indicative that the enzyme has a slightly lower affinity for the substrate in the presence on the nanoparticles. This along with the decrease in maximum velocity (13.8 %) implies that the inhibition is non-competitive. The 3.7 % change in the K_m of *Hs*LAP was very low and most likely because of experimental errors and deviations. The standard deviation indicates that the K_m figures are almost the same hence the only change considered significant was that of V_{max}.

Table 4.2 The kinetic parameters of *Hs*LAP (with / without AgNPs) obtained using the non-linear regression and the Hanes-Woolf linear transformation of the Michaelis-Menten kinetics.

Reaction	Plot	Variables			
		K_m (mM)	V_{max} (μmol.ml^{-1}.min^{-1})	k_{cat} (min^{-1})	k_{cat} / K_m (M^{-1}.min^{-1})
*Hs*LAP + 10 μM AgNPs	Non-linear regression	15.78±2.25	16.78±0.74	1.49×10^3	9.45×10^4
	Hanes-Woolf	16.42	16.88	1.5×10^3	9.14×10^4
*Hs*LAP	Non-linear regression	14.67±1.5	19.17±0.59	1.7×10^3	1.16×10^5
	Hanes-Woolf	15.83	19.59	1.74×10^3	1.1×10^5

4.4.4.3.Comparison of the effects of AgNPs on recombinant *Pf* and *Hs*LAPs

There appears to be a considerable difference in the interaction of AgNPs with *Pf*LAP and *Hs*LAP. Both enzymes' activities are inhibited in the presence of 10 μM AgNPs, with *Pf*LAP's activity being more severely affected. The K_m of *Pf*LAP in the presence of nanoparticles increased by 44.4 % while that of the *Hs*LAP only increased by a 3.7 %. This difference is suggestive of two possible factors which would need further investigation; (i) AgNPs have greater affinity and possibly form a stronger complex with *Pf*LAP than with *Hs*LAP or (ii) the binding site of AgNPs on *Pf*LAP plays a more important role in catalysis compared to the binding sites on *Hs*LAP. The results obtained in the present study suggest that *Pf*LAP undergoes a mixed inhibition model in the presence of 10 μM AgNPs as an increase in K_m is observed along with a decrease in maximum velocity. In contrast, in the presence of 10 μM AgNPs, *Hs*LAP conforms to a non-competitive inhibition model as the K_m remains constant while the maximum velocity decreases. The nature of the interactions in the present study suggest that the binding of AgNPs to the LAP enzymes occurs irrespective of whether the substrate is bound or not. This property is synonymous with non-competitive inhibition. The catalytic efficiency of *Pf*LAP decreased 0.45 fold, while that of *Hs*LAP decreased by 0.17 fold. Relative to *Hs*LAP, *Pf*LAP had an almost 3 fold decrease in catalytic efficiency and a 15 fold decrease in affinity towards the L*p*NA.

The mechanism of the interaction of AgNPs among other nanoparticles with enzymes and other biomolecules is not fully understood, but is proposed to occur via attractions to thiol bearing

moieties such as cysteine and metheonine residues in proteins (Choi *et al*., 2003; Elechiguerra *et al*., 2005; Gondikas, 2012). The structure of the proteins would play a major role in the extent of the effect of the nanoparticles as there is high likelihood of interaction with residues that are exposed on the surface of the protein than concealed residues. The LAP enzymes used in the present study contained the same number of cysteine residues in their structure as calculated using the online tool Amino Acid Calculator. It is therefore hypothesised that the structure of *Pf*LAP has a higher number of exposed thiol-bearing residues than that of *Hs*LAP hence the much higher extent of inhibition of *Pf*LAP. However no detailed records of the crystallised structures have been published to date and this hypothesis remains to be proven.

4.5. Conclusions

The current chapter's main objective was to investigate the effect of AgNPs on *Pf*LAP and *Hs*LAP and compare the two enzymes' activities. This was initiated by the synthesis and characterisation of AgNPs (sections 4.3.1 and 4.3.2) which gave spherical nanoparticles and conformed to the required size range. Sizes ranged from 3-10 nm, with a predominant size range of 5-6 nm. Nanoparticles sized between 1 and 10 nm are considered satisfactory for the purposes of interactions with enzymes as previously suggested by Elechiguerra *et al.* (2005). AgNPs were found to be stable for two weeks with high fidelity in size and shape while their distribution showed a slight increase in density. The ideal AgNP concentration for interacting with LAPs was investigated by incubating the respective enzyme with the various AgNP concentrations and was found to be 10 μM.

Based on the data obtained in the current chapter, it is apparent that AgNPs are able to selectively supress the activity of *Pf*LAP to a much larger extent than *Hs*LAP by affecting the enzyme affinity to the substrate and the catalytic efficiency. This postulation is supported by the 15 fold increase in the K_m of *Pf*LAP relative to that of *Hs*LAP and the approximately 3 fold decrease in catalytic efficiency of *Pf*LAP relative to that of *Hs*LAP.

Chapter 5: Final discussions, conclusions and future recommendations

5.1. General discussions and conclusions

Much progress has been made in the fight against malaria in the last decade as evidenced by a drop in the transmission and deaths; there were 219 million cases of malaria in 2010 as compared to an estimated 300-500 million in 2000. Deaths declined to 610 000 - 970 000 in 2010 from 700 000 - 2.7 million in 2000 (Breman, 2001; WHO, 2012). Despite the progress in the fight against malaria, its debilitating effects remain, particularly among Africa's children. It has often been said that "African children are the future of the continent" (Garcia, 2008), and from this statement it can be extrapolated that malaria threatens the very future of Africa. Medical research against malaria has achieved remarkable breakthroughs such as the discovery of chloroquine in the middle of the 20th century and the much recent discovery of artemisinins. However the parasites have been equal to the task by developing resistance to all of the current drugs hence there is a need for more options.

As a result of extensive research, a number of potential malaria biomedical targets have been proposed. Haemoglobin digestion, a process essential for the supply of vital amino acids for the growth of malaria parasites has been one of the proposed malaria biomedical targets. In particular, the neutral metallopeptidase *Pf*LAP has been identified as a viable biomedical target and results to date have emphasised its importance (Gardiner *et al*., 2006; Stack *et al*., 2007; Cunningham *et al*., 2008; McGowan *et al*., 2010; Skinner-Adams *et al*., 2010; Thriviege *et al*., 2012). The high specialization and a higher level of expression of *Pf*LAP when compared to its counterpart *Pf*AAP underscores its importance in haemoglobin break down and the survival of the parasite in the human host. Various experiments such as gene knock out experiments and the inhibition studies using parasites over-expressing *Pf*LAP have all echoed the importance of *Pf*LAP. It is for these reasons that the present study has been conducted, in order to develop novel therapeutic agents towards exploiting this biomedical target.

The objectives set out for the present study were achieved by over-expressing and purifying *Pf*LAP and *Hs*LAP. A truncated version of the enzyme was expressed as previously done by Stack *et al*. (2007). This was done after attempts to amplify and express the full length gene were unsuccessful. Stack *et al*. (2007) had previously failed to express active full length *Pf*LAP in a heterologous system hence the decision in the current study to express the truncated version as they had obtained success with it. Optimum parameters for *Pf*LAP were 2 mM Mn^{2+}, 25 °C and a pH of 8, while *Hs*LAP had optimum activity at pH 7, a temperature of 37 °C and 2 mM Mn^{2+}. Kinetic parameters were also determined and *Pf*LAP had a K_m of 42.7 mM and a V_{max} of 59.9 μmol.ml^{-1}.min^{-1} while *Hs*LAP had a K_m of 16.72 mM and a V_{max} of 17.21 μmol.ml^{-1}.min^{-1}. *Pf*LAP had a k_{cat} of 6.85×10^2 min^{-1} and a k_{cat} / K_m of 1.6×10^4 M^{-1}.min^{-1} while *Hs*LAP had a k_{cat} of 1.72×10^3 min^{-1} and a k_{cat} / K_m of 1.03×10^5 M^{-1}.min^{-1}. Silver nanoparticles were synthesised using microwave irradiation and were observed to be spherical in morphology with an average size of 6 nm. The silver nanoparticles gave a plasmon resonance band at 420 nm and were stable for two weeks at room temperature in the dark.

The present study sought to investigate the effects of PVP stabilised silver nanoparticles on recombinant *Pf*LAP and *Hs*LAP and compare the results. The hypothesis of the study highlighted that due to differences in the amino acid structures of *Pf*LAP and *Hs*LAP, silver nanoparticles would selectively affect the activity of one enzyme in a way that differs from the other. The results obtained in the study showed that the silver nanoparticles have an inhibitory effect on both enzymes. Although both enzymes showed a decrease in activity, *Pf*LAP was inhibited 3 fold more than the *Hs*LAP thus supporting the hypothesis. The difference in the magnitude of the effects of silver nanoparticles on the enzymes can be attributed to the structural differences that exist between the enzymes as depicted by the different gene sequences (Cunningham *et al.,* 2008; Poreba *et al*., 2012).

One of the proposed mechanisms of the interaction of silver nanoparticles with biomolecules is through their ability to form bonds with sulphur bearing groups of amino acid residues such as cysteine and methionine (Choi *et al*., 2003; Rai *et al*., 2012). It is believed that such interactions disrupt the tertiary and possibly the quaternary structure of enzymes thereby affecting their function (Klueh *et al*., 2000). Using the online amino acid calculating software Amino Acid

Calculator (MacCoss, 2004), the numbers of cysteine and methionine residues in *Pf*LAP and *Hs*LAP were almost equal with the only difference being that *Pf*LAP had one methionine residue more than *Hs*LAP. These observations confirm that the differences between these enzymes exist in structure and not in the amount of sulphur bearing groups. The differences in structure imply that exposure and accessibility of sulphur bearing moieties to nanoparticles may be more enhanced in one enzyme variant and not the other.

The *Pf*LAP enzyme used in this study was a truncated version, as previously expressed by Stack *et al.* (2007). The full length version of the enzyme consists of an additional three cysteine residues and it is possible that the results from the truncated enzyme studies might differ from the full length *Pf*LAP because of the structural differences. This would be of particular relevance if the cysteine residues were available for interaction with silver nanoparticles. The truncated asparagine rich N-terminal was reported to be unimportant in the catalytic function of the enzyme as depicted by its ability to maintain catalysis despite truncation (Stack *et al*., 2007). It remains possible that a conformational change in this part of the native enzyme may be important in the conformation and structure of the whole enzyme.

The structure of *Pf*LAP as presented by McGowan *et al.* (2009) reveals the importance of methionine residues in the S1 pocket which is a part of the enzyme important for catalysis. Because methionine residues comprise sulphur atoms, their presence in the S1 pocket presents a possible channel by which silver nanoparticles exert their effects on *Pf*LAP. Cunningham *et al.* (2008) reported on the significant differences in the S1 sub-sites of *Pf*LAP and *Hs*LAP and it is speculated that these differences may be part of the reason for the discrepancies in the way *Pf*LAP and *Hs*LAP respond to treatment with silver nanoparticles. However this remains a matter of speculation and can only be verified once the mechanism of action of *Hs*LAP has been elucidated.

*Pf*LAP is mainly expressed during the erythrocytic stages of *P. falciparum* growth in the human host (Thrivierge *et al*., 2012); this means that the red blood cells would be the target cells of any therapeutic agent targeting *Pf*LAP. Rothen-Rutishauser *et al.* (2006) reported the ability of silver enhanced GNPs to cross the membrane of erythrocytes into their cytosol, the site of *Pf*LAP

activity. Targeting of the erythrocytes may be achieved by exploiting the ligands or receptors which are used by merozoites when invading erythrocytes. Duraisingh *et al.* (2003) reported on the importance of the erythrocyte receptor glycophorin C for invasion by *P. falciparum* merozoites. If ligands for this receptor can be designed and attached to functionalized silver nanoparticles, erythrocytes can be targeted and the nanoparticles can be delivered to their target destination. This would prevent possible toxicity against non-target cells.

Silver nanoparticles also selectively inhibit *P. falciparum* triosephosphate isomerase while having minimal effects on the human version of the enzyme (De Moor, 2013). These results indicate that silver nanoparticles may be used to target more than one biomedical target thereby increasing their effectiveness as potential therapeutic agents. Another potential target of silver nanoparticles whose importance in the survival of *P. falciparum* remains to be sufficiently validated is the neutral aminopeptidase *Pf*AAP which functions alongside *Pf*LAP in the breakdown of dipeptides. The ability of any therapeutic agent to target more than one biomedical target greatly reduces chances of drug resistance, a phenomenon which has made the fight against malaria very difficult.

5.2. Future recommendations

The results of the current study revealed that the structural differences between *Pf*LAP and *Hs*LAP may cause the two enzymes to respond differently when interacted with various chemotherapeutic agents. There still remains more work to be done to conclusively validate silver nanoparticles among other forms of nanotechnology as possible chemotherapeutic agents for malaria therapy. Firstly, a way to express the full length form of *Pf*LAP would need to be devised as the native enzyme would give a better indication of what would happen in the parasite. Despite the retention of catalysis by the truncated enzyme, the presence of extra cysteine residues in the full length version of the enzyme may be important in how the native enzyme responds to interaction with silver nanoparticles.

The size of nanoparticles used may also be varied to ascertain the effect of different sizes of nanoparticles on the enzymes. This would be necessary as the effect of nanoparticles on different microbes and biomolecules is size dependent (Elechiguerra *et al*., 2005; Morones *et al*., 2005; Lu

et al., 2008; Lara *et al*., 2009). In which case, nanoparticles larger than 10 nm would be used since the majority of nanoparticles used in the present study were below 10 nm. However the limitations on the sizes of metallic nanoparticles that can be taken up by erythrocytes need to be considered so as to prevent using nanoparticles which wouldn't be taken up by cells. Furthermore, the silver nanoparticles used for interaction with LAP may be stabilized and functionalized with agents other than PVP.

Apart from the PVP stabilization, other channels for the preparation of monodisperse nanoparticles would be to use a protein cage such as apoferritin, which could ensure delivery of the nanoparticles to infected erythrocytes (Galvez *et al*., 2008; Kasyutich *et al*., 2010). Burns and Pollack (1988) reported that erythrocytes infected with *P. falciparum* are capable of taking up apoferritin by endocytosis, a feat which is not possible in healthy erythrocytes. There are good chances that AgNPs synthesized in apoferritin cages can therefore be taken up by infected erythrocytes without affecting the healthy cells. Other advantages of using apoferritin are that it is non-toxic and produces uniform monodispersed nanoparticles (Galvez *et al*., 2008). Ma-Ham *et al.* (2011) reported that apoferritin does not affect the efficacy of therapeutic agents when it is used as a cage for delivering drugs to target sites. Liposomes may also be used to encapsulate silver nanoparticles and deliver them to infected cells. Liposomes have been successfully used in drug delivery in humans and they present an interesting option for the delivery of metallic nanoparticles to relevant targets.

Monolayer protected clusters (MPC) and mixed monolayer protected clusters (MMPC) may also be used in the synthesis of nanoparticles to enhance their functionality (Sarathy *et al*., 1997; Kim *et al*., 2004). The shape of nanoparticles interacted with LAP needs to be varied as this has also been found to have a significant bearing on how biological systems respond to nanoparticles. Argawal *et al*. (2013) found that mammalian epithelial and immune cells were able to take up nanodiscs in a better way than they took up nanorods. This would be accomplished by varying the stoichiometry of the precursor reagents or the pH of the reactions during nanoparticle synthesis (Pal *et al.,* 2007).

Considering the different effects of various metallic nanoparticles on cells or biological molecules (Pujalte *et al*., 2011), it would be worthwhile to investigate the effects of other types of nanoparticles such as gold, platinum and titanium oxide. Given the efficacy of silver nanoparticles against whole microorganisms such as various bacteria and viruses, it would be interesting to find out their effect on whole *P. falciparum* cells. This would be worthwhile especially considering that silver nanoparticles may have other biomedical targets within the protozoa besides LAP. Also considering the toxicity of silver nanoparticles against some mammalian cells; it would be worthwhile to investigate the effect that they have towards healthy and infected erythrocytes. The problem of redundancy of functions by enzymes as observed in the falcipains which are found in the *P. falciparum* digestive vacuole needs to be considered as *Pf*AAP has broad substrate specificity (section 1.3.3). This presents an alternative channel through which *P. falciparum* may be able to still hydrolyze leucine containing dipeptides when *Pf*LAP is inhibited. It is therefore worthwhile to investigate the effects of silver nanoparticles on the activity of *Pf*AAP.

With the growing threat of drug resistance coupled with the slow pace at which malaria elimination is happening in Africa, the need for innovative strategies to combat malaria cannot be overemphasized. One of the major challenges remains as the selectivity of therapeutic agents towards parasite biomedical targets without affecting the corresponding human homologs. Though the knowledge of malaria parasites is increasing, their adaptation seems to be happening faster than humans can cope and as a result malaria exists to this day. The case of malaria in Africa is not just a health issue but also a social and economic issue which needs to be addressed in order for Africa to progress towards a better standard of life. Considering the toll that malaria takes on African societies socially and economically, it may be said that part of the answer to Africa's social and economic woes lies in the discovery of effective chemotherapeutic agents which will aid in the elimination of malaria from the continent.

References

Al-Jamal, W.T., Kostarelos, K., 2011. Liposomes: from a clinically established drug delivery system to a nanoparticle platform for theranostic nanomedicine. Acc. Chem. Res. 44, 1094–104.

Alivisatos, A.P., 1996. Semiconductor clusters, nanocrystals, and quantum dots. Science. 271, 933–937.

Allen, M.P., Yamada, A.H., Carpenter, F.H., 1983. Kinetic parameters of metal-substituted leucine aminopeptidase from bovine lens. Am. Chem. Soc. 22, 3778–3783.

Andrews, P., 1964. Estimation of the molecular weights of proteins by Sephadex gel-filtration. Biochem. J. 91, 222–33.

Agarwal, R., Singh, V., Jurney, P., Shi, L., Sreenivasan, S. V, Roy, K., 2013. Mammalian cells preferentially internalize hydrogel nanodiscs over nanorods and use shape-specific uptake mechanisms. Proc. Natl. Acad. Sci. U. S. A. 110, 17247–52.

Arora, S., Jain, J., Rajwade, J.M., Paknikar, K.M., 2008. Cellular responses induced by silver nanoparticles: *In vitro* studies. Toxicol. Lett. 179, 93–100.

Asharani, P. V, Low, G., Mun, K., Hande, M.P., Valiyaveettil, S., 2009. Cytotoxicity and genotoxicity of silver. Am. Chem. Soc. 3, 279–290.

Bell, D., Wongsrichanalai, C., Barnwell, J., 2006. Ensuring quality and access for malaria diagnosis: how can it be achieved? Nat. Rev. Microbiol. 7–20.

Bergmans, H., Die, I. Van, Hoekstra, W., 1981. Transformation in *Escherichia coli*: stages in the process. J. Bacteriol. 146, 564–570.

Bhumkar, D.R., Joshi, H.M., Sastry, M., Pokharkar, V.B., 2007. Chitosan reduced gold nanoparticles as novel carriers for transmucosal delivery of insulin. Pharm. Res. 24, 1415–26.

Bisswanger, H., 2008. Enzyme Kinetics Principles and Methods, 2nd ed. Wiley - VCH, Weinheim. pp. 75-76.

Bitter, G., Egan, K.M., 1984. Expression of heterologous genes in *Saccharomyces cerevisiae* from vectors utilizing the glyceraldehyde-3-phosphate dehydrogenase gene promoter. Gene 32, 263–74.

Block, H., Maertens, B., Spriestersbach, A., Brinker, N., Kubicek, J., Fabis, R., Labahn, J., Schäfer, F., 2009. Immobilized-metal affinity chromatography (IMAC): a review. Methods Enzymol. 463, 439–73.

Bloland, P.B., 2001. Drug resistance in malaria. WHO Press. Geneva. pp. 2-22

Bolanos-Garcia, V.M., Davies, O.R., 2006. Structural analysis and classification of native proteins from *E. coli* commonly co-purified by immobilised metal affinity chromatography. Biochim. Biophys. Acta 1760, 1304–13.

Braydich-Stolle, L., Hussain, S., Schlager, J.J., Hofmann, M.C., 2005. *In vitro* cytotoxicity of nanoparticles in mammalian germline stem cells. Toxicol. Sci. 88, 412–9.

Brust, M., Fink, J., Schiffrina, D.B.D.J., Kielyb, C., 1995. Synthesis and reactions of functionalised gold nanoparticles. Mater. Sci. 1655–1656.

Burley, S.K., David, P.R., Taylor, a, Lipscomb, W.N., 1990. Molecular structure of leucine aminopeptidase at 2.7-A resolution. Proc. Natl. Acad. Sci. U. S. A. 87, 6878–82.

Cereghino, J.L., Cregg, J.M., 2000. Heterologous protein expression in the methylotrophic yeast *Pichia pastoris*. FEMS Microbiol. Rev. 24, 45–66.

Chen, P.C., Mwakwari, S.C., Oyelere, A.K., 2008. Gold nanoparticles: From nanomedicine to nanosensing. Nanotechnol. Sci. Appl. 1, 45–65.

Chi, M.C., Lyu, R.C., Lin, L.L., Huang, H.B., 2008. Characterization of *Bacillus kaustophilus* leucine aminopeptidase immobilized in Ca-alginate/k-carrageenan beads. Biochem. Eng. J. 39, 376–382.

Chien, A., Edgar, D.B., Trela, J.M., 1976. Deoxyribonucleic Acid polymerase from the extreme thermophile *Thermus aquaticus*. J. Bacteriol. 127, 1550–1557.

Chithrani, B.D., Ghazani, A., Chan, W.C.W., 2006. Determining the size and shape dependence of gold nanoparticle uptake into mammalian cells. Nano Lett. 6, 662–8.

Choi, S.H., Lee, S.H., Hwang, Y.M., Lee, K.P., Kang, H.D., 2003. Interaction between the surface of the silver nanoparticles prepared by γ-irradiation and organic molecules containing thiol group. Radiat. Phys. Chem. 67, 517–521.

Coatney, G. R., 1963. Pitfalls in a discovery: the chronicle of chloroquine. Am. J. Trop. Med. Hyg. 12, 121-128.

Collins, W.E., Jeffery, G.M., Collins, W.E., Jeffery, G.M., 2007. *Plasmodium malariae* : parasite and disease. Clin. Microbiol. Rev. 20, 579–592.

Collins, J., Hohn, B., 1978. Cosmids: a type of plasmid gene-cloning vector that is packageable *in vitro* in bacteriophage lambda heads. Proc. Natl. Acad. 75, 4242–4246.

Connor, E.E., Mwamuka, J., Gole, A., Murphy, C.J., Wyatt, M.D., 2005. Gold nanoparticles are taken up by human cells but do not cause acute cytotoxicity. Small 1, 325–7.

Copeland, R., 2004. Enzymes: a practical introduction to structure, mechanism, and data analysis. Wiley – VCH, New York. pp. 115, 120, 145.

Couvreur, P., Vauthier, C., 2006. Nanotechnology: intelligent design to treat complex disease. Pharm. Res. 23, 7.

Cox-singh, J., Hiu, J., Lucas, S.B., Divis, P.C., Zulkarnaen, M., Chandran, P., Wong, K.T., Adem, P., Zaki, S.R., Singh, B., Krishna, S., 2010. Severe malaria-a case of fatal *Plasmodium knowlesi* infection with post-mortem findings. Malar. J. 9, 1–7.

Crowe, J.E., Weitkamp, J.H., 2001. Improved efficiency and reliability of RT-PCR using tag-extended RT primers and temperature gradient PCR. Biotechniques 31, 466–472.

Cunningham, E., Drag, M., Kafarski, P., Bell, A., 2008. Chemical target validation studies of aminopeptidase in malaria parasites using alpha-aminoalkylphosphonate and phosphonopeptide inhibitors. Antimicrob. Agents Chemother. 52, 3221–8.

Dalal, S., Klemba, M., 2007. Roles for two aminopeptidases in vacuolar hemoglobin catabolism in *Plasmodium falciparum*. J. Biol. Chem. 282, 35978–87.

Dagert, M., Ehrlich, S., 1979. Prolonged incubation in calcium chloride improves the competence of *Escherichia coli* cells. Gene 6, 23–28.

Dennison, C., Natarajan, S., 1999. A guide to protein isolation. Kluwer Academic, New York, NY. Pp 52, 55-56.

Despommier, D.D., Gwadz, R.W., Hotez, P.J., Knirsch, C.A., 2005. Parasitic Diseases. Apple Trees P roductions, New York. pp. 50-53.

Dieffenbach, C.W., Lowe, T.M., Dveksler, G.S., 1993. General concepts for PCR primer design. Genome R 3, 30–37.

Domínguez-Vera, J.M., Gálvez, N., Sánchez, P., Mota, A.J., Trasobares, S., Hernández, J.C., Calvino, J.J., 2007. Size-controlled water-soluble Ag nanoparticles. Eur. J. Inorg. Chem. 4823–4826.

Dronamraju, K. R., 2006. Malaria: genetic and evolutionary aspects, Vol. 5. Springer. pp. 125

Dwosh, H.A., Hong, H.H.L., Austgarden, D., Herman, S., Schabas, R., 2003. Identification and containment of SARS in a community hospital. Can. Med. Ass. 168, 1415–1420.

Eisenthal, R., 1974. The direct linear plot. A new graphical procedure for estimating enzyme kinetic parameters. Biochem. J 139, 715–720.

Elechiguerra, J.L., Burt, J.L., Morones, J.R., Camacho-Bragado, A., Gao, X., Lara, H.H., Yacaman, M.J., 2005. Interaction of silver nanoparticles with HIV-1. J. Nanobiotechnology 3, 6.

Elechiguerra, J.L., Larios-Lopez, L., Liu, C., Garcia-Gutierrez, D., Camacho-Bragado, A., Yacaman, M.J., 2005. Corrosion at the Nanoscale: The case of silver nanowires and nanoparticles. Chem. Mater. 17, 6042–6052.

Emerich, D.F., Thanos, C.G., 2007. Targeted nanoparticle-based drug delivery and diagnosis. J. Drug Target. 15, 163–83.

Fairbanks, G., Steck, T. L., & Wallach, D. F. H., 1971. Electrophoretic analysis of the major polypeptides of the human erythrocyte membrane. Biochemistry, 10, 2606-2617.

Farokhzad, O.C., Langer, R., 2009. Impact of nanotechnology on drug delivery. ACS Nano 3, 16–20.

Fidock, D.A., Rosenthal, P.J., Croft, S.L., Brun, R., Nwaka, S., 2004. Antimalarial drug discovery: efficacy models for compound screening. Nat. Rev. Drug Discov. 3, 509–20.

Florens, L., Washburn, M.P., Raine, J.D., Anthony, R.M., Grainger, M., Haynes, J.D., Moch, J.K., Muster, N., Sacci, J.B., Tabb, D.L., Witney, A. a, Wolters, D., Wu, Y., Gardner, M.J., Holder, A. a, Sinden, R.E., Yates, J.R., Carucci, D.J., 2002. A proteomic view of the *Plasmodium falciparum* life cycle. Nature 419, 520–6.

Gaberc-Porekar, V., Menart, V., 2001. Perspectives of immobilized-metal affinity chromatography. J. Biochem. Biophys. Methods 49, 335–60.

Gallup, J.L., Sachs, J.D., 2000. The economic burden of malaria. CID Work. Pap. 52, 1–9.

Garcia, M., Pence, A. R., Evans, J. L., 2008. Africa's future, Africa's challenge: early childhood care and development in Sub-Saharan Africa. World Bank Publications.

Gardiner, D.L., Trenholme, K.R., Skinner-Adams, T.S., Stack, C.M., Dalton, J.P., 2006. Overexpression of leucyl aminopeptidase in *Plasmodium falciparum* parasites. Target for the antimalarial activity of bestatin. J. Biol. Chem. 281, 1741–5.

Gardner, M.J., Hall, N., Fung, E., White, O., Berriman, M., Hyman, R.W., Carlton, J.M., Pain, A., Nelson, K.E., Bowman, S., Paulsen, I.T., James, K., Eisen, J. a, Rutherford, K., Salzberg, S.L., Craig, A., Kyes, S., Chan, M.-S., Nene, V., Shallom, S.J., Suh, B., Peterson, J., Angiuoli, S., Pertea, M., Allen, J., Selengut, J., Haft, D., Mather, M.W., Vaidya, A.B., Martin, D.M. a, Fairlamb, A.H., Fraunholz, M.J., Roos, D.S., Ralph, S. a, McFadden, G.I., Cummings, L.M., Subramanian, G.M., Mungall, C., Venter, J.C., Carucci, D.J., Hoffman, S.L., Newbold, C., Davis, R.W., Fraser, C.M., Barrell, B., 2002. Genome sequence of the human malaria parasite *Plasmodium falciparum*. Nature 419, 498–511.

Gavigan, C.S., Dalton, J.P., Bell, a, 2001. The role of aminopeptidases in haemoglobin degradation in *Plasmodium falciparum*-infected erythrocytes. Mol. Biochem. Parasitol. 117, 37–48.

GE Healthcare., 2010. Gel Filtration: Principles and Methods. General Electric Company. https://www.gelifesciences.com/gehcls_images/GELS/Related%20Content/Files/1314807262343/litdoc18102218_20131220222557.pdf. Accessed: 12/11/2013

Gelb, M.H., 2007. Drug discovery for malaria: a very challenging and timely endeavor. Curr. Opin. Chem. Biol. 11, 440–5.

Gething, P.W., Patil, A.P., Smith, D.L., Guerra, C.A., Elyazar, I.R.F., Johnston, G.L., Tatem, A.J., Hay, S.I., 2011. A new world malaria map : *Plasmodium falciparum* endemicity in 2010. Malar. J. 10, 378.

Ghosh, P., Han, G., De, M., Kim, C.K., Rotello, V.M., 2008. Gold nanoparticles in delivery applications. Adv. Drug Deliv. Rev. 60, 1307–15.

Giaever, G., Chu, A.M., Ni, L., Connelly, C., Riles, L., Véronneau, S., Dow, S., Lucau-Danila, A., Anderson, K., André, B., Arkin, A.P., Astromoff, A., El-Bakkoury, M., Bangham, R., Benito, R., Brachat, S., Campanaro, S., Curtiss, M., Davis, K., Deutschbauer, A., Entian, K.-D., Flaherty, P., Foury, F., Garfinkel, D.J., Gerstein, M., Gotte, D., Güldener, U., Hegemann, J.H., Hempel, S., Herman, Z., Jaramillo, D.F., Kelly, D.E., Kelly, S.L., Kötter, P., LaBonte, D., Lamb, D.C., Lan, N., Liang, H., Liao, H., Liu, L., Luo, C., Lussier, M., Mao, R., Menard, P., Ooi, S.L., Revuelta, J.L., Roberts, C.J., Rose, M., Ross-Macdonald, P., Scherens, B., Schimmack, G., Shafer, B., Shoemaker, D.D., Sookhai-Mahadeo, S., Storms, R.K., Strathern, J.N., Valle, G., Voet, M., Volckaert, G., Wang, C., Ward, T.R., Wilhelmy, J., Winzeler, E. a, Yang, Y., Yen, G., Youngman, E., Yu, K., Bussey, H., Boeke, J.D., Snyder, M., Philippsen, P., Davis, R.W., Johnston, M., 2002. Functional profiling of the *Saccharomyces cerevisiae* genome. Nature 418, 387–91.

Giddings, G., Allison, G., Brooks, D., Carter, A., 2000. Transgenic plants as factories for biopharmaceuticals. Nat. Biotechnol. 18, 1151–5.

Gilbert, H. F., 2000. Basic concepts in biochemistry a student's survival guide 2nd ed. McGraw-Hill Companies, London. pp.96-115

Gräslund, S., Nordlund, P., Weigelt, J., Hallberg, B. M., Bray, J., Gileadi, O., Knapp, S., Oppermann, U., Arrowsmith, C., Hui, R., Ming, J., dhe-Paganon, S., Park, A.S., Yee, A., Edwards, A., Vincentelli, R., Cambillau, C., Rosalind, K., Sung-Hou, K., Rao, Z., Shi, Y., Terwilliger, T.C., Kim, C., Hung, L., Waldo, G.S., Peleg, Y., Albeck, T.U., Dym, O., Prilusky, J., Sussman, J. L., Stevens, R.C., Lesley, S.A., Wilson, I.A., Collart, F., Dementieva, I., Donnelly, M.I., Eschenfeldt, W.H., Kim, Y., Stols, L., Wu, R., Zhou, M., K Burley, S.K., Emtage, J.S., Sauder, J.M., Thompson, D., Bain, K., Gheyi, J.L.T., Zhang, F., Atwell, F., Almo, S.C., Bonanno, J.B., Fiser, A., Swaminathan, S., Studier, F.W., Chance, M.R., Sali1, A., Acton, T.B., Xiao, R., Zhao, L., Ma, L.C., Hunt, J.F., Tong, L.,

Cunningham, K., Inouye, M., Anderson, S., Janjua, D., Shastry, R., Ho, C.K., Wang, C., Wang, H., Jiang, M., Montelione, G.T., Owens, R.J., Daenke, S., Schütz, A., Heinemann, U., Yokoyama, S., Gunsalus, K.C., 2008. Protein production and purification. Nat. Methods 5, 135–146.

Grosjean, H., Fiers, W., 1982. Preferential codon usage in prokaryotic genes : the optimal codon-antidon and the selective codon usage in efficiently expressed genes. Gene. 18, 199–209.

Gu, Y.Q., Walling, L.L., 2002. Identification of residues critical for activity of the wound-induced leucine aminopeptidase (LAP-A) of tomato. Eur. J. Biochem. 269, 1630–40.

Guan, Y., Peiris, J.S.M., Lipatov, a S., Ellis, T.M., Dyrting, K.C., Krauss, S., Zhang, L.J., Webster, R.G., Shortridge, K.F., 2002. Emergence of multiple genotypes of H5N1 avian influenza viruses in Hong Kong SAR. Proc. Natl. Acad. Sci. U. S. A. 99, 8950–5.

Hamilton, C., 1997. A binary-BAC system for plant transformation with high-molecular-weight DNA. Gene 200, 107–116.

Han, G., Chari, N.S., Verma, A., Hong, R., Martin, C.T., Rotello, V.M., 2005. Controlled recovery of the transcription of nanoparticle-bound DNA by intracellular concentrations of glutathione. Bioconjug. Chem. 16, 1356–9.

Han, G., You, C.-C., Kim, B., Turingan, R.S., Forbes, N.S., Martin, C.T., Rotello, V.M., 2006. Light-regulated release of DNA and its delivery to nuclei by means of photolabile gold nanoparticles. Angew. Chemie 118, 3237–3241.

Hannig, G., Makrides, S., 1998. Strategies for optimizing heterologous protein expression in *Escherichia coli*. Trends Biotechnol. 16, 54–60.

Hay, S.I., Guerra, C.A., Tatem, A.J., Noor, A.M., Snow, R.W., 2004. The global distribution and population at risk of malaria : past , present , and future. Lancet Infect. Dis. 4, 327–336.

Hellwig, S., Drossard, J., Twyman, R.M., Fischer, R., 2004. Plant cell cultures for the production of recombinant proteins. Nat. Biotechnol. 22, 1415–22.

Hochuli, E., Döbeli, H., Schacher, A., 1987. New metal chelate adsorbent selective for proteins and peptides containing neighbouring histidine residues. J. Chromatogr. A 411, 177–184.

Holland, P.M., Abramson, R.D., Watson, R., Gelfand, D.H., 1991. Detection of specific polymerase chain reaction product by utilizing the 5′-3′ exonuclease activity of *Thermus aquaticus* DNA polymerase. Proc. Natl. Acad. Sci. U. S. A. 88, 7276–80.

Houdebine, L.-M., 2009. Production of pharmaceutical proteins by transgenic animals. Comp. Immunol. Microbiol. Infect. Dis. 32, 107–21.

Howell, J.M., Winstone, T.L., Coorssen, J.R., Turner, R.J., 2006. An evaluation of *in vitro* protein-protein interaction techniques: assessing contaminating background proteins. Proteomics 6, 2050–69.

Huang, X., Jain, P.K., El-Sayed, I.H., El-Sayed, M. A, 2007. Gold nanoparticles: interesting optical properties and recent applications in cancer diagnostics and therapy. Nanomedicine (Lond). 2, 681–93.

Hussain, S.M., Hess, K.L., Gearhart, J.M., Geiss, K.T., Schlager, J.J., 2005. *In vitro* toxicity of nanoparticles in BRL 3A rat liver cells. Toxicol. *In Vitro* 19, 975–83.

Iijima, S., Ichihashi, T., 1993. Single-shell carbon nanotubes of 1-nm diameter. Nat. 363, 603-605.

Innis, M. A., Gelfand, D. H., Sninsky, J. J., White, T. J. (Eds.)., 1990. PCR protocols: a guide to methods and applications. Academic press. pp. 137.

Inoue, H., Nojima, H., Okayama, H., 1990. High efficiency transformation of *Escherichia coli* with plasmids. Gene. 96, 23–28.

Janes, K. a, Calvo, P., Alonso, M.J., 2001. Polysaccharide colloidal particles as delivery systems for macromolecules. Adv. Drug Deliv. Rev. 47, 83–97.

Jensen, M.R., Lauritzen, C., Dahl, S.W., Pedersen, J., Led, J.J., 2004. Binding ability of a HHP-tagged protein towards Ni^{2+} studied by paramagnetic NMR relaxation: the possibility of obtaining long-range structure information. J. Biomol. NMR 29, 175–85.

Ji, J.H., Jung, J.H., Kim, S.S., Yoon, J.-U., Park, J.D., Choi, B.S., Chung, Y.H., Kwon, I.H., Jeong, J., Han, B.S., Shin, J.H., Sung, J.H., Song, K.S., Yu, I.J., 2007. Twenty-eight-day inhalation toxicity study of silver nanoparticles in Sprague-Dawley rats. Inhal. Toxicol. 19, 857–71.

Jia, H., Nishikawa, Y., Luo, Y., Yamagishi, J., Sugimoto, C., Xuan, X., 2009. Characterization of a leucine aminopeptidase from *Toxoplasma gondii*. Mol. Biochem. Parasitol. 170, 1–6.

Johnson, I.S., 1983. Human insulin from recombinant DNA technology. Science 219, 632–7.

Kabisch, J., Thürmer, A., Hübel, T., Popper, L., Daniel, R., Schweder, T., 2013. Characterization and optimization of *Bacillus subtilis* ATCC 6051 as an expression host. J. Biotechnol. 163, 97–104.

Kager, P., 2002. Malaria control: constraints and opportunities. Trop. Med. Int. Heal. 7, 1042–1046.

Kang, J.-M., Ju, H.-L., Sohn, W.-M., Na, B.-K., 2011. Molecular cloning and characterization of a M17 leucine aminopeptidase of *Cryptosporidium parvum*. Parasitol. 138, 682–690.

Kim, T., Kim, H., Lee, S., Na, B., Lin, K., 2010. Prevalence of *Plasmodium vivax* VK210 and VK247 subtype in Myanmar. Malar. J. 9, 195–201.

Kimsey, R.B., 1992. Host association and the capacity of sand flies as vectors of lizard malaria in Panama. Int. J. Parasitol., 22**,** 657–664.

Klueh, U., Wagner, V., Kelly, S., Johnson, a, Bryers, J.D., 2000. Efficacy of silver-coated fabric to prevent bacterial colonization and subsequent device-based biofilm formation. J. Biomed. Mater. Res. 53, 621–31.

Kohno, H., Kanda, S., Kanno, T., 1986. Immunoaffinity purification and characterization of leucine aminopeptidase from human liver. J. Biol. Chem. 261, 10744–8.

Kunst, F., Ogasawara, N., Moszer, I., Albertini, a M., Alloni, G., Azevedo, V., Bertero, M.G., Bessières, P., Bolotin, a, Borchert, S., Borriss, R., Boursier, L., Brans, a, Braun, M., Brignell, S.C., Bron, S., Brouillet, S., Bruschi, C. V, Caldwell, B., Capuano, V., Carter, N.M., Choi, S.K., Codani, J.J., Connerton, I.F., Danchin, a, 1997. The complete genome sequence of the gram-positive bacterium *Bacillus subtilis*. Nature 390, 249–56.

Lara, H.H., Ayala-Núñez, N. V., Ixtepan Turrent, L.D.C., Rodríguez Padilla, C., 2009. Bactericidal effect of silver nanoparticles against multidrug-resistant bacteria. World J. Microbiol. Biotechnol. 26, 615–621.

Lara, H.H., Ixtepan-Turrent, L., Garza-Treviño, E.N., Rodriguez-Padilla, C., 2010. PVP-coated silver nanoparticles block the transmission of cell-free and cell-associated HIV-1 in human cervical culture. J. Nanobiotechnology 8, 15.

Lara, H.H., Ayala-Nuñez, N. V, Ixtepan-Turrent, L., Rodriguez-Padilla, C., 2010. Mode of antiviral action of silver nanoparticles against HIV-1. J. Nanobiotech. 8, 1.

Larson, D.R., Zipfel, W.R., Williams, R.M., Clark, S.W., Bruchez, M.P., Wise, F.W., Webb, W.W., 2003. Water-soluble quantum dots for multiphoton fluorescence imaging *in vivo*. Science 300, 1434–6.

Last, J. M., 1988. A Dictionary of Epidemiology. 2nd ed. Oxford University Press, New York. pp. 98.

Laurent, T., Killander, J., 1964. A theory of gel filtration and its exeperimental verification. J. Chromatogr. A 14, 317–330.

Ledeme, N., Vincent-Fiquet, O., Hennon, G., Plaquet, R., 1983. Human liver L-leucine aminopeptidase: evidence for two forms compared to pig liver enzyme. Biochimie 65, 397–404.

Lee, J.-Y., Song, S.-M., Seok, J.-W., Jha, B.K., Han, E.-T., Song, H.-O., Yu, H.-S., Hong, Y., Kong, H.-H., Chung, D.-I., 2010. M17 leucine aminopeptidase of the human malaria parasite *Plasmodium vivax*. Mol. Biochem. Parasitol. 170, 45–8.

Lesniak, W., Bielinska, A.U., Sun, K., Janczak, K.W., Shi, X., Baker, J.R., Balogh, L.P., 2005. Silver/dendrimer nanocomposites as biomarkers: fabrication, characterization, *in vitro* toxicity, and intracellular detection. Nano Lett. 5, 2123–30.

Li, L.-C., Dahiya, R., 2002. MethPrimer: designing primers for methylation PCRs. Bioinformatics 18, 1427–31.

Lopez, J., Prezioso, V., 2001. A better way to optimize : two-step gradient PCR. Eppend. BioNews 3–4.

Lu, L., Sun, R.W., Chen, R., Hui, C., Ho, C., Luk, J.M., Lau, G.K.K., 2007. Silver nanoparticles inhibit hepatitis B virus replication 253–262.

Ma, J.K.-C., Drake, P.M.W., Christou, P., 2003. The production of recombinant pharmaceutical proteins in plants. Nat. Rev. Genet. 4, 794–805.

Malwest, 2012. Integrated Surveillance and control programme for West Nile Virus and malaria in Greece. http://www.malwest.gr/en-us/malaria/informationforhealth careprofessionals/plasmodiumlifecycle.aspx , Accessed 30/7/2012

Martin, R., Kirk, K., 2007. Transport of the essential nutrient isoleucine in human erythrocytes infected with the malaria parasite *Plasmodium falciparum*. Blood 109, 2217–2224.

Matsui, M., Fowler, J.H., Walling, L.L., 2006. Leucine aminopeptidases: diversity in structure and function. Biol. Chem. 387, 1535–44.

Matsumoto, H., Rogi, T., Yamashiro, K., Kodama, S., Tsuruoka, N., Hattori, a, Takio, K., Mizutani, S., Tsujimoto, M., 2000. Characterization of a recombinant soluble form of human placental leucine aminopeptidase/oxytocinase expressed in Chinese hamster ovary cells. Eur. J. Biochem. 267, 46–52.

Mantle, D., Lauffart, B., Gibson, A., 1990. Characterization of aminopeptidases in human kidney soluble fraction. Clin. Chim. Acta 187, 105–114.

McGowan, S., Oellig, C., Birru, W. A., Caradoc-Davies, T.T., Stack, C.M., Lowther, J., Skinner-Adams, T., Mucha, A., Kafarski, P., Grembecka, J., Trenholme, K.R., Buckle, A.M., Gardiner, D.L., Dalton, J.P., Whisstock, J.C., 2010. Structure of the *Plasmodium falciparum* M17 aminopeptidase and significance for the design of drugs targeting the neutral exopeptidases. Proc. Natl. Acad. Sci. U. S. A. 107, 2449–54.

Mellor, J., Dobson, M.J., Roberts, N., Kingsman, J., Kingsman, S.M., 1985. Factors affecting heterologous gene expression in *Saccharomyces cerevisiae*. Gene 33, 215–26.

Mendis, K., Sina, B., Marchesini, P., Carter, R., 2001. The neglected burden of *Plasmodium vivax* malaria. Am. J. Trop. Med. Hyg. 64, 97–106.

Miller, L.H., Baruch, D.I., Marsh, K., Doumbo, O.K., 2002. The pathogenic basis of malaria. Nature 415, 673–9.

Miller, L. H., Mason, S. J., Clyde, D. F., McGinniss, M. H., 1976. The resistance factor to *Plasmodium vivax* in blacks: the Duffy-blood-group genotype, FyFy. New Eng. J. Med., 295, 302-304.

Miroux, B., Walker, J., 1996. Over-production of Proteins in *Escherichia coli*: Mutant hosts that allow synthesis of some membrane proteins and globular proteins at high levels. J. Mol. Biol. 260, 289–298.

Mohanraj, V.J., Chen, Y., 2006. Nanoparticles – A Review. Pharmacotherapy 5, 561–573.

Monaco, A., Larin, Z., 1994. YACs, BACs, PACs and MACs: Artificial chromosomes as research tools. Trends Biotechnol. 280–286.

Morones, J.R., Elechiguerra, J.L., Camacho, A., Holt, K., Kouri, J.B., Ramírez, J.T., Yacaman, M.J., 2005. The bactericidal effect of silver nanoparticles. Nanotech. 16, 2346–53.

Moyer, C.A., Brentano, L., Gravens D.L., Margraf, H.W., Monafo, W.W., JR., 1965. Treatment of large human burns with 0.5 % silver nitrate solution. Arch. Surg. 90, 812-867.

Mullis, K., Faloona, F., Scharf, S., 1986. Specific enzymatic amplification of DNA in vitro: the polymerase chain reaction. Cold Spring Harb. Symp. Quant. Biol. L1, 263–273.

Nchinda, T., 1998. Malaria: a re-emerging disease in Africa. Emerg. Infect. Dis. 4, 398–403.

Olliaro, P.L., Yuthavong, Y., 1999. An overview of chemotherapeutic targets for antimalarial drug discovery targets for malaria. Pharmacol. Ther. 81, 91–110.

Owais, M., Varshney, G.C., Choudhury, A., Chandra, S., Gupta, C.M., 1995. Chloroquine encapsulated in malaria-infected liposomes effectively controls chloroquine-resistant *Plasmodium berghei* infections in mice . Antimicrob. Agents Chemother. 39, 180-184.

Oya, M., Yoshino, M., Asano, M., 1974. Human placental aminopeptidase isozymes. Experientia 30, 985–6.

Pal, A., Shah, S., Devi, S., 2008. Microwave-assisted synthesis of silver nanoparticles using ethanol as a reducing agent. Mater. Chem. Phys. 114, 530–532.

Palomares, L. A., Estrada-Mondaca, S., Ramírez, O.T., 2004. Production of recombinant proteins: challenges and solutions. Methods Mol. Biol. 267, 15–52.

Pastoriza-santos, I., Liz-marza, L.M., 2002. Formation of PVP-protected metal nanoparticles in DMF. Society 2888–2894.

Pennisi, E., 2002. Malaria parasite genome sequenced. Science. 298, 33–34.

Pezza, J., Kucera, R., Luo Sun, M.S., 2012. Polymerase Fidelity: What is it, and what does it mean for your PCR? umzug.newenglandbiolabs.de 3–5.

Phyo, A., Nkhoma, S., Stepniewska, K., Ashley, E., 2012. Emergence of artemisinin-resistant malaria on the western border of Thailand: a longitudinal study. Lancet 6736, 1–7.

Pluthero, F.G., 1993. Rapid purification of high-activity Taq DNA polymerase. Nucleic Acids Res. 21, 4850–1.

Pokharel, D.R., Rathaur, S., 2008. Purification and characterization of a leucine aminopeptidase from the bovine filarial parasite *Setaria cervi*. Acta Trop. 106, 1–8.

Pollack, Y., Katzen, A. L., Spira, D. T., Golenser, J., 1981. The genome of *Plasmodium falciparum*. I: DNA base composition. Nucleic Acids Res. 10, 539–546.

Pollock, D.P., Kutzko, J.P., Birck-Wilson, E., Williams, J.L., Echelard, Y., Meade, H.M., 1999. Transgenic milk as a method for the production of recombinant antibodies. J. Immunol. Methods 231, 147–57.

Porath, J., 1959. Gel filtration of proteins, peptides and amino acids. Biochim. Biophys. Acta 39, 193–207.

Porath, J., Flodin, P., 1959. Gel Filtration: A method for desalting and group separation. Nature 4676, 1657–1659.

Poreba, M., Sivaraman, K.K., Oellig, C. a, Huynh, K., Atkinson, S.C., Perugini, M. A., Trenholme, K.R., Gardiner, D.L., Salvesen, G., Drag, M., Dalton, J.P., Whisstock, J.C., McGowan, S., 2012. X-ray crystal structure and specificity of the *Plasmodium falciparum* malaria aminopeptidase PfM18AAP. J. Mol. Biol. 422, 495–507.

Prato, M., Kostarelos, K., 2008. Functionalized carbon nanotubes in drug design and discovery. Acc. Chem. Res. 41, 60-68.

Pujalté, I., Passagne, I., Brouillaud, B., Tréguer, M., Durand, E., Ohayon-Courtès, C., L'Azou, B., 2011. Cytotoxicity and oxidative stress induced by different metallic nanoparticles on human kidney cells. Part. Fibre Toxicol. 8, 10.

Rai, M.K., Deshmukh, S.D., Ingle, a P., Gade, a K., 2012. Silver nanoparticles: the powerful nanoweapon against multidrug-resistant bacteria. J. Appl. Microbiol. 112, 841–52.

Rao, R.N., Rogers, S., 1979. Plasmid pKC7: a vector containing ten restriction endonuclease sites suitable for cloning DNA segments. Gene 7, 79–82.

Rawlings, N.D., Barrett, a J., 1993. Evolutionary families of peptidases. Biochem. J. 290, 205–18.

Ritchie, R., Prvan, T., 1996. Current statistical methods for estimating the K_m and V_{max} of Michaelis-Menten kinetics. Biochem. Educ. 2, 196–206.

Roch, K. Le, Zhou, Y., Blair, P., Grainger, M., 2003. Discovery of gene function by expression profiling of the malaria parasite life cycle. Science. 301, 1503–1508.

Romanowska, E., 1970. Sepharose gel filtration method of purification of lipopolysaccharides. Anal. Biochem. 389, 383–389.

Rosenthal, P.J., 2003. Antimalarial drug discovery: old and new approaches. J. Exp. Biol. 206, 3735–3744.

Sachs, J., Malaney, P., 2002. The economic and social burden of malaria. Nature 415, 680–685.

Sahdev, S., Khattar, S., Saini, K., 2008. Production of active eukaryotic proteins through bacterial expression systems: a review of the existing biotechnology strategies. Mol. Cell. Biochem. 307, 249–264.

Sahoo, S.K., Parveen, S., Panda, J.J., 2006. The present and future of nanotechnology in human health care. Nanomedicine 3, 20–31.

Salata, O. V., 2004. Applications of nanoparticles in biology and medicine. J. Nanobiotech. 6, 1–6.

Sanderink, G., Artur, Y., Siest, G., 1988. Human aminopeptidases: a review of the literature. Clin. Chem. Lab. 26, 795–807.

Sanvicens, N., Marco, M.P., 2008. Multifunctional nanoparticles-properties and prospects for their use in human medicine. Trends Biotechnol. 26, 425–33.

Saxena, A., Tripathi, R.M., Singh, R.P., 2010. Biological synthesis of silver nanoparticles by using onion *(allium cepa*) extract and their antibacterial activity. Dig. J. Nanomater. Biostructures 5, 427–432.

Segel, I., 1951. Enzyme Kinetics: Behavior and analysis of rapid equilibrium and steady-state enzyme systems. John Wiley Sons, New York. pp.30-38.

Schochetman, G., Ou, C. Y., & Jones, W.K., 1988. Polymerase chain reaction. J. Infect. Dis. 158, 1154–1157.

Shiloach, J., Kaufman, J., Guillard, A. S., Fass, R., 1996. Effect of glucose supply strategy on acetate accumulation, growth, and recombinant protein production by *Escherichia coli* BL21 (lambdaDE3) and *Escherichia coli* JM109. Biotechnol. Bioeng. 49, 421–8.

Sies, H., 1999. Glutathione and its role in cellular functions., Free Rad. Biol. and Med. 27, 916–921.

Singh, M., Singh, S., Prasad, S., Gambhir, I., 2008. Nanotechnology in medicine and antibacterial effect of silver nanoparticles. Digest J. Nanomater. Biostruct. 3.3, 115-122.

Skinner-Adams, T.S., Stack, C.M., Trenholme, K.R., Brown, C.L., Grembecka, J., Lowther, J., Mucha, A., Drag, M., Kafarski, P., McGowan, S., Whisstock, J.C., Gardiner, D.L., Dalton, J.P., 2010. *Plasmodium falciparum* neutral aminopeptidases: new targets for anti-malarials. Trends Biochem. Sci. 35, 53–61.

Slater, A. F., 1993. Chloroquine: mechanism of drug action and resistance in *Plasmodium falciparum*. Pharmacol. Ther. 57, 203–35.

Sørensen, M.A., Kurland, C.G., Pedersen, S., 1989. Codon usage determines translation rate in *Escherichia coli*. J. Mol. Biol. 207, 365–377.

Sørensen, H., Mortensen, K., 2005. Advanced genetic strategies for recombinant protein expression in *Escherichia coli*. J. Biotechnol. 115, 113–128.

Spackman, D., Smith, E., Brown, D., 1955. Leucine aminopeptidase IV. Isolation and properties of the enzyme from swine kidney. J. Biol. Chem. 212, 255–269.

Sriram, M.I., Kanth, S.B.M., Kalishwaralal, K., Gurunathan, S., 2010. Antitumor activity of silver nanoparticles in Dalton's lymphoma ascites tumor model. Int. J. Nanomedicine 5, 753–62.

Srivastava, S., 2013. Genetics of Bacteria. Springer India, Delhi. pp. 95-107.

Stack, C.M., Lowther, J., Cunningham, E., Donnelly, S., Gardiner, D.L., Trenholme, K.R., Skinner-adams, T.S., Teuscher, F., Grembecka, J., Mucha, A., Kafarski, P., Lua, L., Bell, A., Dalton, J.P., 2007. Characterization of the *Plasmodium falciparum* M17 leucyl aminopeptidase: A protease involved in amino acid regulation with potential for antimalarial drug. J. Biol. 282, 2069–2080.

Struhl, K., Stinchcomb, D.T., Scherer, S., Davis, R.W., 1979. High-frequency transformation of yeast: autonomous replication of hybrid DNA molecules. Proc. Natl. Acad. Sci. U. S. A. 76, 1035–9.

Studier, F.W., Moffatt, B.A., 1986. Use of bacteriophage T7 RNA polymerase to direct selective high-level expression of cloned genes. J. Mol. Biol. 189, 113–130.

Studier, F.W., 1991. Use of bacteriophage T7 lysozyme to improve an inducible T7 expression system. J. Mol. Biol. 219, 37–44.

Studier, F., 2005. Protein production by auto-induction in high-density shaking cultures. Protein Expr. Purif. 41, 207–234.

Su, X.Z., Wu, Y., Sifri, C.D., Wellems, T.E., 1996. Reduced extension temperatures required for PCR amplification of extremely A+T-rich DNA. Nucleic Acids Res. 24, 1574–5.

Sun, Y., Xia, Y., 2002. Shape-controlled synthesis of gold and silver nanoparticles. Science 298, 2176–9.

Sutherland, C.J., Tanomsing, N., Nolder, D., Oguike, M., Jennison, C., Pukrittayakamee, S., Dolecek, C., Hien, T.T., Rosa, V.E., Arez, A.P., Michon, P., Escalante, A.A., Nosten, F., Burke, M., Lee, R., Blaze, M., Otto, T.D., Barnwell, J.W., Pain, A., Williams, J., White, N.J., Day, N.P.J., Snounou, G., Lockhart, P.J., Chiodini, P.L., Imwong, M., Polley, S.D., 2010. Two non-recombining sympatric forms of the human malaria parasite *Plasmodium ovale* occur globally. J. Infect. 201, 1544–1550.

Talgorn, E., Gao, Y., Aerts, M., Kunneman, L.T., Schins, J.M., Savenije, T.J., van Huis, M. a, van der Zant, H.S.J., Houtepen, A.J., Siebbeles, L.D., 2011. Unity quantum yield of photogenerated charges and band-like transport in quantum-dot solids. Nat. Nanotechnol. 6, 733–9.

Taylor, A., 1993. Aminopeptidases: structure and function. FASEB J. 32, 290–298.

Teklehaimanot, A., and Mejia, P., 2008. Malaria and poverty. Ann. New York Ac. Sci.1136, 32–37.

Thivierge, K., Mathew, R.T., Nsangou, D.M.M., Silva, D., Skinner-Adams, T.S., Trenholme, K.R., Brown, C.L., 2012. Anti-malaria drug development targeting the M1 alanyl and M17 leucyl aminopeptidases. Arkivoc, iv, 330–346.

Timmis, K. N., 2002. *Pseudomonas putida*: a cosmopolitan opportunist par excellence. Env. Microbio. 4, 779-781.

Timmons, L., Court, D.L., Fire, A, 2001. Ingestion of bacterially expressed dsRNAs can produce specific and potent genetic interference in *Caenorhabditis elegans*. Gene 263, 103–12.

Tindall, K., Kunkel, T., 1988. Fidelity of DNA synthesis by the *Thermus aquaticus* DNA polymerase. Biochemistry 27, 6008–6013.

Tortosa, P., Dubnau, D., 1999. Competence for transformation: a matter of taste. Curr. Opin. Microbiol. 2, 588–92.

Toshima, N., Yonezawa, T., 1998. Bimetallic nanoparticles - novel materials for chemical and physical applications. New J. Chem. 22, 1179–1201.

Tuppy, H., Wiesbauer, W., Wintersberger , Z., Silva, D., 1962. Physiological chemistry, Wiley, London.

Umezawa, H., Ishizuka, M., Aoyagi, T., & Takeuchi, T., 1976. Enhancement of delayed-type hypersensitivity by bestatin, an inhibitor of aminopeptidase B and leucine aminopeptidase. J. Antibio., 29, 857.

Venter, J.C., Adams, M.D., Myers, E.W., Li, P.W., Mural, R.J., Sutton, G.G., Smith, H.O., Yandell, M., Evans, C.A., Holt, R.A., Gocayne, J.D., Amanatides, P., Ballew, R.M., Huson, D.H., Russo, J., Zhang, Q., Kodira, C.D., Zheng, X.H., Chen, L., Skupski, M., Subramanian, G., Thomas, P.D., Zhang, J., Miklos, G.L.G., Smith, H., Wortman, J.R., Nelson, C., Broder, S., Clark, A.G., Nadeau, J., Mckusick, V.A., Zinder, N., Levine, A.J., Roberts, R.J., Simon, M., Slayman, C., Hunkapiller, M., Bolanos, R., Delcher, A., Fasulo, D., Flanigan, M., Florea, L., Halpern, A., Hannenhalli, S., Kravitz, S., Levy, S., Bonazzi, V., Brandon, R., Cargill, M., Chandramouliswaran, I., Charlab, R., Evangelista, C., Gabrielian, A.E., Gan, W., Ge, W., Gong, F., Gu, Z., 2001. The Sequence of the Human Genome. Science. 291, 1304–1351.

Weber, J.L., 1987. Analysis of sequences from the extremely A + T-rich genome of *PIasmodium falciparum*. Gene 52, 103–109.

Wellems, T.E., 2002. *Plasmodium* chloroquine resistance and the search for a replacement antimalarial drug. Science 298, 124–6.

White, N., 2007. *Plasmodium knowlesi*: the fifth human malaria parasite. Clin. Infect. Dis. 46, 172–173.

Whitesides, G.M., 2003. The “right” size in nanobiotechnology. Nat. Biotechnol. 21, 1161–5.

WHO, 1957. Expert Committee on Malaria 6th Report. WHO technical report series. Geneva, Switzerland. WHO Press.

WHO, 1987. The biology of malaria parasites. WHO Scientific group. WHO technical report series, Geneva, Switzerland. WHO Press.

WHO, 2012. World malaria report. Geneva, Switzerland. WHO Press.

Wilkes, S.H., Prescott, J.M., 1985. The slow, tight binding of bestatin and amastatin to aminopeptidases. J. Biol. Chem. 260, 13154–62.

Wiser, Mark F., 2011. Protozoa and human disease. Garland Science, New York.

Wright, S., 1986. Recombinant DNA technology and its social transformation, 1972-1982. Osiris 2, 303–60.

Wurm, F.M., 2004. Production of recombinant protein therapeutics in cultivated mammalian cells. Nat. Biotechnol. 22, 1393–8.

Yamada, T., 1984. Causal relationships between infant mortality and fertility in developed and less developed countries. 1528.

Zeng, Q., Xu, J., Fu, R., Ye, Q., 2001. Functional polymer affinity matrix for purifying hexahistidine-tagged recombinant protein. J. Chromatogr. A 921, 197–205.

Zhang, L., Gu, F.X., Chan, J.M., Wang, A.Z., Langer, R.S., Farokhzad, O.C., 2008. Nanoparticles in medicine : therapeutic applications and developments. Clin. Pharmacol. Ther. 83, 761–769.

Zhao, M., Sun, L., Crooks, R.M., 1998. Preparation of copper nanoclusters within dendrimer templates. J. Am. Chem. Soc. 62.

Zimmer, S.M., Burke, D.S., 2009. Historical perspective--Emergence of influenza A (H1N1) viruses. N. Engl. J. Med. 361, 279–85.

Zucker, J., 1996. Changing patterns of autochthonous malaria transmission in the United States: a review of recent outbreaks. Emerg Infect Dis 2, 37–43.

Appendices

Appendix A: Growth media and constituents

Media	Quantity	Constituents	Treatment
Luria Broth	1 L	10 g Tryptone 5 g Yeast Extract 5 g NaCl	Autoclave
SOB	1 L	20 g Tryptone 5 g Yeast extract 0.584 $g.l^{-1}$ NaCl 0.186 $g.l^{-1}$ KCl 2.034 $g.l^{-1}$ $MgCl_2$-$6H_2O$ 2.464 $g.l^{-1}$ $MgSO_4$-$7H_2O$	Autoclave
SOC	1 L	Add 20 $ml.l^{-1}$ of sterile glucose per litre of SOB media after autoclaving.	
ZY	1 L	10 g tryptone 5 g yeast extract	Autoclave
20x NPS solution	200 ml	0.5 M $(NH_4)_2SO_4$ 1 M of KH_2PO_4 1 M Na_2HPO_4	Filter sterilize into a sterile bottle using a 0.22 μm sterile filter.
50x (505/5052)	100 ml	250 $g.l^{-1}$ glycerol, 25 $g.l^{-1}$ glucose, 100 $g.l^{-1}$ α-lactose	Filter sterilize into a sterile bottle using a 0.22 μm sterile filter.
1 M $MgSO_4$	100 ml	12 g in ddH_2O	Filter sterilize into a sterile bottle using a 0.22 μm sterile filter.
TB-Buffer	250 ml	10 mM HEPES 15 mM $CaCl_2$ 250 mM KCl 55 mM $MnCl_2$	Mix all components except the $MnCl_2$ then adjust to pH 6.7 with KOH or HCl and add the $MnCl_2$ and filter sterilize with a 0.22 μm filter and store at 4°C
ZYP505/5052	1 L	50 ml of 20x NPS 20 ml of 50x 505/5052 2 ml of 1 M $MgSO_4$ and 1 L of ZY media.	Add other ingredients into autoclaved 1 L ZY media under sterile conditions.

Appendix B: SDS-PAGE reagents

Media	Constituents	Treatment
SDS-PAGE Resolving gels 10 %	1.215 ml 30 %/0.8 % Acrylamide/Bis-Acrylamide, 485 µl 3 M Tris-HC*l*, pH 8.8 1.944 ml sterile dddH_2O 91 µl 10 % SDS 12.5 µl 10 % ammonium persulphate (APS) 2.5 µl Tetramethylethylenediamine (TEMED)	APS and TEMED added just prior to pouring of the gel. Once poured a few drops of H_2O saturated Tert-Amyl alcohol (2-Methyl-2-butanol) were added to prevent evaporation and ensure it set level. Gels were allowed 1 hour to set before pouring the stacking gel
SDS-PAGE Stacking gels 4 %	0.2 ml 30%/0.8% Acrylamide/Bis-Acrylamide 105 µl 0.5 M Tris-HC*l*, pH 6.8 1.185 ml sterile ddH_2O 15 µl 10% SDS 15 µl 10% APS 2.5 µl TEMED	Before pouring the stacking gel, Tert-Amyl alcohol was washed thoroughly off the top of the running gel using ddH_2O. After pouring 10/15 tooth combs were inserted into the gels and left to set for 1 hour.
SDS-PAGE 10x running buffer	30.28 g Tris 144 g Glycine 10 g SDS	Prior to use, the buffer was diluted to 1x using ddH_2O
SDS-PAGE TD solution	1 ml 10 % SDS 50 µl β-mercaptoethanol	
SDS-PAGE TS solution	13.3 ml 3 M Tris-HCl, pH 8.8 2 ml 0.5 M EDTA 40 ml Glycerol	This solution was prepared and stored at 4 °C.
SDS-PAGE loading dye TD + TS	200 µl TS solution 50 µl of TD solution	Loading dye was prepared fresh all the time.
Fairbanks destaining solutions	Fairbanks A, 0.05 % coomassie blue R-250, 25 % isopropanol, and 10 % acetic acid Fairbanks B, 0.005 % coomassie blue R-250, 10 % isopropanol, and 10 % acetic acid Fairbanks C, 0.002 % coomassie blue R-250, and 10% acetic acid Fairbanks D, 10 % acetic acid	
Native gels were prepared by replacing 10 % SDS with water in the SDS-PAGE gel recipe.		

Appendix C: Molecular Cloning

*Pf*LAP complete coding strand

ATGTATTTTTCTTCCTTATGTAAATTTTTGCCAATATCTGAAAAAGAAAAGATATATTTAAATATTGTAAAAAAACG
CTTCTGTAAATCAAATATATATTATAATAATAATAATAATAATATTATTAATTATAATAAGAGAGGTTTAAAATTTT
ATCCTTTTTGTAATAATTTAAAAAAAAATATAAATTTTGTAAATATTAATAATAAGAAGGGAATAAATTTTCATAGT
ATAAATAAAGAAAGAAAAATGGCAAGTGAAGTACCACAAGTTGTTTCCTTAGATCCAACAAGTATTCCTATTGAATA
TAATACTCCTATACATGATATAAAAGTTCAGGTTTATGATATAAAAGGAGGTTGTAATGTTGAAGAAGGATTAACTA
TTTTCTTAGTTAATAATCCTGGTAAAGAAAATGGGCCAGTTAAAATTAGCTCAAAAGTTAATGATAAAAATGTGAGC
GAATTTTTAAAAGATGAAAATATGGAAAAATTTAATGTTAAATTAGGAACATCAAAACATTTCTACATGTTTAATGA
TAATAAAAATTCAGTTGCTGTTGGTTATGTAGGATGTGGATCAGTTGCTGATTTAAGTGAAGCTGATATGAAAAGAG
TTGTATTATCATTAGTCACTATGTTACATGATAATAAACTTTCTAAATTAACTGTTGTTTTTGAAATTAATGTTGAT
AAAAATTTATTCCGTTTTTTCTTAGAAACATTATTTTATGAATATATGACCGATGAAAGGTTCAAATCTACTGATAA
AAATGTTAATATGGAATATATCAAACATTTAGGTGTATACATAAACAATGCTGATACTTATAAGGAAGAAGTTGAAA
AAGCTCGTGTTTATTATTTTGGTACTTATTATGCTTCTCAACTTATTGCTGCACCATCCAACTATTGTAATCCTGTA
TCTTTATCTAATGCAGCTGTAGAGCTAGCTCAAAAATTAAATTTAGAATATAAAATTCTAGGAGTAAAAGAACTTGA
AGAATTAAAAATGGGAGCCTATTTATCTGTGGGTAAAGGTAGTATGTATCCAAATAAATTTATTCATTTAACATATA
AAAGCAAAGGAGATGTCAAAAAAAAAATTGCATTAGTAGGAAAAGGTATTACATTCGATTCAGGAGGATACAATTTA
AAAGCTGCTCCAGGATCTATGATAGATTTAATGAAATTTGATATGAGTGGATGTGCAGCCGTTTTAGGTTGTGCTTA
TTGTGTAGGTACACTTAAACCAGAAAATGTTGAAATTCATTTTCTAAGTGCCGTTTGTGAAAATATGGTCTCTAAAA
ATTCCTATCGTCCAGGGGATATTATTACAGCATCAAATGGTAAAACTATAGAAGTTGGTAATACAGATGCTGAAGGA
AGATTAACATTAGCTGATGCTTTAGTATATGCTGAAAAATTAGGTGTTGATTATATTGTAGATATAGCTACATTAAC
AGGTGCTATGCTATATTCATTAGGTACAAGCTATGCTGGTGTTTTTGGTAATAATGAAGAACTTATCAATAAAATAT
TGAACTCTTCAAAAACTTCAAACGAACCAGTCTGGTGGTTACCAATTATTAATGAATACAGAGCAACATTAAATTCA
AAATATGCTGATATTAATAATATCTCATCAAGTGTTAAAGCTTCATCTATTGTGGCCTCATTATTTTTAAAAGAATT
TGTTCAAAATACTGCTTGGGCACATATTGATATTGCTGGTGTTTCATGGAATTTCAAAGCTAGAAAACCAAAAGGTT
TTGGTGTGCGTTTATTGACAGAATTTGTACTCAATGACGCTCTATAA

Truncated *Pf*LAP sequence

AAAATGGCAAGTGAAGTACCACAAGTTGTTTCCTTAGATCCAACAAGTATTCCTATTGAATATAATACTCCTATACA
TGATATAAAAGTTCAGGTTTATGATATAAAAGGAGGTTGTAATGTTGAAGAAGGATTAACTATTTTCTTAGTTAATA
ATCCTGGTAAAGAAAATGGGCCAGTTAAAATTAGCTCAAAAGTTAATGATAAACAGGTGAGCGAATTTTTAAAAGAT
GAAAATATGGAAAAATTTAATGTTAAATTAGGAACATCAAAACATTTCTACATGTTTAATGATAATAAAAATTCAGT
TGCTGTTGGTTATGTAGGATGTGGATCAGTTGCTGATTTAAGTGAAGCTGATATGAAAAGAGTTGTATTATCATTAG
TCACTATGTTACATGATAATAAACTTTCTAAATTAACTGTTGTTTTTGAAATTAATGTTGATAAAAATTTATTCCGT
TTTTTCTTAGAAACATTATTTTATGAATATATGACCGATGAAAGGTTCAAATCTACTGATAAAAATGTTAATATGGA
ATATATCAAACATTTAGGTGTATACATAAACAATGCTGATACTTATAAGGAAGAAGTTGAAAAAGCTCGTGTTTATT
ATTTTGGTACTTATTATGCTTCTCAACTTATTGCTGCACCATCCAACTATTGTAATCCTGTATCTTTATCTAATGCA
GCTGTAGAGCTAGCTCAAAAATTAAATTTAGAATATAAAATTCTAGGAGTAAAAGAACTTGAAGAATTAAAAATGGG
AGCCTATTTATCTGTGGGTAAAGGTAGTATGTATCCAAATAAATTTATTCATTTAACATATAAAAGCAAAGGAGATG
TCAAAAAAAAAATTGCATTAGTAGGAAAAGGTATTACATTCGATTCAGGAGGATACAATTTAAAAGCTGCTCCAGGA
TCTATGATAGATTTAATGAAATTTGATATGAGTGGATGTGCAGCCGTTTTAGGTTGTGCTTATTGTGTAGGTACACT
TAAACCAGAAAATGTTGAAATTCATTTTCTAAGTGCCGTTTGTGAAAATATGGTCTCTAAAAATTCCTATCGTCCAG
GGGATATTATTACAGCATCAAATGGTAAAACTATAGAAGTTGGTAATACAGATGCTGAAGGAAGATTAACATTAGCT
GATGCTTTAGTATATGCTGAAAAATTAGGTGTTGATTATATTGTAGATATAGCTACATTAACAGGTGCTATGCTATA
TTCATTAGGTACAAGCTATGCTGGTGTTTTTGGTAATAATGAAGAACTTATCAATAAAATATTGCAGTCTTCAAAAA
CTTCAAACGAACCAGTCTGGTGGTTACCAATTATTAATGAATACAGAGCAACATTAAATTCAAAATATGCTGATATT
AATCAGATCTCATCAAGTGTTAAAGCTTCATCTATTGTGGCCTCATTATTTTTAAAAGAATTTGTTCAAAATACTGC
TTGGGCACATATTGATATTGCTGGTGTTTCATGGAATTTCAAAGCTAGAAAACCAAAAGGTTTTGGTGTGCGTTTAT
TGACAGAATTTGTACTCAATGACGCTCTATAA

Truncated *Pf*LAP sequence optimised for expression in *E. coli* and with *Eco*RI and *Nde*I restriction sites.

```
CATATGGCGAGCGAAGTTCCGCAGGTGGTCTCACTGGACCCGACGAGCATCCCGATTGAATACAACACGCCGATCCA
TGACATTAAGGTGCAGGTCTATGATATTAAAGGCGGTTGCAACGTGGAAGAAGGCCTGACCATCTTTCTGGTTAACA
ATCCGGGCAAAGAAAACGGTCCGGTGAAGATTAGCTCTAAAGTCAATGATAAGCAAGTGAGCGAATTTCTGAAGGAC
GAAAACATGGAAAAGTTTAACGTGAAGCTGGGCACCTCTAAGCATTTCTACATGTTCAACGATAACAAGAACAGTGT
TGCGGTCGGTTACGTTGGCTGTGGTTCCGTCGCGGATCTGTCAGAAGCCGACATGAAACGTGTGGTTCTGTCGCTGG
TTACCATGCTGCACGATAATAAGCTGAGCAAACTGACGGTCGTGTTCGAAATCAATGTGGACAAAAACCTGTTTCGT
TTCTTTCTGGAAACGCTGTTCTATGAATACATGACCGATGAACGCTTTAAAAGCACGGACAAGAACGTCAACATGGA
ATACATCAAGCATCTGGGCGTGTACATCAACAATGCAGATACCTATAAAGAAGAAGTGGAAAAGGCTCGCGTTTATT
ACTTCGGCACGTATTACGCGTCTCAGCTGATTGCGGCCCCGAGTAATTATTGCAACCCGGTGTCCCTGTCAAACGCA
GCTGTTGAACTGGCGCAAAAACTGAATCTGGAATACAAAATTCTGGGCGTTAAGGAACTGGAAGAACTGAAAATGGG
TGCCTACCTGTCGGTGGGCAAAGGTAGCATGTATCCGAACAAGTTTATCCATCTGACCTACAAGTCCAAAGGCGATG
TCAAAAAGAAAATTGCGCTGGTTGGCAAAGGTATCACGTTCGACTCAGGCGGTTATAATCTGAAAGCGGCCCCGGGT
TCCATGATTGATCTGATGAAGTTTGACATGTCAGGCTGCGCAGCTGTTCTGGGTTGCGCCTATTGTGTCGGCACCCT
GAAACCGGAAAACGTGGAAATCCACTTCCTGTCTGCAGTCTGTGAAAATATGGTGTCGAAAAACAGCTATCGTCCGG
GCGATATTATCACCGCCAGTAACGGCAAGACGATTGAAGTTGGCAATACCGATGCAGAAGGTCGTCTGACCCTGGCA
GACGCACTGGTGTACGCTGAAAAACTGGGTGTGGATTATATTGTTGACATCGCAACCCTGACGGGCGCTATGCTGTA
TTCTCTGGGTACCAGTTACGCAGGCGTTTTCGGTAACAACGAAGAACTGATCAACAAGATCCTGCAAAGTTCCAAGA
CCTCGAATGAACCGGTGTGGTGGCTGCCGATTATCAATGAATACCGTGCAACGCTGAACAGCAAATATGCTGATATT
AATCAGATCTCATCGAGCGTTAAAGCGTCTAGTATTGTCGCCTCCCTGTTTCTGAAGGAATTTGTTCAAAACACCGC
ATGGGCTCACATTGATATCGCGGGTGTCAGCTGGAATTTTAAAGCCCGTAAGCCGAAAGGCTTCGGTGTGCGCCTGC
TGACGGAATTTGTTCTGAATGACGCCCTGTAAGAATTC
```

Human Cytosolic LAP

```
GGCTCTTTTAAATGACCCCAGGCGTCGTGTATTGAATCCTAGACTCACGTCCGTCTCGCCGGCGCCCGAGCCAGTCC
GCGCGCACCGCGTCTGCGTCCCCGAAAGCCCCGCCCGCAAGGGCTGCCCTGCCTACCTGGTCTCCGACGTGCTCGTC
TGGAGGGCGGTGCGAGGGGCCGAGCCGACGAGATGTTCTTGCTGCCTCTTCCGGCTGCGGGGCGAGTAGTCGTCCGA
CGTCTGGCCGTAGTACGTTCTGGGAGCCGGAGTCTCTCCACCGCAGACATGACGAAGGGCCTTGTTTTAGGAATCTA
TTCCAAAGAAAAAGAAGATGATGTGCCACAGTTCACAAGTGCAGGAGAGAATTTTGATAAATTGTTAGCTGGAAAGC
TGAGAGAGACTTTGAACATATCTGGACCACCTCTGAAGGCAGGGAAGACTCGAACCTTTTATGGTCTGCATCAGGAC
TTCCCCAGCGTGGTGCTAGTTGGCCTCGGCAAAAAGGCAGCTGGAATCGACGAACAGGAAAACTGGCATGAAGGCAA
AGAAAACATCAGAGCTGCTGTTGCAGCGGGGTGCAGGCAGATTCAAGACCTGGAGCTCTCGTCTGTGGAGGTGGATC
CCTGTGGAGACGCTCAGGCTGCTGCGGAGGGAGCGGTGCTTGGTCTCTATGAATACGATGACCTAAAGCAAAAAAAG
AAGATGGCTGTGTCGGCAAAGCTCTATGGAAGTGGGGATCAGGAGGCCTGGCAGAAAGGAGTCCTGTTTGCTTCTGG
GCAGAACTTGGCACGCCAATTGATGGAGACGCCAGCCAATGAGATGACGCCAACCAGATTTGCCGAAATTATTGAGA
AGAATCTCAAAAGTGCTAGTAGTAAAACCGAGGTCCATATCAGACCCAAGTCTTGGATTGAGGAACAGGCAATGGGA
TCATTCCTCAGTGTGGCCAAAGGATCTGACGAGCCCCCAGTCTTCTTGGAAATTCACTACAAAGGCAGCCCCAATGC
AAACGAACCACCCCTGGTGTTTGTTGGGAAAGGAATTACCTTTGACAGTGGTGGTATCTCCATCAAGGCTTCTGCAA
ATATGGACCTCATGAGGGCTGACATGGGAGGAGCTGCAACTATATGCTCAGCCATCGTGTCTGCTGCAAAGTTAAAT
TTGCCCATTAATATTATAGGTCTGGCCCCTCTTTGTGAAAATATGCCCAGCGGCAAGGCCAACAAGCCGGGGGATGT
TGTTAGAGCCAAAAACGGGAAGACCATCCAGGTTGATAACACTGATGCTGAGGGGAGGCTCATACTGGCTGATGCGC
TCTGTTACGCACACACGTTTAACCCGAAGGTCATCCTCAATGCCGCCACCTTAACAGGTGCCATGGATGTAGCTTTG
GGATCAGGTGCCACTGGGGTCTTTACCAATTCATCCTGGCTCTGGAACAAACTCTTCGAGGCCAGCATTGAAACAGG
GGACCGTGTCTGGAGGATGCCTCTCTTCGAACATTATACAAGACAGGTTGTAGATTGCCAGCTTGCTGATGTTAACA
ACATTGGAAAATACAGATCTGCAGGAGCATGTACAGCTGCAGCATTCCTGAAAGAATTCGTAACTCATCCTAAGTGG
GCACATTTAGACATAGCAGGCGTGATGACCAACAAAGATGAAGTTCCCTATCTACGGAAAGGCATGACTGGGAGGCC
CACAAGGACTCTCATTGAGTTCTTACTTCGTTTCAGTCAAGACAATGCTTAGTTCAGATACTCAAAAATGTCTTCAC
TCTGTCTTAAATTGGACAGTTGAACTTAAAAGGTTTTTGAATAAATGGATGAAAATCTTTTAACGGAGACAAAGGAT
GGTATTTAAAAATGTAGAACACAATGAAATTTGTATGCCTTGATTTTTTTTTCATTTCACACAAAGATTTATAAAGG
TAAAGTTAATATCTTACTTGATAAGGATTTTTAAGATACTCTATAAATGATTAAAATTTTTAGAACTTCCTAATCAC
TTTTCAGAGTATATGTTTTTCATTGAGAAGCAAAATTGTAACTCAGATTTGTGATGCTAGGAACATGAGCAAACTGA
AAATTACTATGCACTTGTCAGAAACAATAAATGCAACTTGTTGTGAAAAAAAAAAAAAAAAAAAAAA
```

*Hs*LAP gene codon optimised for expression in *E. coli* and with *Eco*RI and *Nde*I restriction sites.

```
CATATGTTCCTGCTGCCGCTGCCGGCTGCTGGTCGTGTCGTCGTTCGTCGTCTGGCTGTCCGTCGTTTTGGTAGTCG
CTCACTGTCAACCGCTGATATGACCAAAGGCCTGGTTCTGGGTATTTATTCCAAGGAAAAAGAAGATGACGTCCCGC
AGTTTACCTCAGCGGGCGAAAACTTCGACAAGCTGCTGGCCGGTAAACTGCGTGAAACGCTGCAGATCTCGGGTCCG
CCGCTGAAGGCAGGTAAAACCCGCACGTTTTACGGCCTGCATCAAGATTTCCCGTCAGTGGTTCTGGTTGGCCTGGG
TAAAAAGGCGGCCGGCATTGACGAACAGGAAAACTGGCACGAGGGTAAAGAAAATATTCGTGCAGCTGTGGCAGCAG
GTTGCCGTCAGATCCAAGATCTGGAACTGAGCTCTGTGGAAGTTGATCCGTGTGGTGACGCACAGGCAGCTGCAGAA
GGTGCAGTGCTGGGTCTGTATGAATACGATGACCTGAAGCAGAAAAAGAAAATGGCGGTTTCTGCCAAACTGTATGG
CAGTGGTGATCAGGAAGCGTGGCAAAAAGGCGTCCTGTTTGCAAGCGGTCAGAACCTGGCTCGTCAACTGATGGAAA
CCCCGGCAAATGAAATGACCCCGACGCGCTTCGCTGAAATTATCGAAAAGAACCTGAAATCGGCCAGTTCCAAGACC
GAAGTTCATATTCGTCCGAAAAGCTGGATCGAAGAACAGGCAATGGGCAGCTTTCTGTCTGTGGCTAAAGGTTCTGA
TGAACCGCCGGTTTTCCTGGAAATTCACTACAAAGGCAGTCCGAACGCGAATGAACCGCCGCTGGTCTTTGTGGGCA
AGGGTATCACCTTCGATAGTGGCGGTATTTCCATCAAAGCATCAGCTAATATGGATCTGATGCGCGCAGACATGGGC
GGTGCCGCAACCATTTGCTCGGCTATCGTGAGCGCTGCGAAACTGAACCTGCCGATTAATATTATCGGTCTGGCCCC
GCTGTGTGAAAACATGCCGAGCGGCAAGGCGAATAAACCGGGTGATGTCGTGCGTGCCAAGAACGGCAAAACCATTC
AGGTCGATAATACGGACGCAGAAGGTCGCCTGATCCTGGCGGATGCCCTGTGCTATGCGCATACCTTTAACCCGAAA
GTGATCCTGAATGCCGCAACCCTGACGGGTGCAATGGACGTCGCTCTGGGTTCCGGTGCAACCGGTGTGTTTACGAA
CTCATCGTGGCTGTGGAATAAACTGTTCGAAGCATCAATTGAAACCGGCGATCGTGTGTGGCGCATGCCGCTGTTTG
AACACTATACGCGTCAGGTTGTCGATTGCCAACTGGCGGACGTTAACAATATCGGCAAATACCGCTCTGCAGGTGCT
TGTACCGCTGCGGCCTTTCTGAAGGAATTTGTTACGCATCCGAAATGGGCGCACCTGGATATTGCCGGTGTTATGAC
CAACAAGGACGAAGTCCCGTACCTGCGTAAGGGTATGACGGGTCGTCCGACCCGTACGCTGATCGAATTTCTGCTGC
GCTTCAGTCAGGATAATGCCTAAGAATTC
```

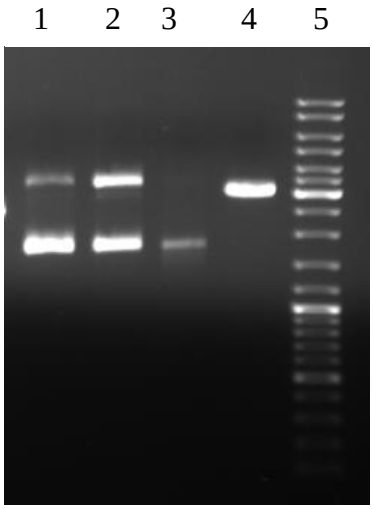

A gel showing the double digestion results of the samples sent for sequencing alongside the controls. Lane 1 – Clonejet with insert (sample A), lane 2 Clonejet with insert (sample B), lane 3 – insert , lane – 4 Clonejet and lane 5 – DNA ladder.

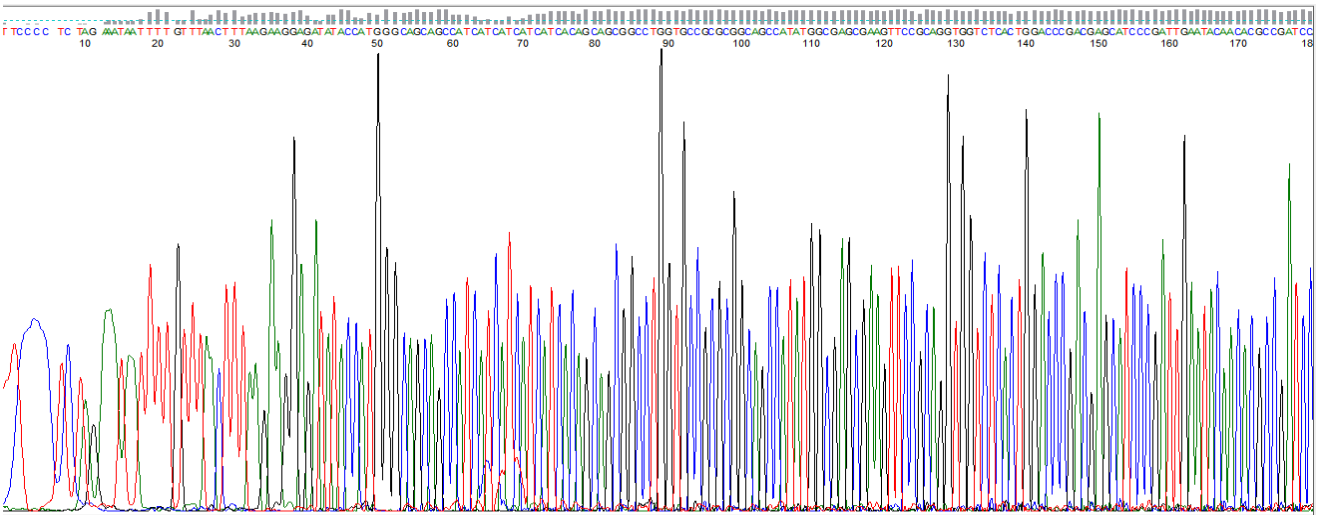

A segment of the *Pf*LAP electropherogram as analysed using Geospiza's FinchTV ver 1.4.0. it shows the initiation codon (ATG) at approximately base 50 and the His-tag sequence which follows.

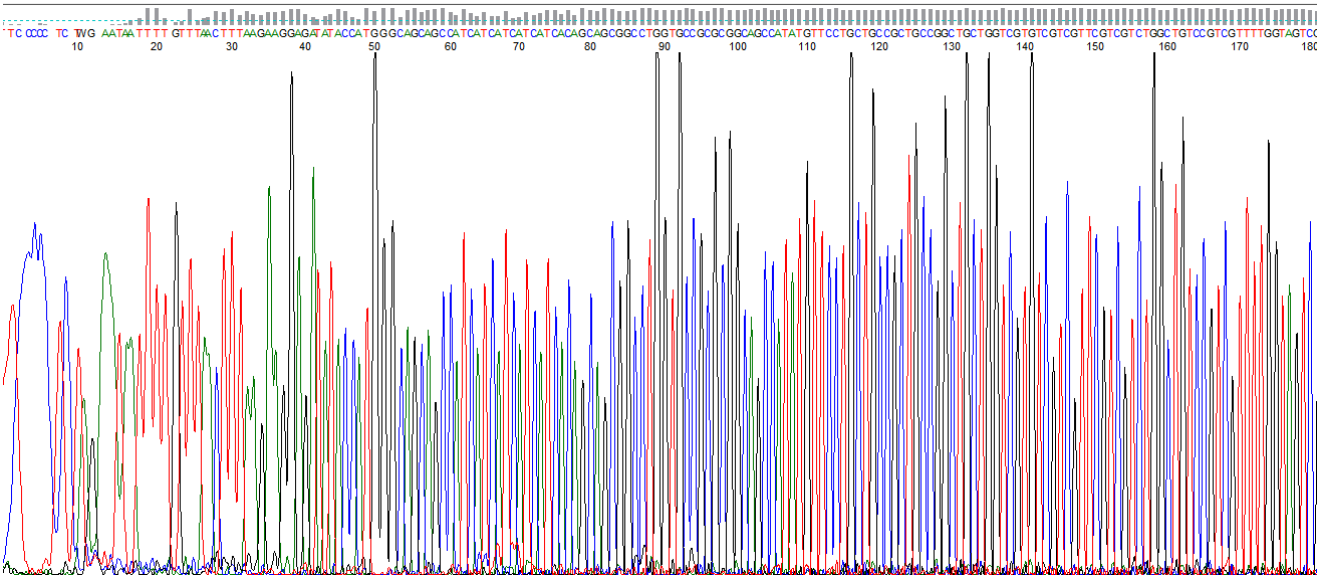

A segment of the *Hs*LAP electropherogram as analysed using Geospiza's FinchTV ver 1.4.0. It shows the initiation codon (ATG) at approximately base 50 and the His-tag sequence which follows.